COLLOIDAL PARTICLE-SURFACE INTERACTIONS IN ATMOSPHERIC AND AQUATIC SYSTEMS

A Dissertation
Presented to
The Academic Faculty

by

Eunhyea Chung

In Partial Fulfillment
of the Requirements for the Degree
Doctor of Philosophy in the
School of Civil and Environmental Engineering

Georgia Institute of Technology
May 2011

COLLOIDAL PARTICLE-SURFACE INTERACTIONS IN ATMOSPHERIC AND AQUATIC SYSTEMS

Approved by:

Dr. Sotira Yiacoumi, Advisor
School of Civil and Environmental Engineering
Georgia Institute of Technology

Dr. Jaehong Kim
School of Civil and Environmental Engineering
Georgia Institute of Technology

Dr. Costas Tsouris
School of Civil and Environmental Engineering
Georgia Institute of Technology

Dr. Todd Sulchek
School of Mechanical Engineering
Georgia Institute of Technology

Dr. Spyros Pavlostathis
School of Civil and Environmental Engineering
Georgia Institute of Technology

Date Approved: March 18, 2011

To my beloved family, Chanhyuk Chung, Youngbok Woo, and Jaehoon Chung

ACKNOWLEDGEMENTS

I would like to show my gratitude to my advisor, Dr. Sotira Yiacoumi, and Dr, Costas Tsouris who were abundantly helpful and offered invaluable support, encouragement and friendship throughout my study at Georgia Tech. Deepest gratitude are also due to my committee members, Professor Spyros Pavlostathis, Professor Jaehong Kim, and Professor Todd Sulchek; without whose patience, knowledge, and assistance, this study would not have been successful. I thank Dr. Guangxuan Zhu for his assistance during the past few years at Georgia Tech. My appreciation is also given to people from the Oak Ridge National Laboratory, especially to Dr. Lavrik, Dr. Datskos, Mark Walker, Dr. McFarlane, Dr. Ida Lee, Dr. John Ankner, Dr. Wei Wang, and Candice Halbert for their valuable help.

I would like to thank my current and previous lab mates, Patricia, Chia-hung, Douglas, Hyojin, and Ketki for their great help and friendship. I owe my sincere gratitude to my friends at Georgia Tech, especially to Soonchul, Myunghwa, Dr. Min Cho, Sujin, Hyunwook, and Sung Hu. I also wish to express my gratitude to my former advisor in Korea, Dr. Hyo-taek Chon for his great advices and support.

I would like to give my deepest appreciation to my parents and brother for their unconditional love and endless support which enabled me to complete my Ph.D. work successfully.

TABLE OF CONTENTS

LIST OF TABLES

LIST OF FIGURES

LIST OF SYMBOLS

A_H	Hamaker constant
A_H^{air}	Hamaker constant in air
A_H^{air}	Hamaker constant in water
$A_{particle}$	Surface area of the particle
a	Height of the spherical particle; Molecular spacing
b_i	Neutron scattering length of atom, i
b/V	Scattering length density of the subphase
b_s/V_s	Scattering length density of the incident medium
d	Thickness of the species
E	Electric field
e	Charge of an electron
F	Force
$F_{capillary}$	Capillary force
$F_{pressuredifference}$	Force due to the pressure difference
$F_{surfacetension}$	Surface tension force
F_{vdW}	van der Waals force
H	Distance between a particle and a surface
h	Separation distance between the surfaces
k	Scattering vector within the species
k_B	Boltzmann constant
$k_{cantilever}$	Spring constant of the cantilever

k_i	Neutron beam wave vectors
l	Line where the meniscus meets the particle
N	Number of contact points between the two objects
n	Refractive index
n_∞	Number of ions in the bulk solution
$n_{i,\infty}$	Number concentration in the bulk solution of ion, i
N_i	Number concentration of atom, i
P	Vapor pressure
P_0	Saturated vapor pressure
q	Electrostatic charge
$q_{particle}$	Electrostatic charge of particle
R	Radius of a particle
$R(\theta)$	Reflectivity
$R_F(\theta)$	Reflectivity of an ideal interface
R_{gas}	Gas constant
$r_{0,1}$	Reflection coeffiecient
$r_{0,1}^*$	Complex conjugate of the reflection coeffiecient
r_i	Radius of the spherical particle i
r_1 , r_2	Principle radii of the meniscus curvature
T	Temperature
z	Distance from a surface
z_i	Charge valence
z_{tip}	Position of the AFM tip
$z_{substrate}$	Position of the substrate

α, β, γ	Weight coefficient
β_{abs}	Absorption factor
ΔP	Pressure difference
Δz	Deflection of a probe
ε_0	Vacuum permittivity
ε	Dielectric permittivity
Φ	Potential
Φ_{vdW}	van der Waals interaction potential
ϕ	Angle of meniscus
ϕ_{edl}	Electrical double-layer potential
ϕ_i	Reduced potential
$\lvert\phi(Q)\rvert^2$	Modulus squared of the Fourier transform of the scattering density gradient
γ	Surface tension of water
λ	Neutron wavelength
θ	Angle of the neutron beam
θ_c	Critical angle
θ_i	Contact angles of the surfaces
ρ	Scattering length density
ρ_a	Scattering length density in air
ρ_s	Mean scattering length density in the bulk of the subphase
σ	Charge density
$\sigma_{surface}$	Surface charge density

$\sigma_{substrate}$	Surface charge density of the substrate
υ^0	Molar volume of water
ψ_i	Surface potential
$\psi_{substrate}$	Potential of the substrate
ψ_{tip}	Potential of the AFM tip

LIST OF ABBREVIATIONS

AFM	Atomic force microscopy
Bt	*Bacillus thuringiensis*
DLVO	Derjaguin-Landau-Verwey-Overbeek
DSL	Dynamic light scattering
NR	Neutron reflectometry
QCM	Quartz crystal microbalance
SEM	Scanning electron microscope
SLD	Scattering length density
SSPM	Scanning surface potential microscopy
STEM	Scanning/transmission electron microscopy
TEOS	Tetraethyl orthosilicate

SUMMARY

Colloidal particles suspended in a liquid or gas phase often interact with solid-liquid or solid-gas interfaces. In this study, experimental data through atomic force microscopy (AFM) and neutron reflectometry (NR) and theoretical results of colloidal particle-surface interactions were obtained and compared. Atmospheric and aquatic environments were considered for the interactions of microbial colloidal particles and nano-sized silica particles with planar surfaces. Spores of *Bacillus thuringiensis* (*Bt*), members of the *Bacillus cereus* group, were examined as the microbial particles simulating the pathogens *Bacillus cereus* and *Bacillus anthracis* which are potentially dangerous to human health. Model planar surfaces used in this study include gold which is an electrically conductive surface, as well as mica and silica which are charged, nonconductive surfaces.

A mathematical model was developed to calculate the adhesion force between a spherical particle and a planar surface in atmospheric systems as the sum of the capillary force and the van der Waals force. The electrostatic interaction was initially neglected in the model. The two-force mechanisms that were considered are functions of relative humidity. The capillary force increases as the relative humidity value increases, whereas the van der Waals force decreases as the humidity increases. Adhesion force measurements by AFM were conducted using a particle or a *Bt*-spore modified AFM cantilever probe. The measured adhesion force between a silica particle and a gold surface is comparable to the model calculations, while there is some disagreement between the measured adhesion force for the *Bt* spore-gold surface system and the

calculated values. The discrepancy may be the result of neglecting the electrostatic force, and of the surface roughness of the spore that was observed from the imaging studies.

In continuation of the study, the electrostatic force was investigated as one of the components of the adhesion force between *Bt* spores and planar surfaces in atmospheric systems. The surface potentials of a *Bt* spore and a non-conductive surface, such as mica, were experimentally obtained using a combined AFM-scanning surface potential microscopy (SSPM) technique. The surface charge of the mica and the *Bt* spore decreases with increasing humidity. The Coulombic force was introduced for the spore-mica system and an electrostatic image force was introduced for the spore-gold system. The Coulombic force for spore-mica (both charged, non-conductive surfaces) is repulsive because the components are similarly charged, while the image force for the spore-gold system is attractive. The magnitude of both forces decreases with increasing humidity as a result of the decreasing surface charge density as humidity increases. The electrostatic forces were added to other force components, e.g., van der Waals and capillary forces, to obtain the adhesion force for each system. The repulsive Coulombic force for the spore-mica system decreases the magnitude of the adhesion force, while the attractive image force for the spore-gold system increases the previously obtained adhesion force. It was shown that the electrostatic (Coulombic and image) forces play a significant role in the adhesion force between spores and planar surfaces.

In this part of the study, bacterial spore interactions with planar surfaces in aquatic environments, including adhesion forces and force-distance profiles, were investigated. The characteristics of *Bt* spores were determined using electron microscopy and electrokinetic measurements. The surface potentials of the spores and mica surface

used in the experiments were measured as a function of pH and ionic strength. The Derjaguin-Landau-Verwey-Overbeek (DLVO) theory was employed to predict the interaction force between the spore and planar surfaces as a function of the separation distance, and a force balance was used to explain the adhesion force or "pulling-off" force. Theoretical estimations were compared to experimental measurements obtained from AFM. The DLVO-based calculations are consistent with AFM force measurements, while the calculated adhesion force shows some deviations from the measurements. The deviations can be minimized by considering the roughness of the *Bt* spore and substrate surfaces.

Neutron reflectometry was used as a method to investigate particle deposition and aggregation near a flat surface in aqueous solutions. This experimental technique has some advantages compared to other experimental tools, such as the capability to capture a large population of particles that represent the behavior of the whole system, as well as to observe particles within several nanometers from the surface. The results agree well with DLVO calculations between a particle and a surface, confirming that NR is a promising method for the study of interactions of particles close to a solid surface.

The results obtained in this research provide insights into the fundamental mechanisms of colloidal particle interactions with environmental surfaces in both atmospheric and aquatic systems, contributing to the understanding of the phenomena driving interfacial processes such as deposition, aggregation, and sedimentation. Thus, the results obtained can help us describe the behavior of contaminant colloidal particles in environmental systems and subsequently devise better means for their removal from environmental surfaces.

CHAPTER 1

INTRODUCTION

1.1 Interfacial Processes and Colloidal Forces

Interfaces and colloidal particles including microbial particles are ubiquitous in environmental systems. As the size of a system becomes smaller, the ratio of interfacial area to volume becomes bigger; thus interfacial processes have more significance in smaller systems. The interface of two phases, such as solid-liquid or solid-gas, may involve colloidal particles suspended in a liquid or gaseous phase. Examples of interfacial processes involving colloidal particles include deposition, aggregation, and sedimentation among others. In addition, there are microbiological processes such cellular attachment (or detachment) onto surfaces or adsorption of nutrients on the cellular membrane of microbial agents. The behavior of bioaerosols in atmospheric systems is also strongly influenced by interfacial processes. Such processes may occur in both natural and engineered environments.

Interfacial processes may be driven by several types of interaction forces between colloidal particles and interfaces in aquatic or atmospheric environmental systems. One such type is the van der Waals force that arises from the attractive force between transient dipoles or quadrupoles in molecules; thus, the van der Waals force, also called dispersion force, is exhibited by non polar molecules (Israelachvili 1998). Electrostatic interaction is another type of force arising when two bodies are charged (Hiemenz and Rajagopalan 1997). This force can be expressed by Coulomb's law and is either attractive or repulsive depending on the charges of the two bodies. While the van der Waals attraction and the electrostatic interaction forces occur in both aquatic and atmospheric systems, another type of force, called the capillary force, appears only in atmospheric environments.

When a particle rests on a planar surface, water is condensed due to the pressure difference and surface tension in the area between the two objects. The capillary force is calculated as the sum of a force due to surface tension and a capillary pressure force that depends on the surrounding relative humidity. Even though there are other types of forces, such as the magnetic force and the short-range Born repulsion force, the capillary, van der Waals, and electrostatic interaction forces are considered as the basic forces in interfacial systems.

There are existing mathematical models that can be used to quantify surface interaction forces. The interaction force, such as the adhesion force between a particle and a surface in an atmospheric environment, is estimated by the addition of the van der Waals attraction, electrostatic interaction, and capillary forces (Cross and Picknett 1963; Ouyang et al. 2001; Biggs et al. 2002). Solid-gas interfacial processes with fine particles, such as aerosols, deposited onto a surface could be explained by this method; however, the calculation of each component has limitations due to the inaccuracies in the values of parameters or the difficulties in measuring the variables.

The Derjaguin-Landau-Verwey-Overbeek (DLVO) theory has traditionally been used to describe solid-liquid interfaces (Hiemenz and Rajagopalan 1997). The DLVO theory describes the force between charged surfaces interacting through a liquid medium. It combines the effects of the van der Waals attraction and electrostatic interactions. This theory explains colloidal systems with symmetric electrolytes at low concentrations. There are several systems, however, that cannot be predicted by the DLVO theory; for example, asymmetric electrolytes at high concentration, which can be encountered in many natural and engineered systems (Hahn and O'Melia 2004; Taboada-Serrano et al. 2005). Monte Carlo simulation has been proven an effective method to predicting the behavior of ions near charged surfaces (Yang et al. 2002; Taboada-Serrano et al. 2005). Molecular modeling deals with systems of relatively small dimensions compared to the experimental systems. Increasing the dimensions of the system is often challenging due

to computational limitations. Even with these limitations, Monte Carlo simulation can be used to explain the behavior of asymmetric electrolytes that cannot be described by the DLVO theory.

There are several experimental methods that can be used to provide a better understanding of various interfacial processes. The quartz crystal microbalance is used for the investigation of the behavior of colloidal particles, polymers, and lipid films and biomolecules on surfaces (Caruso et al. 1997; Lvov et al. 1997; Marx 2003). The device measures the change in resonance frequency of a quartz crystal resonator, which is disturbed by the accumulation or removal of particles at the surface of the resonator. It can be used to monitor the deposition rate or the adsorption affinity of colloidal particles to surfaces. Another example of experimental methods to quantify surface interactions is atomic force microscopy (AFM). In AFM, a particle probe (i.e., a microcantilever with a colloidal particle attached to it) approaches toward a surface and retracts from the surface. From the recorded deflection of the cantilever, the interactive force between the particle and the surface can be calculated as the product between the cantilever deflection and the cantilever spring constant. Neutron reflectometry provides structural information of the distribution of particles along a direction perpendicular to surfaces (Zhou and Chen 1995). The technique involves an incoming neutron beam at a flat surface, and its reflection from the surface is measured in terms of scattering length density as a function of depth. The obtained reflectivity profile can be used to determine the thickness, material composition, periodicity, and roughness of any thin film layered on the substrate.

In the present work, a combination of experimental data and theoretical calculations is used to provide a better understanding of the relative importance of interfacial forces under various environmental conditions.

1.2 Behavior of Microbial Colloidal Particles

There have been several studies reported in the literature on applying an experimental methodology or a simulation approach to determine the macroscopic behavior of biological aerosols. This determination has several implications related to environmental engineering including the detection of atmospheric pollutants, estimation of pathogenic transport through the atmosphere, and air filtration processes. Airborne bacteria or fungi can be transported through the stratosphere in either their vegetative state or their dormant form. Transport of microbial colloidal particles is an important issue with respect to spreading pathogenic microorganisms (Griffin 2004; Smith et al. 2010). The dispersion of aerosol particles or biological agents as potential materials for bioterrorism was investigated through experimental simulation in an aerosol chamber (Utrup et al. 2003; Ho and Duncan 2005; Lai et al. 2008), or by sampling outdoor air (Fuzzi et al. 1997; Kuske 2006), or through computer-model simulation in high rise buildings (Reshetin and Regens 2003; Reshetin and Regens 2004).

Besides environmental-engineering related applications, studies on the interfacial behavior of bioaerosols have also implications in other fields related to microbiological ecology, hygiene in the medical field and food science, and pathology (Ubbink and Schar-Zammaretti 2005). Spore adhesion on spacecrafts was also investigated for cleaning, sterilization, validation, and recontamination prevention of the surface (Venkateswaran et al. 2004; Lin 2006). In addition, global transport or dispersion of biological aerosols or pathogens was investigated by air sampling to determine the atmospheric microbiological ecology (Bovallius et al. 1978; Westbrook and Isard 1999; Kellogg and Griffin 2006).

The fate and transport of biological colloids was studied in aqueous systems, as well. Microorganisms or biological colloids can be considered as contaminants in groundwater or subsurface systems and can also facilitate the transport of other contaminants, such as heavy metals (Pang et al. 2004; Custodio 2006). In addition,

biocolloids including bacterial spores can be used as tracers for sewage dispersion. The transport of spores was tested and visualized by laboratory-scale soil-column experiments or field-scale experiments under saturated or unsaturated condition (Kinoshita et al. 1993; Jiang et al. 2006; Keller and Auset 2007; Harvey et al. 2008), and the factors affecting the process of spore transport through a soil column were investigated (Camesano et al. 1999; Kim et al. 2009). In addition, the advection-dispersion model was tested for microbial colloids in filtration processes (Pang et al. 2005). These studies have implications in groundwater contamination (a public-health problem), subsurface bioremediation, subsurface ecology, water-treatment process design, and risk assessment of pathogen contamination.

Previous studies on the fundamental mechanisms behind microscopic interfacial processes between microbial colloids and environmental surfaces provide a good background resource for understanding the macroscopic behavior of biocolloids in atmospheric and aquatic environments.

1.3 Scope and Objectives

This study combines experimental and theoretical work to examine the fundamental mechanisms behind interfacial processes occurring in atmospheric and aquatic environments. This objective is accomplished through various experimental measurements and comparisons between experimental data and mathematical modeling results.

The overall objective of the present thesis is to provide a better understanding of the interfacial interaction forces in atmospheric and aqueous environments. The following specific objectives were proposed in order to achieve the overall goal:

- Study the adhesion force between a particle (inorganic or biological) and a planar surface in atmospheric environments.

- Assess the relative importance of the adhesion force components between a spherical particle and a planar surface in atmospheric environments through mathematical modeling calculations.
- Study the interfacial force and its components between a biological agent and model surfaces in aqueous environments.
- Assess the factors influencing the interaction of colloidal particles with surfaces through experimental data and theoretical calculations.
- Examine the potential of neutron reflectometry as a tool to investigate particle-surface interactions.

1.4 Organization of Thesis

Chapter 1 introduces the interfacial processes and colloidal forces acting on particles suspended in a liquid or gaseous phase. Chapter 1 also discusses the importance of studying the behavior of microbial colloids in environmental systems. The scope and objectives of this research are included in this chapter as well.

A review related to theoretical modeling and experimental methods is described in Chapter 2. Detailed descriptions of the DLVO theory, adhesion force modeling and calculations, neutron reflectometry, and operation procedure of the AFM can be found in Chapter 2.

Chapter 3 describes the mechanisms of adhesion between a particle, such as a *Bacillus thuringiensis* spore, and an electrically conductive surface such as gold in atmospheric environments. The adhesion force, also called pulling-off force, measured by AFM is discussed and the components of the force are evaluated through a mathematical model. In the model, the effects of such parameters as particle size and properties of the materials, including the Hamaker constant and hydrophobicity or contact angle, are

investigated. In addition, the role of the relative humidity in the adhesion force is also discussed via experimental and theoretical approaches in Chapter 3.

The adhesion force between a colloidal particle and an electrically non-conductive surface is discussed in Chapter 4. The comparison of AFM experimental data and model calculations showed a discrepancy, therefore, it was needed to modify the model. An electrostatic interaction force was introduced in the model as a new component of the adhesion force. The role of the electrostatic interaction in the modified model is discussed in this chapter. A possible additional force component in the system with conductive surface is also discussed.

In Chapter 5, not only the adhesion force but also other types of force measurements that can be obtained through AFM, specifically the 'force-distance curve', is also discussed for microbial colloids and planar surfaces in aquatic environments. The force-distance curve is compared to the calculated force-distance or potential-distance curve using the DLVO theory. Similarly to the atmospheric system, the adhesion force for aqueous environments is investigated both experimentally and theoretically.

Neutron reflectometry experiments are conducted to probe the classical theory, specifically the electrical double layer force. In Chapter 6, the results from neutron reflectometry experiments under various conditions of electrolytes are compared to theoretical calculations. The concentration distribution of particles near a charged surface is determined by fitting modeling results to neutron reflectivity data. The concentration profile of colloidal particles near the surface obtained in this way is explained by means of the DLVO theory.

Major conclusions of this research and recommendations for future studies are presented in Chapter 7.

CHAPTER 2

COLLOIDAL PARTICLE-SURFACE INTERACTIONS: THEORETICAL MODELS AND EXPERIMENTAL MEASUREMENTS

2.1 Theory for Colloidal Particle–Surface Interactions

2.1.1 Adhesion Forces in Atmospheric Environments

Mathematical models for the adhesion force between a spherical particle and a planar surface in atmospheric systems have been reported in the literature (Cross and Picknett 1963; Sedin and Rowlen 2000; Butt et al. 2006; Farshchi-Tabrizi et al. 2006). Three main components – the van der Waals force, the capillary force, and the electrostatic force – are generally considered in the modeling of the adhesion force (Xiao and Qian 2000; Ouyang et al. 2001). These forces are functions of the electrostatic potential, shape, size, and roughness of particles, as well as the relative humidity. For the capillary force calculation, two components are considered: one is a surface tension force and the other is a force due to the pressure difference, and the circular approximation is used to describe the shape of the meniscus between the particle and surface (Orr et al. 1975). Figure 2.1 shows the schematic of the spherical particle on the planar surface at a certain height and circular shaped meniscus.

The capillary force is calculated as the sum of the surface tension force and the force due to the pressure difference:

$$F_{capillary} = F_{surfacetension} + F_{pressuredifference} = 2\pi d\gamma \sin(\theta_1 + \phi) + \pi d^2 \Delta P \qquad (2.1)$$

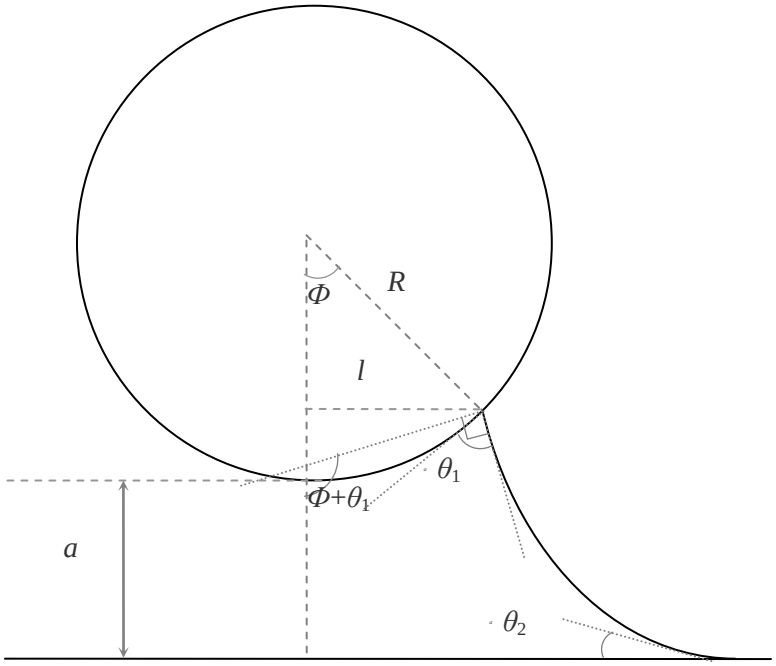

Figure 2.1 Spherical particle on a planar surface at the height, *a*, and meniscus with circular shaped curvature.

where γ is the surface tension of water. The Young-Laplace equation describes the pressure difference using the principal radii of the curvature as: $\Delta P = \gamma\left(\frac{1}{r_1} - \frac{1}{r_2}\right)$ where r_1 and r_2 are the principal radii of the meniscus curvature.

The radius of the circle on the spherical particle along the line where the meniscus meets the particle, *l*, can be replaced by $R\sin\phi$. Then, the force can be rewritten as:

$$F_{capillary} = \pi R\gamma \sin\phi \left\{ 2\sin(\theta_1 + \phi) + R\sin\phi\left(\frac{1}{r_1} - \frac{1}{r_2}\right)\right\} \tag{2.2}$$

Orr *et al*. (1975) expressed the principal radii using the radius of the particle (*r*), particle height (*a*), contact angles of the materials (θ), and angle of the meniscus (ϕ):

$$r_1 = \frac{R(1-\cos\phi) + a}{\cos(\theta_1 + \phi) + \cos\theta_2} \tag{2.3}$$

$$r_2 = \frac{R\sin\phi}{\sin(\theta_1 + \phi)} \tag{2.4}$$

Thus, the capillary force is calculated using known parameters such as the water surface tension, particle radius, angle of meniscus, contact angles of the surfaces, and the height of the spherical particle:

$$F_{capillary} = \pi R\gamma \sin^2\phi \left\{ \frac{\sin(\theta_1 + \phi)}{\sin\phi} + \frac{\cos(\theta_1 + \phi) + \cos\theta_2}{1 - \cos\phi + (a/R)}\right\} \tag{2.5}$$

The van der Waals force between a spherical particle and a planar surface is obtained by integrating the force between a circular disc and a planar surface as a

function of the properties of the medium surrounding the two objects. Because of the existence of the meniscus between the spherical particle and the surface in the system, the integration consists of two parts; one with water as the medium between the surfaces and the other with air surrounding the system:

$$F_{vdW} = 2\pi \int_0^l \frac{zA_H^{water}}{6\pi H^3} dz + 2\pi \int_l^\infty \frac{zA_H^{air}}{6\pi H^3} dz \qquad (2.6)$$

where A_H^{water} and A_H^{air} are the Hamaker constant in water and air, respectively, and H is the distance between the disc and the surface which can be expressed using the parabolic approximation as $H = a + (x^2 / 2R)$. Therefore, the van der Waals force is described as:

$$F_{vdW} = -\frac{(A_H^{water} - A_H^{air})}{6R} \frac{(a/R)+1-2\cos\phi}{(a/R)+1-\cos\phi} + \frac{A_H^{water}}{6R} \frac{(a/R)-1}{(a/R)^2} - \frac{A_H^{air}}{6R} \frac{1}{(a/R)+1} \qquad (2.7)$$

A value of the angle of the meniscus (ϕ) in the calculation of the van der Waals and capillary forces is determined as a function of the relative humidity (P / P_0) by using the Kelvin equation:

$$\frac{R_{gas} T \ln(P/P_0)}{\gamma \upsilon^0} = -\frac{\cos(\phi + \theta_1) + \cos\theta_2}{R(1-\cos\phi)} + \frac{\sin(\phi + \theta_1)}{R\sin\phi} \qquad (2.8)$$

where R_{gas} and T are the gas constant and absolute temperature, respectively, and υ^0 is the molar volume of water. As shown in the calculation results for model particle and surface (Figure 2.2), the sum of the two forces is influenced by the contact angles of the materials. While the Kelvin equation can be solved numerically, the angle of the

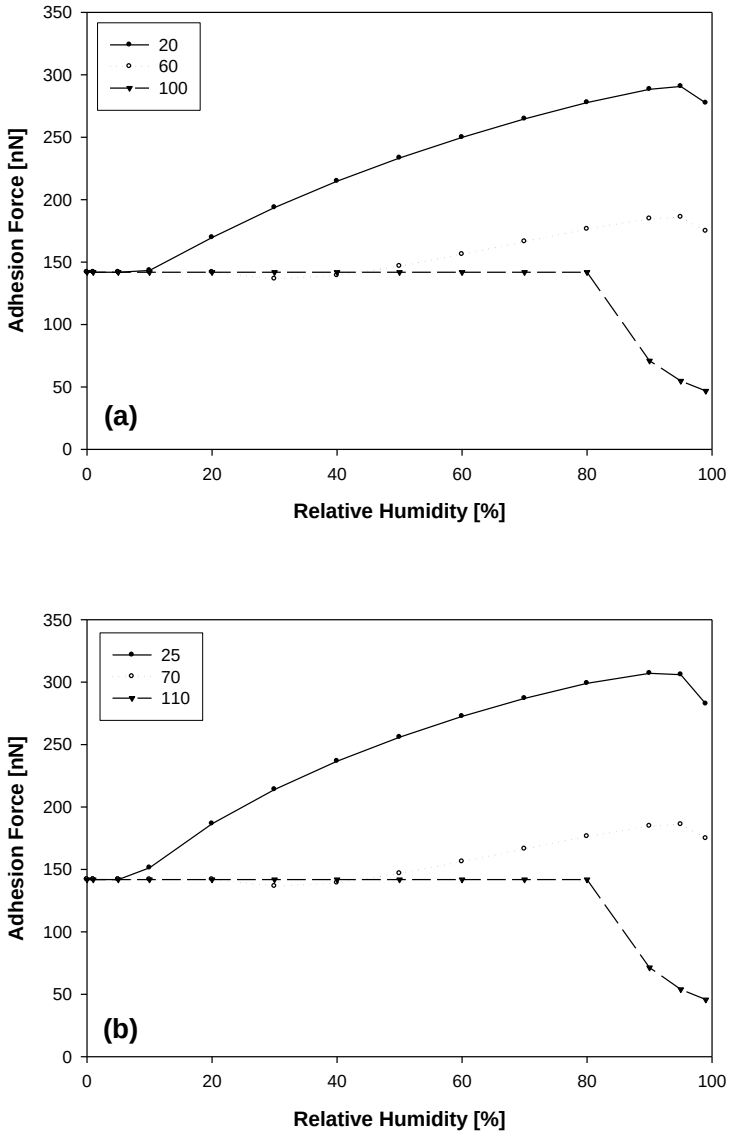

Figure 2.2 Adhesion force calculations for a model particle and a surface and the influence of contact angle θ_1 for the sphere-water-air (a) and the contact angle θ_2 for the planar surface-water-air (b) on the adhesion force.

meniscus is not determined at low relative humidity conditions for the model calculation, which means that the meniscus is not formed up to a critical value of the relative humidity. Below the critical humidity level, the capillary force is zero and the sum of the forces is constant.

The third component of the adhesion force is the electrostatic force which can be calculated from the surface potential or charge density of the two objects. The surface potential of the material is obtained from SSPM measurements and converted into the charge density, as explained further in a subsequent section (Section 2.2.3).
If we assume an infinite size for a planar surface with surface charge density ($\sigma_{surface}$), the electric field, *E*, produced by the surface charge is: $E = \frac{\sigma_{surface}}{2\varepsilon_0}$. The force, *F*, applied to a particle of electrostatic charge ($q_{particle}$) in an electric field *E* is:

$$F = E \cdot q_{particle} = \frac{\sigma_{surface}}{2\varepsilon_0} q_{particle} \tag{2.9}$$

Because the surface charge of the spherical particle can be calculated as the product of the charge density and the surface area, the force can be rewritten as:

$$F_{Coulomb} = E \cdot q_{particle} = \frac{\sigma_{surface}}{2\varepsilon_0} q_{particle} = \frac{\sigma_{surface}\sigma_{particle}}{2\varepsilon_0} A_{particle} \tag{2.10}$$

where $A_{particle}$ is the surface area of the particle.

The Coulombic force arises when two interacting objects have electrostatic surface charges. However, there is another type of electrostatic force acting between a charged particle and a grounded conductive surface. Although the conductive substrate has no surface charge, so the Coulombic force between the particle and the surface is zero,

there is an image charge or image particle arising on the opposite side of a conducting planar surface due to polarization of the conducting surface material by the charged atoms of the particle (Fowlkes and Robinson 1988; Feng and Hays 2003). The interaction force between the image particle due to polarization and the charged particle is called 'electrostatic image force'.

The image force is calculated by the equation:

$$F_{imgae} = \alpha \frac{q_{particle}^{2}}{16\pi\varepsilon_0 R^2} \tag{2.11}$$

where R is the radius of the particle and α is the weight coefficient, which is a function of several parameters such as the dielectric constant or the geometry of the particle. The value of α varies with the charge distribution on the particle surface. If the surface charge of the particle is concentrated close to the contact point on the surface, α increases by up to an order of magnitude (Czarnecki and Schein 2004). Also, if the particle has a symmetrical surface charge distribution, the value of α is 2.27 times greater than the point charged particle system.

Consequently, the adhesion force of a particle on a planar surface in an atmospheric environment can be determined by three factors: (i) van der Waals, (ii) capillary, and (iii) electrostatic (Coulombic or image) forces. There are two important approximations involved in the model development: (i) the shape of the meniscus formed between a spherical particle and a planar surface is circular and (ii) the distribution of the potential between two surfaces is linear.

While the interaction force between a particle and a surface in the atmosphere is described by considering the two interacting objects and the condensed water in-between, the interaction force in aqueous environments can be described by considering the ions in the solution and their interactions with ions accumulating near the particle surface and the

planar surface, as introduced in the following section (Section 2.1.2). The ionic cloud near a solid surface in an aqueous solution is also known as the electrical double layer.

2.1.2 Interparticle Interactions in Aqueous Solutions through the DLVO Theory

Traditionally, the Derjaguin, Landau, Verwey and Overbeek (DLVO) theory has been used in explaining the interaction between two charged colloidal particles in electrolyte solutions (Elimelech et al. 1995; Hiemenz and Rajagopalan 1997; Israelachvili 1998). The theory has two components, the electrostatic and van der Waals interaction whose energy potentials or forces can be expressed as a function of the separation distance between two planar surfaces. Mathematical expressions of potentials and forces between two planar surfaces, between two spherical particles, or between a particle and a planar surface have been reported in the literature (Elimelech et al. 1995; Hiemenz and Rajagopalan 1997; Dorobantu et al. 2009). The electrostatic interaction between charged particles in aqueous solutions is determined by the overlapping electrical double layers formed by ions accumulating near the charged surfaces (Hiemenz and Rajagopalan 1997). The electrical double-layer potential between two planar surfaces per unit area is expressed by:

$$\phi_{edl} = 64 k_B T n_\infty \kappa^{-1} \Gamma_0^2 \exp(-\kappa h) \tag{2.12}$$

where k_B is the Boltzmann constant, T is the absolute temperature, n_∞, is the number concentration of ions in the bulk solution, h is the separation distance between the

surfaces, $\kappa = \left[\frac{e^2}{\varepsilon k_B T} \sum_i z_i^2 n_{i,\infty} \right]^{1/2}$, and $\Gamma_0 = \frac{\exp(ze\psi_0 / 2k_B T) - 1}{\exp(ze\psi_0 / 2k_B T) + 1}$. The parameters *e*, ε, z_i, $n_{i,\infty}$, and ψ_0 represent the charge of an electron, dielectric permittivity, charge valence, number concentration in the bulk solution of ion type *i*, and surface potential, respectively. The interaction potential between two charged spheres can be given by:

$$\Phi = \frac{2\pi r_1 r_2 n_\infty k_B T}{(r_1 + r_2)\kappa^2} \left(\phi_1^2 + \phi_2^2\right) \left[\frac{2\phi_1\phi_2}{\phi_1 + \phi_2} \ln\left(\frac{1 + \exp(-\kappa h)}{1 - \exp(-\kappa h)} \right) - \ln(1 - \exp(-2\kappa h)) \right] \tag{2.13}$$

where r_i is the radius of the spherical particle *i* and ϕ_i is the reduced potential, which is related to the surface potential (ψ_i) by: $\phi_i = \frac{e\psi_i}{k_B T}$. The interaction potential of the system of a spherical particle and a planar surface can be estimated by the two-particle-system mathematical expression by allowing one particle to have an infinite size.

The van der Waals interaction potential between a spherical particle and a surface is given by:

$$\Phi_{vdw} = -A_H R / 6h \tag{2.14}$$

while the van der Waals potential between two planar surfaces can be expressed per unit area:

$$\Phi_{vdw} = -(A_H / 12\pi) / h^2 \tag{2.15}$$

where A_H is the van der Waals constant and R is the radius of the particle (Elimelech et al. 1995). After the addition of the two potential components (i.e., van der Waals and electrostatic interactions) between a spherical particle and a planar surface, the corresponding force can be simply obtained from the derivative of the total potential with respect to the separation distance between the surfaces.

In summary, the interaction between two objects in an aqueous environment has one missing component, the capillary force, compared to the atmospheric system. Moreover, two common components – van der Waals and electrostatic forces – are calculated using different equations for atmospheric and aqueous systems. While the electrostatic interaction in the aqueous solution is described by the interaction of adjacent electrical double layers, which are the clouds of ions near charged surfaces, the electrostatic force in the atmospheric environment is simply calculated using the surface charges. Also, the van der Waals force in the aqueous solution is calculated using a simple equation, while the van der Waals force in the atmospheric system is calculated with consideration of two media – the surrounding atmosphere and condensed water.

2.2 Experimental Measurements of Particle–Surface Interaction

The theoretical estimations of the force or potential energy between a spherical particle and a planar surface can be verified with various experimental measurements such as neutron reflectometry or atomic force microscopy (AFM). While AFM provides the interaction force data between a particle and a surface directly (Chin et al. 2002), neutron reflectometry provides structural information of particle distribution near the surface, which is a result of the interaction force between the particle and the surface (Zhou and Chen 1995). Therefore, the particle distributional information obtained by the

neutron reflectometry measurements is explained by the potential energy (or force) curve calculated from the DLVO theory. Meanwhile, AFM force data can be directly compared to theoretical calculations of the interaction force.

2.2.1 Neutron Reflectometry

Neutron reflectometry provides structural information of surfaces (Penfold and Thomas 1990; Li et al. 1998). The technique involves an incoming neutron beam at a flat surface, and its reflection from the surface is measured in terms of angle and scattering length density as shown in Figure 2.3 (Russell 1990). The obtained reflectivity profile can be used to determine the thickness, material composition, periodicity, and roughness of any thin films layered on the substrate. The neutron reflectometry experiments provide information about the distribution of particles along the direction perpendicular to the flat surface, a result that cannot be provided by other instruments such as the quartz crystal microbalance or AFM. The neutron reflectometry measurements involve a very large population of particles, thus the measurements represent well the average behavior of the whole particle population in the system. In addition, in neutron reflectometry experiments, particles freely move toward and away from the surface in the aqueous solution. Thus, the behavior of a large number of colloidal particles freely floating in the medium and interacting with a surface in the neutron reflectometry experiment will be comparable to the behavior of a real natural or engineered system.

Neutron reflectometry provides structural information near an interface, in the direction normal to the surface. The instrument provides the refractive index profile normal to the interface which is related to the scattering length density and this

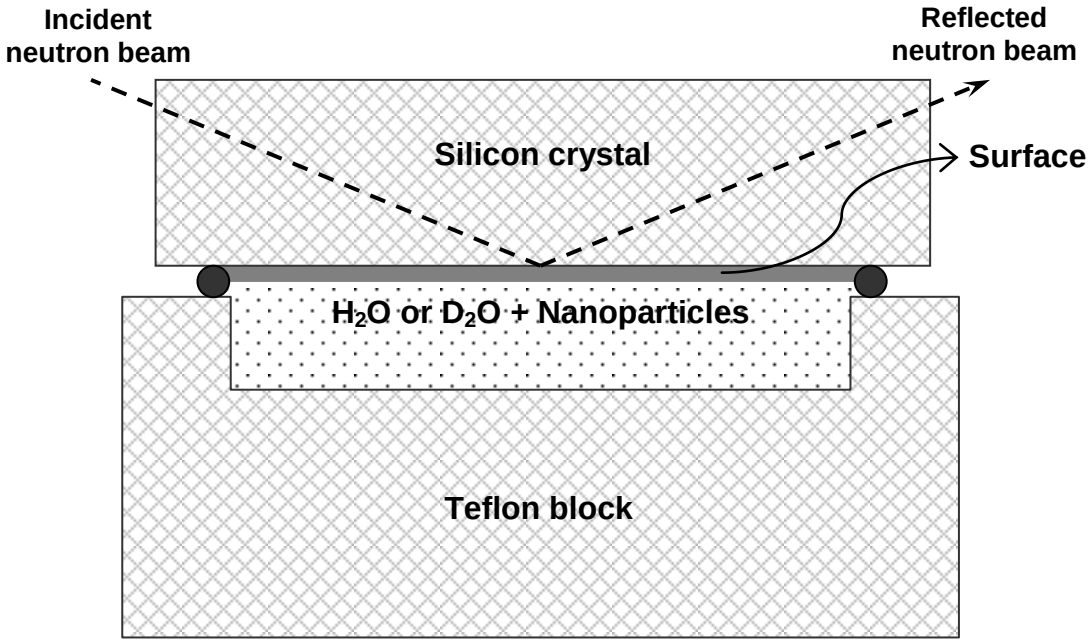

Figure 2.3 Schematic of the neutron reflectometry cell.

information is used in the calculation of the reflectivity. The reflectivity profiles are produced using an approximate method (Grundy et al. 1988; Fragneto-Cusani 2001).

The reflectivity $R(\theta)$ is calculated using the following formula:

$$R(\theta) = R_F(\theta)\left|\phi(Q)\right|^2 \tag{2.16}$$

where $R_F(\theta)$ is the reflectivity of an ideal interface and $\left|\phi(Q)\right|^2$ is the modulus squared of the Fourier transform of the scattering density gradient. The reflectivity expected for an ideal interface is:

$$R_F(\theta) = \left|\frac{\sin^2\theta - (n^2 - \cos^2\theta)^{1/2}}{\sin^2\theta + (n^2 - \cos^2\theta)^{1/2}}\right|^2 \tag{2.17}$$

when $\theta > \theta_c$, or $R_F(\theta) = 1$ when $\theta \le \theta_c$. Here, the critical angle $\theta_c = \cos^{-1} n$ is obtained using the refractive index $n = 1 - \frac{\lambda^2}{2\pi}\rho_s + i\beta_{abs}$, where λ is the neutron wavelength, ρ_s is the mean scattering length density in the bulk of the subphase, and β_{abs} is an absorption factor which is considered not significant for most cases (i.e., $\beta \approx 0$). The scattering density ρ is calculated by the formula: $\rho(z) = \sum_i N_i(z) b_i$, where N_i and b_i are the number density and the neutron scattering length of atom, *i*, respectively.

The Fourier transform of the scattering density gradient is given by:

$$\phi(Q) = \frac{1}{\rho_s - \rho_a} \int_{-\infty}^{\infty} \frac{\partial \rho(z)}{\partial z} \exp(iQz)\, dz \qquad (2.18)$$

where ρ_a is the scattering length density in air, z is the distance perpendicular to the surface and $Q = \frac{4\pi}{\lambda}(n_f^2 - 1 + \sin^2\theta)^{1/2}$ when $\theta > \cos^{-1} n_f$, or $Q = 0$ otherwise.

The experimentally obtained neutron reflectivity curve is analyzed by developing a model and finding the optimal model parameters that best describe the experimental data. The model contains a series of layers of different scattering densities and thicknesses along the normal distance from the surface. The thickness of various layers, which can be detected by this technique, ranges between 10 Å and 5000 Å from the surface. Neutron reflectometry can be employed to measure the structure of thin films; therefore, this technique can be applied to investigate surface or interfacial phenomena, for example, particle aggregation, polymer and surfactant adsorption, and structure of thin films or biological membranes.

2.2.2 Atomic Force Microscopy

In AFM, a colloidal particle of interest attached to a tipless silicon-nitride AFM cantilever using micromanipulators and epoxy glue moves upward/downward on a surface presumed to be perpendicular to the surface (Chin et al. 2002). The interaction force between the particle and the surface during the movement is inferred from the recorded deflection of the cantilever using a laser beam and a photodetector. The laser beam which aims at the backside of the cantilever is reflected to the photodetector. The relative position of the laser beam in the photodetector divided into four segments is determined from an output voltage of each respective photodetector segment. The

recorded deflection of the cantilever is converted into the interaction force after multiplication with the spring constant of the cantilever by Hooke's law:

$$F = k_{cantilever} \Delta z \tag{2.19}$$

where $k_{cantilever}$ corresponds to the spring constant of the cantilever and Δz is the measured deflection of the probe. The spring constant is a function of the properties of the material and the geometric characteristics of the probe. The spring constant can be calculated theoretically, but it can be also experimentally measured. The measuring procedure involves capturing the cantilever's mechanical response to thermal noise. The motion of the probe in response to thermal agitations includes the Brownian motion of the molecules of the encompassing medium such as air or water. The frequency spectrum of the cantilever response is extracted from fluctuations of the cantilever as a function of time. Assuming a single degree of freedom of the cantilever and using the energy equi-partition theorem, a Lorentzian line shape is fitted to the obtained frequency spectrum, which enables an estimate of the spring constant of the probe.

Two sets of data points are recorded during the two-way movements of the particle probe: approaching and retracting. Figure 2.4 shows a schematic of the data plot obtained from AFM force measurements.

While maximum deflection in probe retracting movement is simply converted into the adhesion force (often called 'pulling-off' force) by Hooke's law using the spring constant, the data plot showing the change of the deflection of the cantilever with the

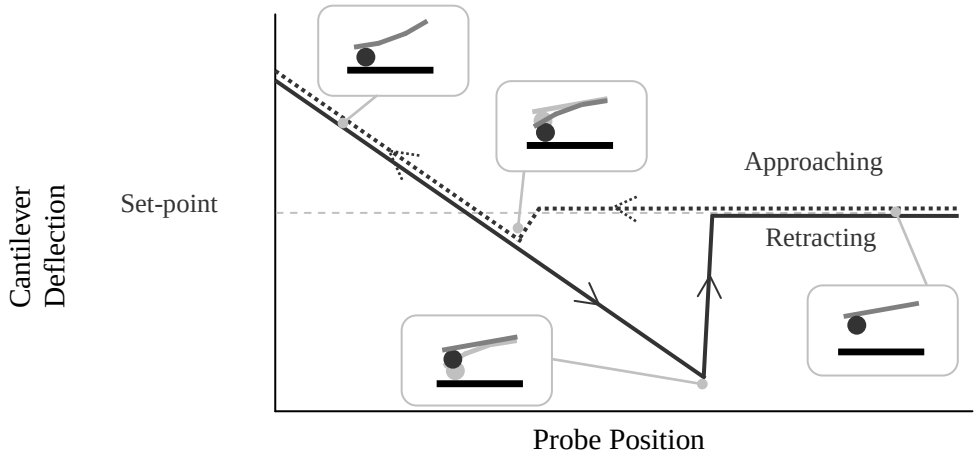

Figure 2.4 Schematic representation of the curve of tip deflection vs. probe position.

vertical position of the cantilever during the approach of the probe toward the surface is converted into the force-separation distance curve as shown in Figure 2.5. The force is calculated as the product of the deflection and the spring constant of the cantilever probe and the separation distance is calculated from the summation of the position and the deflection of the cantilever.

Figure 2.5 (a) and (c) represent an attractive and repulsive inter-particle force and the force-distance curve in Figure 2.5 (b) depicts neither attractive nor repulsive force between the particle and the surface. If there is a repulsive force as strong as an attractive force between two objects, the net force is zero and the force curve will be obtained as in Figure 2.5 (b).

The AFM provides not only force data between the tip and the surface, but also height information of the surfaces using a small sharp tip traveling along the surface of the substrate. In addition, AFM can be combined with other technologies such as scanning surface potential microscopy (SSPM) to measure the surface potential or surface charge density of the substrate. The working mechanism of SSPM that is based on an AFM setup will be introduced in the following section (Section 2.2.3).

2.2.3 Scanning Surface Potential Microscopy

Combination of the two techniques – AFM and scanning surface potential microscopy (SSPM) – provides surface potential information of the substrate. SSPM has been used to investigate electrical or electro-mechanical phenomena at the nanoscale (Kalinin and Gruverman 2007). The tapping-mode AFM technique precedes SSPM potential measurements to provide the surface topography and the corresponding electrostatic potential. The surface morphology of a substrate is obtained by AFM in a

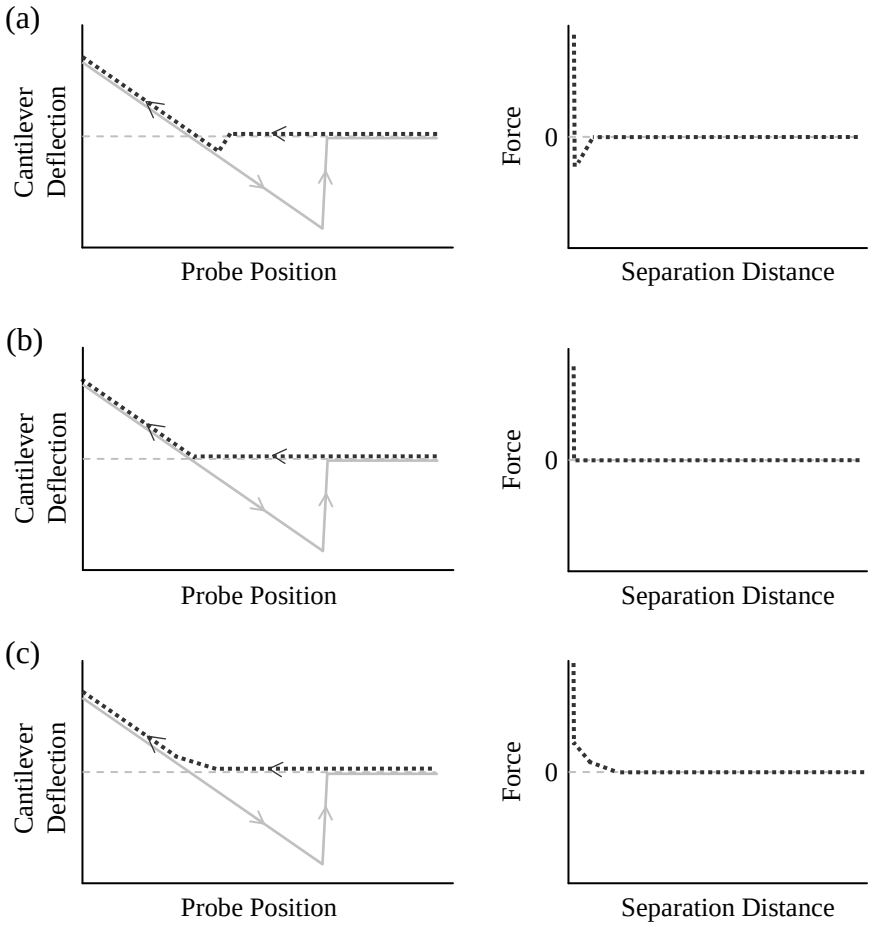

Figure 2.5 Force-distance curves converted from the curves of tip deflection vs. probe position.

tapping-mode using a sharp tip traveling over the substrate. Immediately, following the SSPM measurement, the tip moves based on the height data recorded by AFM. Figure 2.6 shows a schematic of a particle on a conductive substrate in the SSPM instrument in which a tip is moving on the surface.

As depicted in Figure 2.6 (a), the tip scans along the recorded topographical line in the AFM image at a constant height (called a set height) away from the surface. The set height – distance between the tip and the scanning surface – is selected to minimize other short-range forces, such as the van der Waals force. At the second scan, the local electrostatic potential resulting from the electrostatic force between the AFM tip and the sample substrate is recorded and the potential data are plotted in the SSPM potential profile, as shown in Figure 2.6 (b).

The obtained surface potential profile versus distance from the planar surface is used to calculate the surface charge density. The slope of the potential ($\frac{\partial \psi}{\partial z}$) is converted into the surface charge density using the equation: $\frac{\partial \psi}{\partial z} = \frac{\sigma}{2\varepsilon_0}$, where σ is the surface charge density and ε_0 is the vacuum permittivity (Israelachvili 1998). Although this equation is applicable to a planar surface in the absence of any other objects interacting with the surface with respect to the electrical potential, the interacting object (AFM tip in the SSPM measurement system) is ignored in this study in order to obtain an approximate estimation of the surface charge density of the substrate. With the assumption that the potential distribution between the surface and the tip is linear as shown in Figure 2.6 (c), the slope of the potential can be obtained by dividing the potential difference between the two objects by the set height. Because the potential of the tip can be considered the same

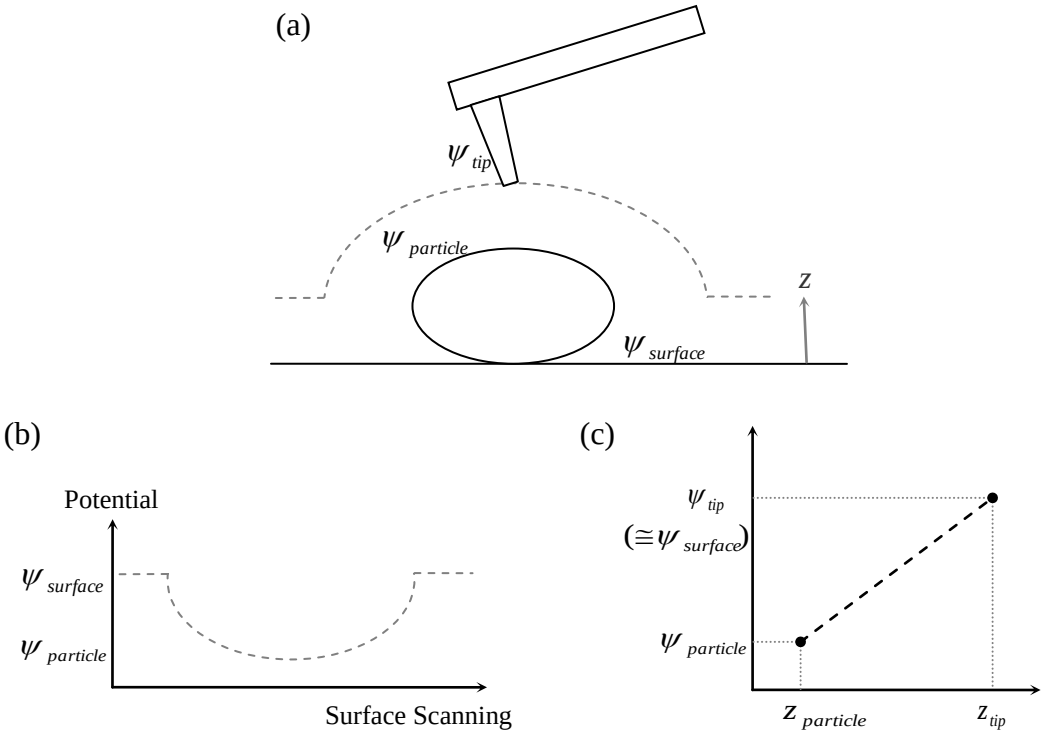

Figure 2.6 Scanning surface potential microscopy (SSPM) measurement of a particle on a conductive substrate and the obtained surface potential profile versus distance to calculate the surface charge density.

as the potential of the background gold surface during SSPM measurements (Jacobs et al. 1998), the potential of the AFM tip (ψ_{tip}) is replaced by the measured potential of the conductive substrate ($\psi_{substrate}$) in the calculations. Therefore, the electrostatic potential data are converted into the surface charge density of the substrate using the equation:

$$\frac{\psi_{substrate} - \psi_{tip}}{z_{substrate} - z_{tip}} = \frac{\sigma_{substrate}}{2\varepsilon_0}.$$

Consequently, theoretical calculations of particle-surface interactions are compared with the experimental measurements of interaction forces between a particle and a surface or the observation of distribution of colloidal particles. This study is helpful in understanding the fundamental mechanisms behind interfacial processes occurring in atmospheric and aquatic environments.

CHAPTER 3

ADHESION OF SPORES OF BACILLUS THURINGIENSIS ON A PLANAR SURFACE

In this chapter, the fundamental mechanisms of the adhesion of colloidal particles on surfaces in atmospheric environments were studied via a combination of experimental and theoretical studies. Spores of *Bacillus thuringiensis* were chosen as a model particle system. The *Bacillus thuringiensis* spores simulate natural or engineered environmental contaminants, such as *Bacillus anthracis* spores.

The objective of this study is to provide a better understanding of how strongly colloidal particles and spores adhere on environmental surfaces. A mathematical model describing the adhesion force between a particle and a planar surface was developed, and the force consisted of van der Waals, capillary, and electrostatic force components. Because an electrically conductive material, such as gold, was used as a substrate surface material, the electrostatic force could be neglected in this part of the study. Model calculations were compared to experimental measurements of the adhesion force obtained via atomic force microscopy to determine the validity of the model. Consequently, the model can be used to predict the adhesion force of colloidal particles and spores onto electrically conductive environmental surfaces. This information may be used to devise methods for the removal of environmental contaminants from natural or engineered surfaces.

3.1 Introduction

Microorganisms, especially bacteria, exist everywhere, and their importance in environmental processes and human activities is well recognized (Madigan et al. 2002).

In nature, bacterial cells live as a microbial community and form biofilms on surfaces. Bacteria in a biofilm interact with other cells as well as with heterogeneous surfaces. Bacterial interactions play a key role in pathology and food science (Ubbink and Schar-Zammaretti 2005). The fact that a bacterial biofilm can be a source of medical implant infections, for example, has been discussed (Costerton et al. 1999; Emerson and Camesano 2004; Waar et al. 2005). Surface adhesion of bacteria is relevant to biological attacks as surfaces become contaminated with the bacterial agent used. Therefore, bacterial interaction forces are important in understanding how bacteria adhere to such common surfaces as metal, glass, or construction materials and how bacteria adhered to these surfaces can be detached. The microbial adhesion force between bacteria and a surface has been studied in either liquid (Ong et al. 1999; Vadillo-Rodriguez and Logan 2006; de Kerchove et al. 2007; Sheng et al. 2007) or atmospheric environments (Thio and Meredith 2008) for several species such as *Escherichia coli* and Pseudomonas.

The adhesion force between a particle and a planar surface in an atmospheric environment has been considered to consist mainly of capillary force (Cross and Picknett 1963; Orr et al. 1975) as the dominating interaction component; however, other force components, such as van der Waals and electrostatic forces, are added for a complete calculation of the total adhesion force (Xiao and Qian 2000; Ouyang et al. 2001).

Capillary forces arise due to water condensation between a particle and a surface. Water vapor in the atmosphere condenses onto the surface to form a water film, and when the particle is in contact with the surface, a water meniscus is formed between the two objects. This geometry leads to the adhesion force due to the surface tension pressure differences. Surface tension arises along the boundary line where condensed water meets the particle surface. Pressure difference, which is a characteristic of the curvature of the water surface, exists between the interior of the condensed water and the surrounding atmosphere. The van der Waals or dispersion force arises between the transient dipoles or quadrupoles in molecules and is calculated by use of the Hamaker constant, a property of

the combination of particle material, surface material, and the medium in between. The van der Waals force is calculated with consideration of two media: (i) surrounding atmosphere and (ii) condensed water.

The electrostatic interaction force between two objects may be calculated through Coulomb's law by use of the charges of interacting objects, the dielectric constant of the medium in between, and the separation distance.

Spores of microbial agents, which are living forms of spore forming bacteria during their life cycle, have previously been studied (Bowen et al. 2000; Prier et al. 2001; Faille et al. 2002). Spores have minimal water content to enhance their resistance to harsh environments, such as dryness and low or high temperature. They have an outer layer (coat) to serve as a barrier against external conditions and to support their structure. While most of the outer membrane of active cells of bacteria is a single-layered or multilayered cell wall consisting of polymer layers of peptidoglycan connected by amino acid bridges or lipopolysaccharide layers, spores have a coat as the outer membrane composed of layers of spore-specific proteins. Spores of the *Bacillus cereus* group, including *Bacillus anthracis* and *Bacillus thuringiensis*, have an additional filmy outer layer (Faille et al. 2002; Madigan et al. 2002). This most outer membrane, namely the exosporium, which covers the spore coat, consists of protein, aminopolysaccharides and neutral polysaccharides, and lipids (Gerhardt et al. 1976; Redmond et al. 2004). The difference between membrane components of bacterial cells and spores is expected to lead to different behavior in terms of adhesion onto a surface.

Spores, like bacteria in their active form, can be contaminants and health hazards. This study is focused on the adhesion of spores on surfaces through combining spore characterization, modeling of surface interactions, and surface force measurements. Spores of *Bacillus thuringiensis* (*Bt*) have been studied as a simulant of *Bacillus anthracis*, which is potentially dangerous to human health. There have been studies (Prier et al. 2001; Thio et al. 2009) of the adhesion force between a biological particle and a

surface in atmospheric conditions based on various experimental methods, including atomic force microscopy (AFM). The adhesion force was quantitatively determined by use of modified AFM probes with pollen particles (Thio et al. 2009); however, the components of the total adhesion force have not been investigated theoretically. Therefore, the aim of this study is to measure the adhesion force between a *Bt* spore and a planar surface, develop a validated model for the prediction of the adhesion force, and identify the mechanisms and all the force components. By comparison between the measurements and model calculations, the model will be verified and the relative contributions of the components of the total adhesion force will be evaluated for different relative humidity levels.

3.2 Experimental Methods

3.2.1 Materials

Spores of *Bt* have been purchased from Raven Laboratories (Omaha, NE) and also produced at Oak Ridge National Laboratory by the following procedure: *Bt* microorganisms were incubated in a 1:10 nutrient broth solution and grown in the solution for 2-4 days. After snap-freezing in liquid nitrogen and centrifugation, spores in the shape of pellets were obtained. The formation of spores was verified under an optical microscope. Both purchased and laboratory-produced spore suspensions were dried on a substrate for measurements under room conditions. A gold-coated silica substrate was used for topographical measurements of spores by AFM. Filter paper (Schleicher & Schuell, 470) was also used as a substrate in order to obtain dried spores that could be attached onto tipless AFM cantilevers for adhesion force measurements. A *Bt* spore or a spherical silica particle of predetermined size was attached onto a tipless silicon-nitride AFM cantilever by use of micromanipulators and epoxy glue. This method had been

employed in our previous work (Chin et al. 2002) to attach silica particles onto tipless AFM cantilevers. For better reproducibility, AFM probes with a silica particle or a *Bt* spore used in this study were prepared by Novascan Technologies (Ames, IA).

The adhesion force between a spore or a particle and a substrate was measured by MultiMode AFM (Veeco Instruments, Plainview, NY). The adhesion force is measured between the AFM probe and a model planar surface as the retraction force normal to the surface. During force measurements, the cantilever with the particle or spore facing the surface moves toward and away from the surface. While the cantilever is approaching the substrate until the tip (silica particle or spore attached onto the cantilever) is in contact with the substrate and retracting away from the substrate, the deflection of the cantilever, which is a result of the interaction between the particle and the substrate, is recorded. The adhesion force is calculated from the maximum deflection occurring during retraction multiplied by the spring constant of the cantilever. The spring constant was directly measured in our laboratory by an AFM procedure. For force measurements via AFM, a gold-coated substrate was used. The silica surface was soaked into sulfuric acid overnight, then rinsed with deionized water, and dried with nitrogen, while the gold surface was rinsed with acetone or ethanol and with deionized water and then dried with nitrogen gas. Because the theory predicts that adhesion force is a function of relative humidity, the adhesion force was measured at a wide range of relative humidity values. A glass cylinder around the head of the AFM was used as a humidity-control chamber, and the humidity was adjusted by the flow rates of saturated and dry air gas.

3.2.2 Spore Characterization: Size and Shape of a *Bt* Spore

Imaging of *Bt* spores was conducted prior to adhesion force measurements via AFM, scanning electron microscopy (SEM), and scanning/transmission electron microscopy (STEM). AFM imaging was performed in contact mode. As shown in Figure

3.1, the spore surface has considerable roughness, an observation that was also reported in the literature (Chada et al. 2003; Giorno et al. 2007). Images of *Bt* spores have also been obtained by STEM (Hitachi-2000) and SEM in the Center for Nanophase Materials Sciences at Oak Ridge National Laboratory. From STEM images, it was found that there are objects of two shapes, a rod-shaped object (approximately 1.3 μm long and 0.8 μm wide) and a rhombus-shaped object of various sizes. The former is the spore and the latter is a parasporal crystal protein made by the microorganisms (Gerhardt et al. 1976). These two types of objects could also be identified in SEM images, but a more detailed structure was observed on the spore surface. In SEM images, ridge structures are shown on the surface of the spores, and the exosporium-assumed objects (i.e., the material connected to the spores and spread onto the surface) are shown in the images. Variations in the spore shape or roughness are also observed in the images. There are mainly spherical or rod-shaped spores but also spores with rough surface, which indicate variations in the shape and roughness of the spores or variations in their water content. A combination of AFM and scanning surface potential microscopy was employed to measure the surface potential of the spores. The electrostatic potential of the spore surface was relatively wide-ranging, from -330 to -850 mV at different relative humidity levels. This relatively high surface charge of *Bt* spores helps the adhesion of spores onto positively charged surfaces.

3.3 Theoretical Calculation of the Adhesion Force in Atmospheric Systems

Mathematical models for the adhesion force between a spherical particle and a planar surface in atmospheric systems have been reported (Cross and Picknett 1963; Sedin and Rowlen 2000; Butt et al. 2006; Farshchi-Tabrizi et al. 2006). Previous studies were focused mainly on the capillary force (Cross and Picknett 1963), but other studies

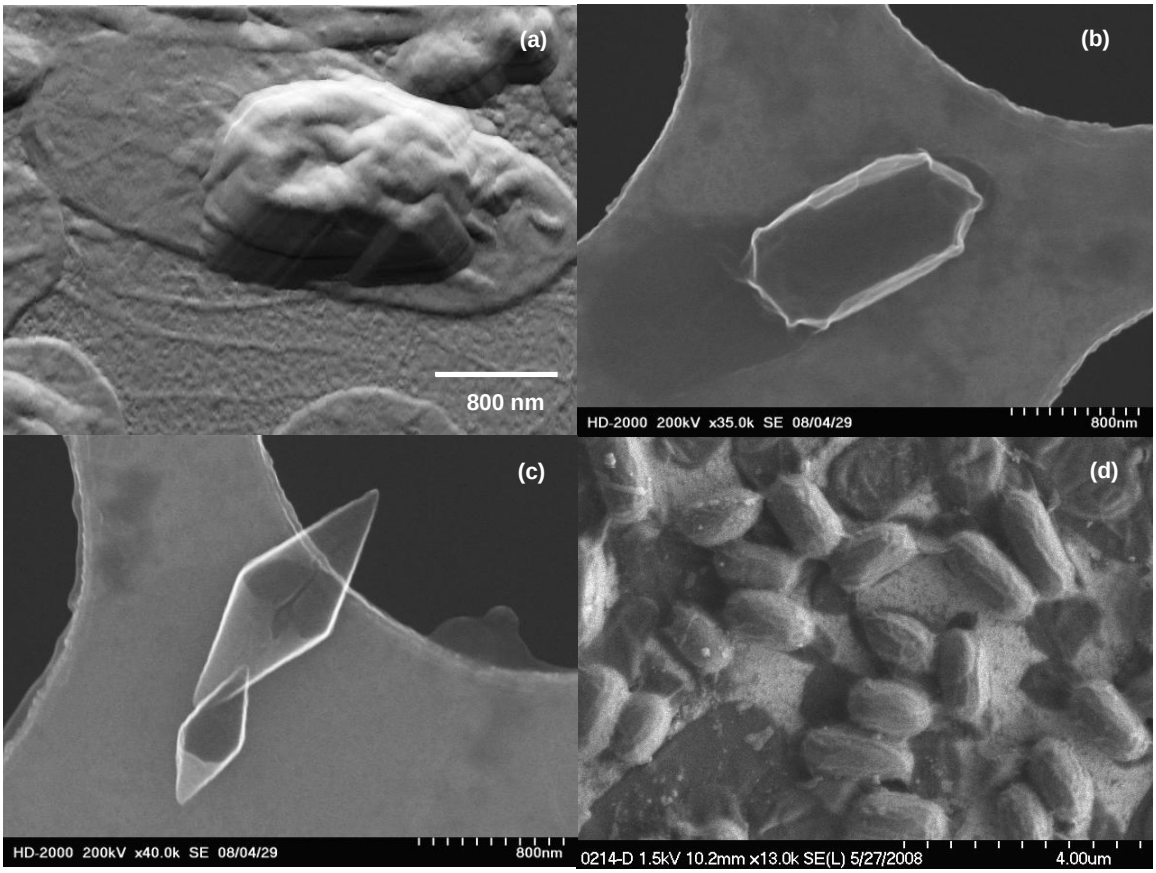

Figure 3.1 Images of *Bt* spores and protein crystals obtained by AFM, STEM, and SEM. (a) spore images by AFM, (b) spore images by STEM, (c) protein crystal images by STEM, and (d) spores and protein crystals in SEM images.

investigated the role of van der Waals and electrostatic forces in the determination of the total adhesion force (Ouyang et al. 2001). In the modeling of adhesion force in this study, the three main components that were considered are van der Waals, capillary, and electrostatic forces. These forces are functions of the electrostatic potential, shape, size, and roughness of particles as well as relative humidity. However, because the gold-coated substrate was electrically conductive, the assumption was made that the surface charge dissipated, so that the electrostatic force could be neglected in the calculations. Thus, the adhesion force is calculated as the sum of capillary and van der Waals forces. In addition, even though the spore is confirmed to be rod-shaped, the object in the model was assumed to be of spherical shape with a smooth surface, so that the roughness of the particle is initially ignored. For capillary and van der Waals forces, the following expressions were used, respectively (Orr et al. 1975; Xiao and Qian 2000):

$$F_{vdw} = -\frac{\left(A_H^{water} - A_H^{air}\right)}{6R}\frac{(a/R)+1-2\cos\phi}{(a/R)+1-\cos\phi} + \frac{A_H^{water}}{6R}\frac{(a/R)-1}{(a/R)^2} - \frac{A_H^{air}}{6R}\frac{1}{(a/R)+1} \tag{3.1}$$

$$F_{capillary} = F_{surface\_tension} + F_{pressure\_difference}$$
$$= \pi\gamma R\sin^2\phi\left[\frac{\sin(\phi+\theta_1)}{\sin\phi} + \frac{\cos(\phi+\theta_1)+\cos\theta_2}{(a/R)+1-\cos\phi}\right] \tag{3.2}$$

There are several parameters in these equations, including the angle of the meniscus of water between the two objects (ϕ), contact angles (θ_1 for particle-air-water, θ_2 for flat surface-air-water), particle radius (R), surface tension of water (γ), intermolecular spacing (a, 0.275 nm), and the Hamaker constants (A_H). Except for the radius of the particle and contact angles, which are experimentally measured, the values of such variables as surface tension of water, the Hamaker constant, and intermolecular spacing were obtained from the literature (Orr et al. 1975; Xiao and Qian 2000; Brown and Jaffe 2006) (see Table 3.1). The angle for meniscus (ϕ) can be calculated by using

the Kelvin equation (equation 3.3) as a function of the relative humidity (P/P_0) with additional variables: temperature (T) and molar volume of water (v^0). R_{gas} is the gas constant.

$$\frac{R_{gas}\,T\ln(P/P_0)}{\gamma v^0} = -\frac{\cos(\phi+\theta_1)+\cos\theta_2}{R(1-\cos\phi)} + \frac{\sin(\phi+\theta_1)}{R\sin\phi} \tag{3.3}$$

In the Kelvin equation, the principal radii were geometrically expressed with the "circle approximation" that describes the shape of the meniscus as a circular curve (Orr et al. 1975). The contact angles of gold (62°) and silica (79°) were measured in this study by a contact angle meter (CAM Plus). The meniscus angle, ϕ, in equation 3.3 was calculated as a function of the relative humidity. As shown in Figure 3.2, the meniscus is not formed below a certain relative humidity value (approximately 30% in the figure). Above the critical relative humidity level, the meniscus angle increases as relative humidity increases. Therefore, the meniscus force is zero below the critical humidity and increases above the critical relative humidity value. The van der Waals force is constant for low humidity conditions, where there is no meniscus formed, and decreases as the humidity level increases. As a sum of the forces, the total adhesion force is composed mainly of the van der Waals force at low relative humidity values (below the critical point), while the main component of the total force is rapidly shifted to the capillary force contribution beyond the critical point. The adhesion force between two hydrophilic surfaces (contact angle with water <5°) has recently been investigated (Asay et al. 2009), and a good comparison between experimental and modeling results, considering the structure of the adsorbed water layer on the surface, was reported. The surfaces used in the present work, however, are hydrophobic with contact angles higher than 60°. The thickness and structure of the water layer adsorbed at the interface between air and a

Table 3.1 Parameters used in model calculations for a 1-μm silica particle or a spore and a gold planar surface.

k	Gas constant	8.314472 J/K·mol
T	Temperature	298 K
γ	Water surface tension	0.07197 kg/sec^2
v^o	Molar volume of water	1.8E-5 m^3/mol
θ	Contact angles	62° (silica), 79° (gold), 80° (spore)
R	Radius of the particle	500 nm
A_H	Hamaker constant	1.29E-19 J (air), 1.68E-20 J (water) for silica-gold surface 1.24E-19 J (air), 1.38E-20 J (water) for spore-gold surface*
a	Intermolecular spacing	0.275 nm

* The Hamaker constant for the spore is applied from the value for the general bacteria form literature.

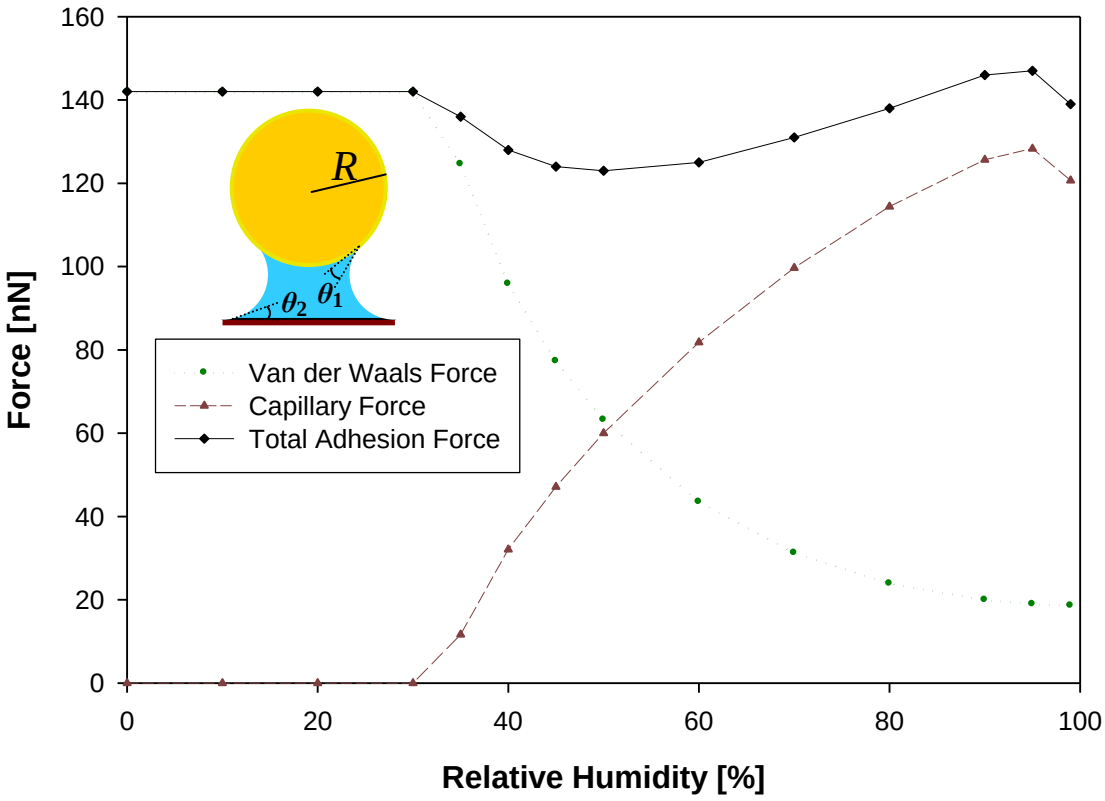

Figure 3.2 Model calculations for the van der Waals, capillary, and total adhesion force for a 1-µm silica particle and a planar gold surface.

hydrophobic solid surface still needs to be investigated. In order to determine the influence of various parameters on the adhesion force for the system of the present work, three different contact angles and two particle sizes were independently considered in the model. It is shown in Figure 3.3 that as the contact angle (θ_1) increases, the critical point increases too. This behavior means that a particle made by a material of high contact angle will allow formation of the meniscus between the particle and the planar surface at higher relative humidity values. Similar behavior was observed for the other contact angle, θ_2. While the contact angles of the materials determine the critical relative humidity value for formation of the water meniscus, the particle size determines the magnitude of the adhesion force. A larger particle size was predicted to have a stronger adhesion force.

3.4 Results and Discussion

3.4.1 Adhesion Force Measurement of a Silica Particle on Surfaces by AFM

To verify model predictions, adhesion force measurements between a silica particle and a gold planar surface have been obtained by use of 1-μm silica AFM probes at different humidity levels (Figure 3.4). The spring constant of each probe was measured by using the thermal tune function of the AFM. A significant difference was found between the spring constant of the cantilever reported by the manufacturer (0.12 N/m) before attachment of the particle and that measured (0.297 N/m) for the 1-μm silica probe. The spring constant is a critical parameter because the adhesion force is directly proportional to the spring constant; therefore, it is important to measure the exact value of the spring constant after modification of the cantilever probe.

To verify formation of the meniscus between the particle and the planar surface, various surface delay times were selected for the measurement before retraction of the

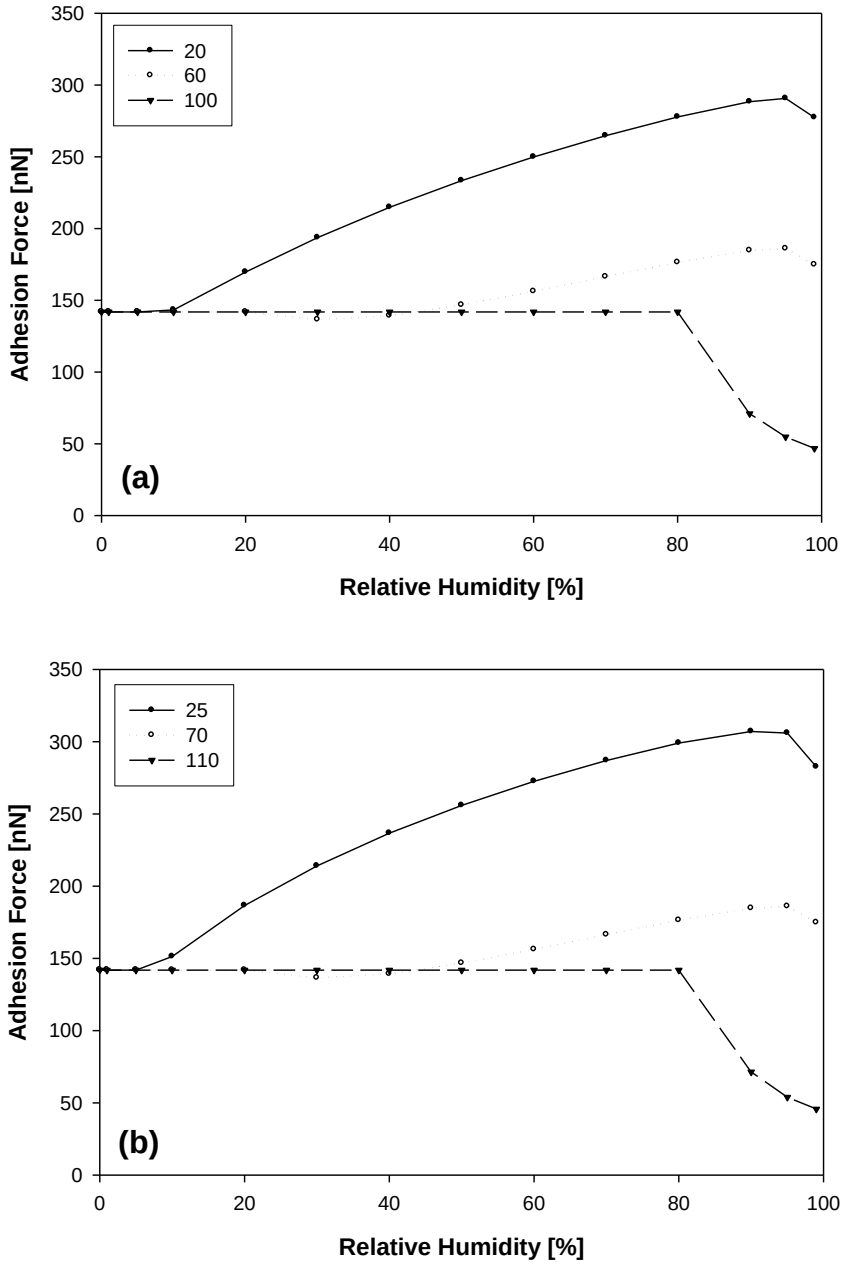

Figure 3.3 Influence of the contact angles on the calculated total adhesion force: (a) effect of contact angle θ_1 for the sphere-water-air and (b) effect of contact angle θ_2 for the planar surface-water-air.

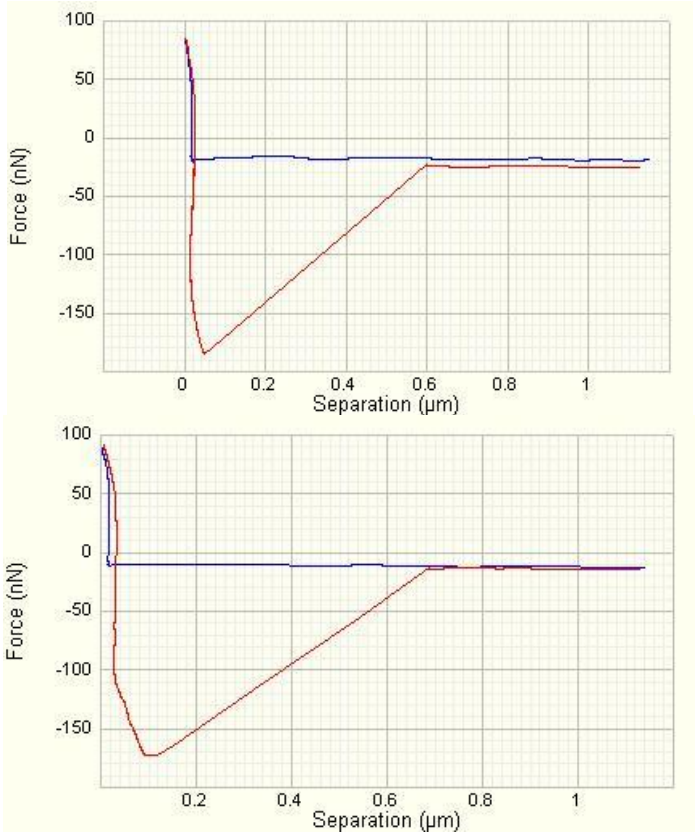

Figure 3.4 Representative force-distance curve for a 1µm silica particle onto a gold surface at relative humidity 35 % (upper) and for a *Bt* spore onto the gold surface at relative humidity 48 % (lower).

cantilever from the surface was initiated. During the delay time, the particle stayed in contact with the planar surface, allowing water condensation to occur between the particle and the surface. By use of the AFM software, the delay time could change up to a maximum of 200 s. The adhesion force was measured with delays of 0, 50, 100, 150, and 200 s at room temperature (22 ℃). It was found that the adhesion force increased slightly as the delay time increased. Delay of 0 s did not allow enough time for the meniscus to be formed, and as the time delay increased, the meniscus formed, approaching equilibrium. All adhesion force measurements were performed with 200 s of delay time, which is the maximum delay time allowed by the instrument. The meniscus was removed before the next force measurement by applying a low-humidity condition with less than 5% relative humidity for at least 15 min between consecutive measurements. Measurements obtained with this procedure were very reproducible. The adhesion force was measured several times for the same conditions and the average value was recorded. The maximum variability of the measurements under the same conditions was within 9% of the measured force.

Force measurements between a 1-μm silica particle and a planar gold surface are plotted in Figure 3.5. The reproducibility was confirmed and the trend and magnification of the experimental data were comparable to modeling results in a relative humidity range between 0% and 60%. The adhesion force could not be obtained by AFM at relative humidity values above 60% because the maximum deflection of the cantilever in higher relative humidity environment could not be physically achieved due to the cantilever retraction limit (～2.5 μm) of the instrument.

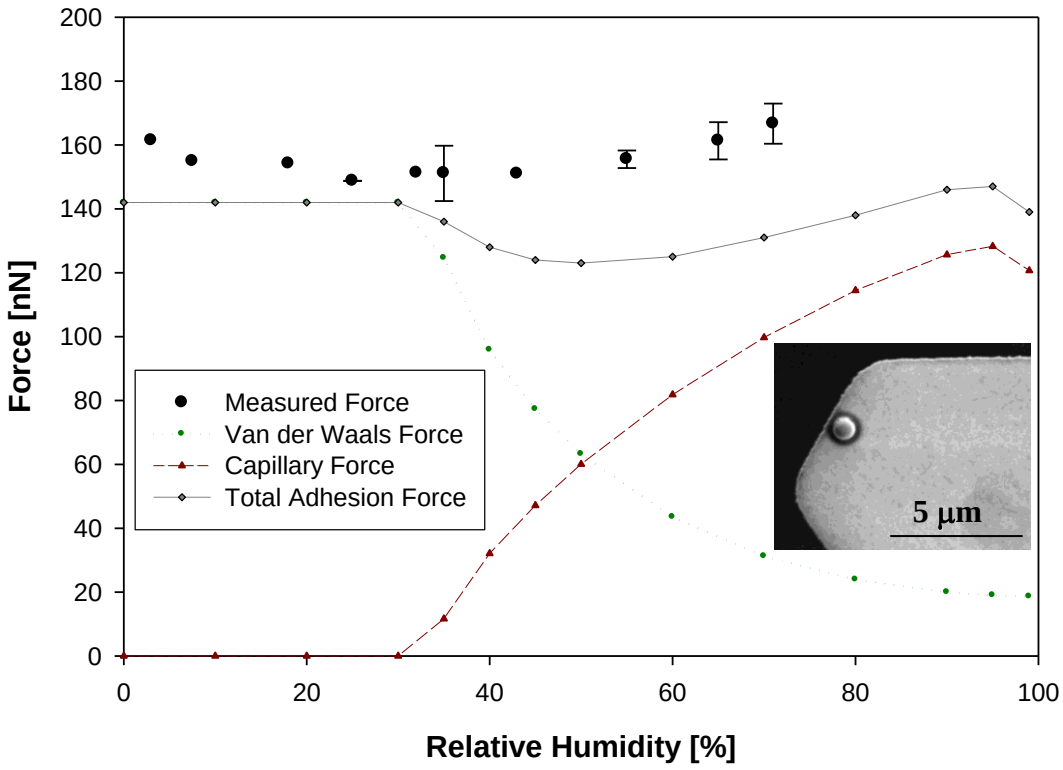

Figure 3.5 Adhesion force measurements by AFM between a 1-µm silica particle (inset) and a gold planar surface under different relative humidity values.

3.4.2 Adhesion Force Measurement of a *Bt* Spore on Surfaces by AFM

Bt spore probes have been produced similarly to silica probes by attaching a spore onto a tipless cantilever (see Figure 3.6). As shown in images, *Bt* spores are not spherical but ellipsoid or rod-shaped. For comparison of the measurements with model calculations, a spherical particle with the same planar surface was assumed in the model, with parameters for the biological material and the gold surface. The particle radius in the model was determined at 498 nm for a sphere of the same volume as an average-size *Bt* spore. The spore was attached to the cantilever along the long axis of the ellipsoid (rod), so the long axis of the ellipsoid (rod) is parallel to the planar surface when the spore is resting on the surface during measurements. Therefore, the area of contact between the two objects is bigger for the spore than for the spherical particle. Similarly, the center of the spore mass is closer to the planar surface than the center of mass of a spherical particle. The bigger contact area between a spore and a planar surface forms a meniscus of larger perimeter and leads to a stronger capillary force. Furthermore, the lower center of mass for the spore leads to a stronger van der Waals force compared to the equivalent spherical particle of the same mass or volume. Therefore, due to these geometrical effects, it was expected that the measured force would be larger than the force calculated for the spherical model particle. The measured adhesion forces between a *Bt* spore and a gold surface in Figure 3.6 show that the measured forces are on the average 20% larger than the calculated values. In addition, no significant change in the measured force was observed, while a change of the force is expected from model calculations. This can be explained by inaccuracies in the contact angle value of the spore. The contact angle value used here was taken from the literature for bacteria in general, not for the specific spores used here. As discussed in the previous section, the contact angle of the material determines the critical point of relative humidity at which the meniscus starts to form. Below the relative humidity critical point, the capillary force is zero and the van der

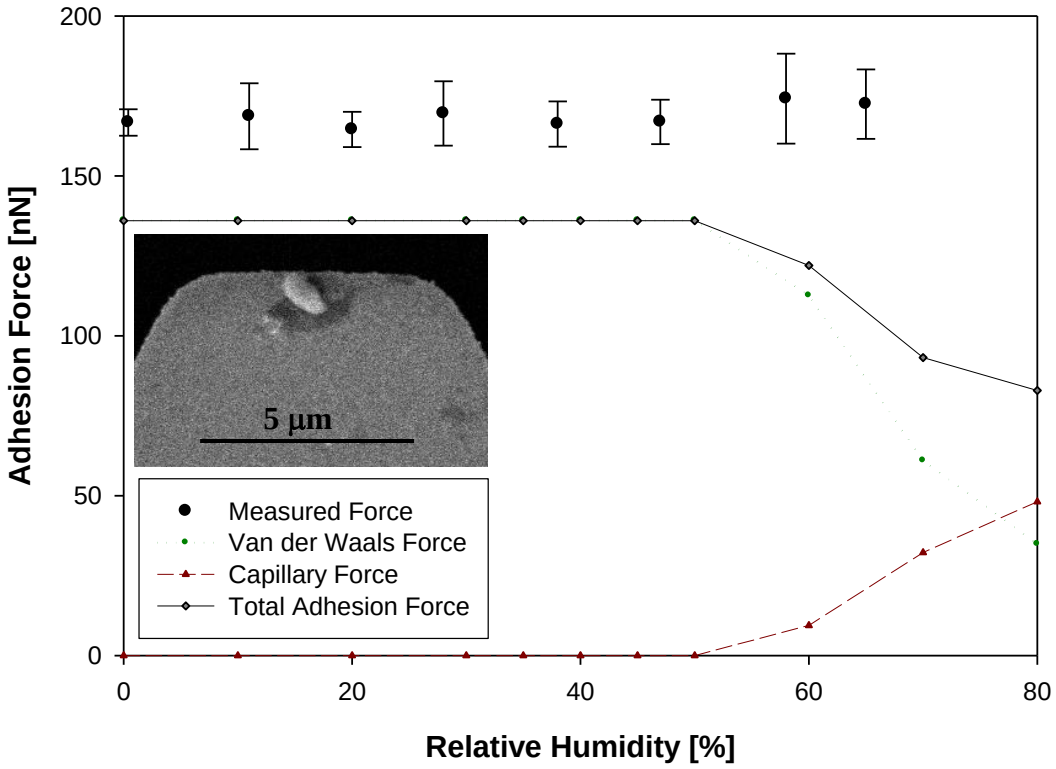

Figure 3.6 Comparison between (i) model calculations for the system of a spherical particle, with the same volume as that of a *Bt* spore, and a planar gold surface and (ii) adhesion force measurements between a *Bt* spore (inset) and a gold surface by AFM.

Waals force is constant. If it is assumed that the actual contact angle of the *Bt* spores is big enough to move the critical point to higher humidity levels (above 70% relative humidity), the constant value of the force measurements at relative humidity values up to 70% can be explained.

3.4.3 Model Modification

Consideration of the actual spore shape in the model was expected to lead to more accurate force calculations. The spherically assumed spore/planar surface system can be modified to account for the geometry of the actual geometrical system in the model by introducing the rod shape of a particle consisting of two hemispheres and one cylinder between the hemispheres. For the modified system, calculation of capillary and van der Waals force had to be modified as well.

If it is assumed that the height and principal radii of the meniscus for the spore/planar surface system are the same as those for the sphere/planar surface system, where the sphere has the same radius as that of the spore hemisphere, the equation used to calculate capillary force can be easily modified because the two components of capillary force are related to the geometrical characteristics of the meniscus. The force due to the pressure difference and the surface tension force are directly proportional to the area and the perimeter of the meniscus boundary, respectively. The van der Waals force can be also modified for the system of a rod-shaped particle and a planar surface. The force is calculated by addition of two elements: one for the two hemispheres and another representing the cylindrical part. The former is calculated as one complete sphere and the latter is described as an equivalent spherical particle having the volume of the cylinder. Two spheres are considered instead of a single sphere having the same volume as the whole rod particle to minimize the gap between the centers of mass of the rod-shaped particle and the spherical particle.

Results from the modified model are presented in Figure 3.7. When compared to the results of the equivalent-volume spherical particle shown in Figure 3.6, the magnitude of the total adhesion force is larger and a substantial increase of capillary force is obtained at high relative humidity values. The discrepancy between calculated and measured values of the adhesion force may be due to surface roughness of the spore surface. Even though it is known that surface roughness can make the capillary force smaller (Farshchi-Tabrizi et al. 2006), this study considered the spore to have a smooth surface; therefore, the roughness of the spore surface did not appear in the calculations.

If it is assumed that the actual contact angle of the spore is greater than the value used in this study and thus the critical point of relative humidity is higher than 70%, then the constant measured force can be explained. In that case, it can be concluded that when the electrostatic force is eliminated, the adhesion force of the *Bt* spore onto a surface is explained by the modified model for a particle and a planar surface system in which the total force consists of the capillary and van der Waals forces.

3.5 Summary

A mathematical model was developed to calculate the adhesion force between a spherical particle and a planar surface as a sum of the capillary force and the van der Waals force. The electrostatic interaction was neglected in the model for the experimental system of this work, which involves an electrically conductive material as the planar surface. The two-force mechanisms that were considered are functions of the relative humidity. The capillary force increases as the relative humidity value increases, whereas the van der Waals force decreases as the humidity increases.

Adhesion force measurements by AFM were conducted using a particle or spore modified AFM cantilever probe. The measured adhesion force between a silica particle and a gold surface was comparable to the model calculation, while there was some

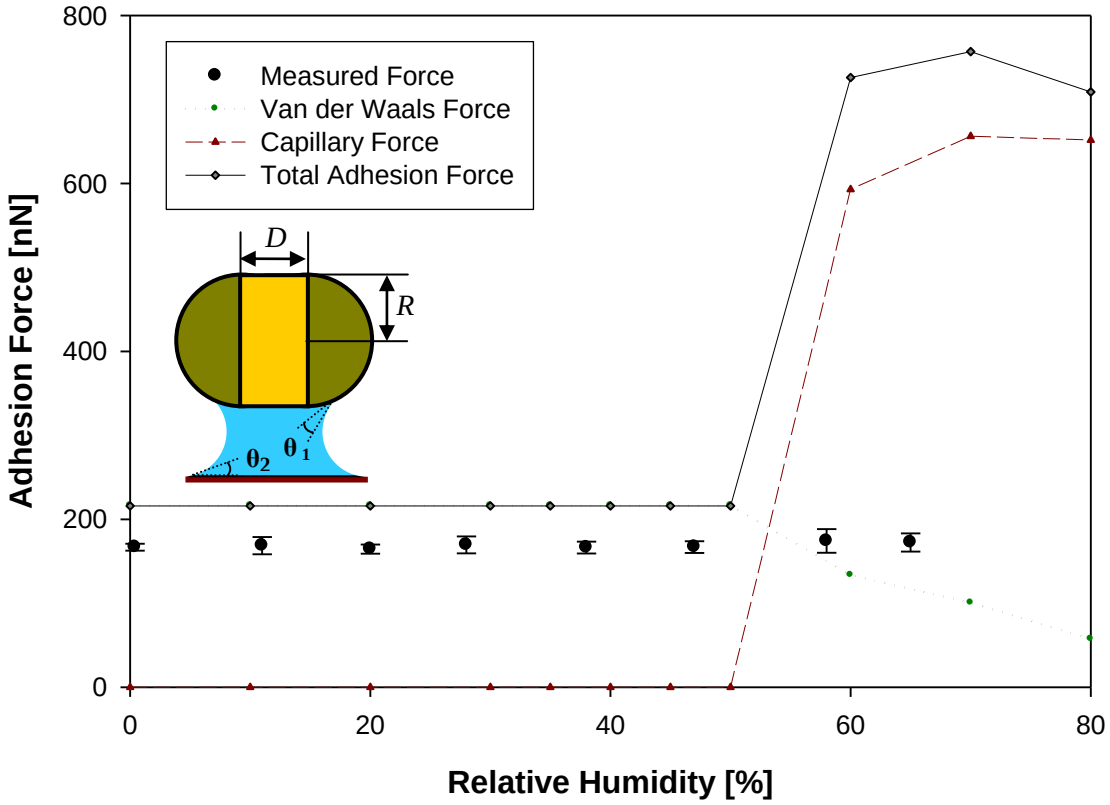

Figure 3.7 Comparison between (i) modified model calculations for the system of a rod-shape particle representing a *Bt* spore and a planar gold surface and (ii) measured adhesion force between a *Bt* spore and gold planar surface by AFM. The schematic shows a rod-shape particle of R=400 nm and D=500 nm representing a 0.8-µm wide and 1.3-µm long spore.

disagreement between the measured adhesion force for the *Bt* spore-gold surface system and the calculated value. In order to minimize the discrepancy, the model was modified using the actual shape and dimensions of the spores. The results of the modified model also showed some discrepancy with the measurements. The discrepancy may be a result of neglecting important parameters in the model, such as the surface roughness of the spore, which was observed in AFM, SEM, and STEM images.

The implications of this study are two-fold: (i) the mechanisms and parameters involved in spore adhesion onto environmental surfaces are identified, contributing to the understanding of the phenomenon, and (ii) the results may help us devise better means for the removal of spores and other biological particles from environmental surfaces.

CHAPTER 4

THE ROLE OF THE ELECTROSTATIC FORCE IN SPORE ADHESION

As shown in Chapter 3, the adhesion force between a spherical particle or a bacterial spore and a planar surface can be estimated as the sum of the capillary force and the van der Waals force. The electrostatic force was not included for the system of a charged particle and an electrically conductive surface. However, when measurements of the adhesion force were conducted for a system involving a non-conductive surface, such as mica, a significant discrepancy between model calculations and AFM measurements was observed. This discrepancy was assumed to be the result of an electrostatic force component that was neglected in the mathematical model.

In this chapter, the electrostatic force is introduced into the model as an additional component of the adhesion force. The Coulombic force can play a significant role in the interaction between two objects such as a highly charged particle (or spore) and a charged planar surface. Furthermore, another type of electrostatic force which is called 'image force' is introduced into the theoretical model for a charged particle and a conductive surface. Addition of the image force into the model can lead to a more accurate estimation of the adhesion force.

4.1 Introduction

The electrostatic force can be an important component in the adhesion force between a particle and a planar surface, especially in a system of small charged particles. The importance of the electrostatic force as a component of the adhesion force has been discussed for powder particles and other surfaces in previous studies (Feng and Hays

2003, Takeuchi 2006, Hays and Sheflin 2005). Even though the interaction of microorganisms with solid surfaces in aqueous environments may include forces additional to the electrostatic interaction (Abu-Lail and Camesano 2006), the electrostatic force is possibly a major component in spore adhesion on surfaces in atmospheric systems. A charged dielectric particle has an electrostatic interaction with either a conducting surface or a nonconductive surface. The electrostatic force can be calculated based on Coulomb's law using the surface charges of the particle and the planar surface. It has also been reported that the electrostatic force may be a major component for the microscale or nanoscale adhesion force in some cases (Ouyang et al. 2001, Kumar et al. 2008).

The evaluation of the adhesion force or its components for small contaminants, such as microorganisms or nanosized particles attached to natural or engineered surfaces, may be important in the decision-making process for the decontamination of environmental systems. The contaminant particles may be removed by physical, chemical, or electrical methods. Detachment of a particle by electrical means has been investigated in previous studies, especially when the contaminant particles have a significant amount of electrical charge and/or the surface material is electrically conductive, which means that an electrical potential can be applied (Feng and Hays 2000, Techaumnat, Kadonaga and Takuma 2009, Watano, Hamashita and Suzuki 2002).

Previously, we investigated the adhesion force between a *Bacillus thuringiensis* (*Bt*) spore and a gold planar surface using atomic force microscopy (AFM) measurements and calculations based on mechanistic modeling (Chung et al. 2010a). Even though microorganisms, and in particular spores, are known to attain electrostatic charge on their surface (Husmark and Ronner 1990), previous experiments were conducted using a *Bt* spore and a gold substrate at conditions for which the electrostatic force could be ignored as a component of the adhesion force. Theoretical and experimental results were comparable for a *Bt* spore and the gold surface system. However, measurements between

the *Bt* spore and a mica surface showed a significant deviation from calculated results, which is believed to be due to the electrostatic force.

The focus in this study is on the importance of electrostatic forces on the adhesion force under a variety of environmental conditions. Coulombic and image forces are introduced in the model to better explain the adhesion force measurements between a *Bt* spore and a mica planar surface and to minimize the difference between theoretical and experimental results for a *Bt* spore and a gold surface system.

4.2 Materials and Methods

Bt spores were purchased from Raven Labs (Omaha, Nebraska). Spore suspension drops were air-dried either on gold-coated silica to be imaged by AFM or on a filter paper from where spores were transferred to a tipless cantilever and fixed there by epoxy glue. Through this procedure, the tipless cantilever was modified into a *Bt* spore probe. Because the spring constant of the tipless cantilever reported by the manufacturer may not be accurate or may change significantly after the mounting of the *Bt* spore, the spring constant of the modified spore probe is measured using the function 'thermal tune' of the AFM. The method involves measurement of the cantilever's mechanical response to thermal agitations, originating from the Brownian motion of the molecules of the encompassing fluid (ambient air). While the tipless cantilever used was reported to have a spring constant of 0.12 N/m, the measured spring constant after mounting of the spore was between 0.25 and 0.3 N/m. The epoxy glue used in this study is commercially available, and the elastic modulus of the glue is high enough so that the epoxy-spore interaction can be ignored. For scanning surface potential microscopy (SSPM) measurements, drops of the spore suspension were placed on substrates and dried over 10 hours in a desiccator before put into the imaging chamber. The imaging chamber was then purged with ultrapure nitrogen to reach 0% humidity and continued to be purge for

four more hours. The humidity was brought up slowing to a desired level for imaging at a speed of ~ 10% per 30 minutes.

A combination of tapping-mode AFM and SSPM with modified Nanoscope IIIa (Veeco instrument, Plainview, NY) controller was used to investigate the surface topography and the corresponding local electrostatic potential of a sample, such as mica or *Bt* spores on gold substrate. Details of the procedure were previously described elsewhere (Lee et al. 2003). In brief, a surface topographical image with height data of 256 points in a line was first recorded by scanning in AFM tapping mode, using a metal-coated Si cantilever AFM probe, followed by 3-dimensional electrical potential mapping. The coating consisted of approximately 25-nm thick layers of chromium and platinum iridium on both sides of the cantilever. Potential mapping was performed by scanning along with the recorded topographical line at a set height of 50 nm from the sample surface using the same AFM probe in the scanning surface potential mapping mode. During the SSPM measurements, an AC voltage with adjustable DC offset was applied to the conducting AFM-tip ($V_{DC} + V_{AC}\cos\omega t$). Surface potential measurements with maximum sensitivity are achieved when the AC voltage applied to the tip has the resonance frequency of the cantilever and the first harmonic component ($\cos\omega t$) of the tip force becomes zero. The oscillation amplitude of the cantilever was zeroed by adjusting the external DC voltage until it matched the sample potential, so that the tip was at the same DC potential as the region of the sample surface underneath it.

Figure 4.1 shows an example of AFM and SSPM measurements for a *Bt* spore on a gold substrate. The measurement provides the topographical surface profile in the AFM mode (left) and surface potential profile in the SSPM mode (right) of the spore on the gold surface. Because the gold surface potential is equal to the metal-coated tip potential, the surface charge of the spore can be calculated by assuming a linear distribution of the potential between tip and spore. All experiments were repeated 4-6 times to ensure reproducibility. A set height of 50 nm was selected to minimize other short-range forces,

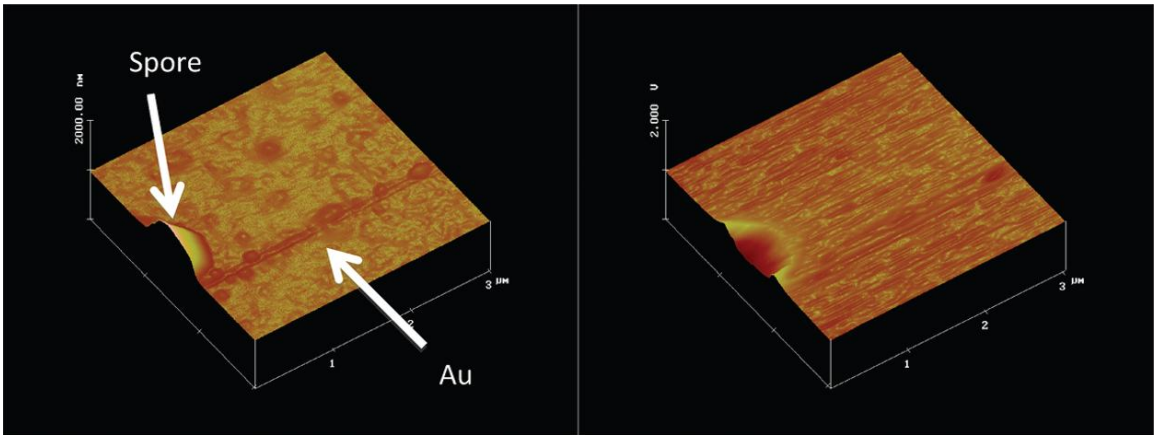

Figure 4.1 AFM (left) and SSPM (right) measurements of a *Bt* spore on gold (Au) surface. The tapping mode AFM imaging is employed and height data are recorded. Surface potential mapping by SSPM follows, providing the surface potential.

such as the van der Waals force. From the SSPM potential data of the sample, the surface charge densities can be calculated. Using the surface potential profile versus distance from the planar surface, the slope of the potential ($\frac{\partial \psi}{\partial z}$) can be converted into the surface charge density using the equation: $\frac{\partial \psi}{\partial z} = \frac{\sigma}{2\varepsilon_0}$, where σ is the surface charge density and ε_0 is the permittivity (Israelachvili 1998). This equation, however, is applicable to one planar surface whose surface charge density is σ, absent any other object interacting with the surface with respect to the electrical potential. In the SSPM measurement system, the tip is traveling above the surface at a distance of 50 nm. We can obtain an approximate estimation of the surface charge density of the substrate by dividing the potential difference between the two objects by the set height (50 nm). The underlying assumption is that the potential distribution between the surface and the tip is linear.

Bt spore probes were used in a multi-mode AFM (Veeco, Plainview, NY) using various substrates such as mica and gold to investigate the adhesion force between a spore and a planar substrate under different humidity levels. The cantilever of the spore probe is made of silicon nitride, which is not conductive. A glass cylindrical chamber was mounted around the head of the AFM for humidity control. Dry air provided by a pressurized cylinder (Airgas) was divided in two streams. One of the streams was passed through a column of water in the form of bubbles (formed by a bubble diffuser) to be humidified. The humidity in the AFM chamber was controlled by adjusting the flow rates of the dry and humidified air streams. A number of 512 data points were extracted from the force curve while the probe was retracting from the substrate. Retraction started after 200 seconds of delay to allow enough time for the formation of the meniscus and for the equilibrium state to be reached. The adhesion force was measured 5-10 times for the same conditions, and the average value was recorded.

4.3 Results

4.3.1 Surface Charge of the Spore and the Planar Surfaces

It is known that the surface structure and the size of the spores depend on the humidity level of the surrounding atmosphere (Driks 2003, Westphal et al. 2003, Plomp et al. 2005). Spore changes with humidity are a result of structure modification of the coat - the outer membrane of the spores. As the humidity is decreased, the degree of roughness on the coat surface of the spore increases and the size of the spore decreases. Not only the size but also the surface charge of the spores is expected to depend on the relative humidity. Thus, all the components of the adhesion force including the electrostatic, van der Waals, and capillary forces are functions of the relative humidity. Therefore, AFM imaging has been employed to quantify the size and morphology of spores, and SSPM measurements were conducted to provide the surface potential at various relative humidity levels, independently of the force measurements, using gold as a model substrate (20, 40, 60, and 80%).

The size variation of *Bt* spores is shown in Table 4.1 under a relative humidity ranging from 20 to 80%. The width values shown in Table 4.1 are averages over at least ten images at each humidity level that were measured along the short axis of the rod. The variations were negligible (within 1 nm) so only the averages are shown. Spore width increases with increasing relative humidity, as expected from the literature (Driks 2003). The measured increasing trend in this study, however, was insignificant; the width at 80% relative humidity increases by 1.8% compared to the value at 20% relative humidity. If it is assumed that the shape of the spore and the ratio of length to width do not change with relative humidity, the surface area will increase by only 3.6% from 20 to 80% relative humidity.

The potentials of the tip and the spore are theoretically required in order to calculate the surface charge as discussed in the preceding section; however, the properties

Table 4.1 AFM/SSPM measurements of *Bt* spores on gold (Au) substrate under different relative humidity levels.

Relative humidity [%]	*Bt* spore width [µm]	*Bt* spore potential [V]	AFM tip potential [V]	Mica potential [V]	AFM tip potential [V]
20	0.772	-0.439	0.43	-5.73	0.44
40	0.776	-0.409	0.43	-4.99	0.44
60	0.779	-0.373	0.43	-4.55	0.44
80	0.786	-0.354	0.42	-4.50	0.44

obtained from the SSPM measurements include the potentials of the background surface, which in the experimental setup is gold and the spore. In the literature about the SSPM working principle (Jacobs et al. 1998), it was found that the potential of the tip can be considered the same as the potential of the background gold surface. Therefore, the measured gold surface potentials were used to find the potential of the AFM tip interacting with the spore surface. From the potential values shown in Table 4.1, at 20% relative humidity, we have: $\frac{\partial \psi}{\partial z} = \frac{\psi_{substrate} - \psi_{tip}}{z} = -0.017 \ V/nm$ at a distance z =50 nm between the tip and the spore surface. The distance, *z*, or a set height in SSPM measurements was selected as 50 nm throughout the experiment and it is expected that a short-range force, such as the van der Waals force, is minimal at that distance. Therefore, the charge density of the *Bt* spore surface is calculated as: $\sigma = 2\varepsilon_0 \frac{\partial \psi}{\partial z} = 0.031 \, \mu C/cm^2$. The estimated surface charge decreases with increasing relative humidity. A 10% decrease was observed when the relative humidity was increased from 20% to 80% (Figure 4.2).

For various reasons, many natural or engineered materials have electric charge on their surface. For instance, the mica surface is charged due to its surface structure. Isomorphous substitution of atoms and functional groups on the surface cause the charge on the surface of mica. There are many studies reporting the surface charges of clay mineral particles such as mica at different conditions of pH or ionic strength in aqueous environments (Hartley, Larson and Scales 1997, Vane and Zang 1997), but an influence of the humidity on the surface charge in atmospheric environments has not been reported. A relationship between the surface charge and the relative humidity has not been established, thus, the surface charge of mica is estimated through SSPM measurements in this study using the same experimental procedure that was utilized for the determination of the surface charge density of the spore (i.e., measurements with a system of mica and

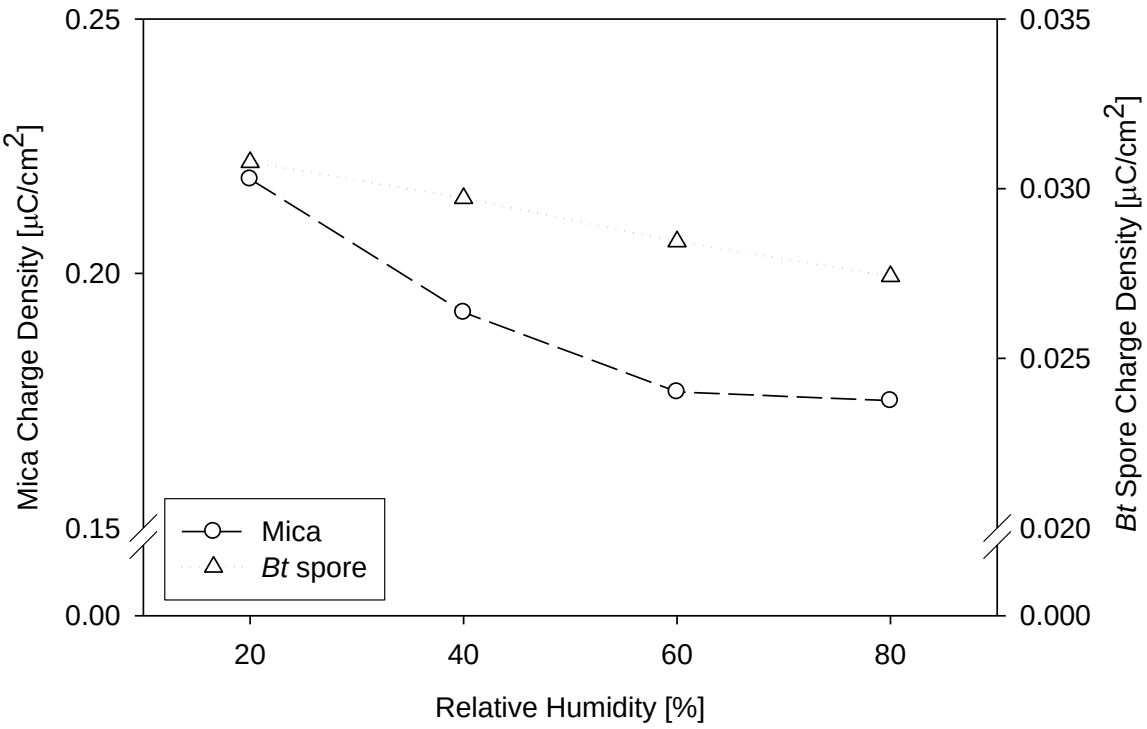

Figure 4.2 Surface charge densities of a *Bt* spore and mica at different humidity levels.

gold). For these measurements, a small piece of mica was placed on top of a gold surface. The electrostatic potential values of the mica surface and AFM tip is shown in Table 4.1. The potential was found as: $\frac{\partial \psi}{\partial z} = \frac{\psi_{substrate} - \psi_{tip}}{z} = -0.123 \ V/nm$ at 20% relative humidity using the same approach. This value was converted to surface charge density for the mica surface as -0.219 $\mu C/cm^2$. This surface charge density is about 10 times greater than that of the spore at the same humidity level. In addition, it was observed that the charge density of the mica also decreases with increasing relative humidity. The decreasing rate of the mica surface charge is, however, bigger than that of the spore (Figure 4.2).

Neglecting the electrostatic interaction between the tip and the planar surface, we estimated the surface charge approximately. However, the values for surface charge density of mica in air calculated in this study are comparable to those reported in previous studies (Shao 1959), indicating that the approximate procedure employed for the evaluation of the surface charge density from potential measurements is acceptable for the system studied here.

4.3.2 Coulombic Force Calculation

From Coulomb's law, it is well known that there is an attractive or repulsive force between charged surfaces. Since the SSPM measurement confirms that *Bt* spores have a significant surface charge density, the Coulombic force is expected to be an important component in its interaction force with another charged surface, such as mica. Since the charge densities of the spore and the planar surface were found to be slightly different at different humidity levels, the electrostatic force is also expected to vary with the relative humidity.

From the surface charge of *Bt* spores (-0.031 μC/cm^2) and the surface charge of mica (-0.219 μC/cm^2) at 20% relative humidity, the electrostatic interaction force can be calculated between the spore and the planar mica surface. If we assume an infinite size for the mica surface with surface charge density (σ), the electric field, *E*, produced by the charged mica surface will be: $E = \frac{\sigma}{2\varepsilon_0}$ where ε_0 is the vacuum permittivity. The force, *F*, applied to a particle of electrostatic charge (*q*) in an electric field *E* is: $F = E \cdot q = \frac{\sigma}{2\varepsilon_0} q$. Because the surface charge of the spore can be calculated as the product of the charge density and the surface area, the force can be rewritten as:

$$F_{Coulomb} = E \cdot q = \frac{\sigma}{2\varepsilon_0} q = \frac{\sigma_{surface}\sigma_{spore}}{2\varepsilon_0} A_{spore} \quad (4.1)$$

where A_{spore} is the surface area of the spore.

The *Bt* spore can be modeled as a rod shaped particle of 0.8-μm width and 1.3-μm length based on SEM or STEM images (Chung et al. 2010a). Assuming that the size change of the spore as a result of humidity occurs with a constant ratio of length to width, we were able to calculate the surface areas of the spore under different humidity levels using the measured width via tapping-mode AFM. The estimated surface area of the *Bt* spore is 2.098 μm^2 at a relative humidity of 20%, and the corresponding electrostatic force was calculated as 79.7 nN. The positive value means a repulsive force between the two objects whose charges are both negative. The calculated electrostatic forces in different humidity environments are given in Table 4.2. The electrostatic force between the *Bt* spore and the mica surface decreases with increasing humidity level as a result of the decreasing surface charge density on both the spore and the mica surfaces (see Figure

4.2). Even though the surface area is reduced, the size variation effect seems insignificant in comparison with the effect of the surface-charge-density change.

4.3.3 Electrostatic Image Force Calculation

A force called "electrostatic image force" arises between a charged particle and its image particle on the opposite side of a conducting planar surface (Feng and Hays 2003, Fowlkes and Robinson 1988). The image charge or image particle arises due to polarization of the conducting surface material by the charged atoms of the particle. The image force is calculated for the *Bt* spore on the planar gold surface. Because the image force is the interaction force between the charged particle and its image due to polarization, the Coulombic interaction between these two objects should always be attractive. In addition, there are other forms of forces caused by application of an external electric field. Previous studies evaluated the total electrostatic image force on a uniformly charged particle under an externally applied electric field as:

$$F_{image} = \alpha \frac{q^2}{16\pi\varepsilon_0 R^2} + \beta qE - \gamma\pi\varepsilon_0 R^2 E^2 \tag{4.2}$$

where q is the particle charge, R is the particle radius, E is the electric field, and ε_0 is the vacuum permittivity (Hays 1995, Hartmann, Marks and Yang 1976). The first term on the right hand side of the equation represents the electrostatic image force between the particle charge and the image charge; the second term represents the force on the charged particle located in the applied electric field, E; and the last term represents the force between dipoles (one in the particle, induced by the external electric field, and the other, an image dipole in the substrate). The coefficients α, β, and γ are functions of several parameters, such as the dielectric constant or the geometry of the particle, and they

determine the relative magnitude of each force. While the properties of both objects (planar surface and particle) are considered in the calculation of the electrostatic force, the image force is a function of particle properties only. No electric field was applied during adhesion force measurements between a spore and a surface in our system; therefore, the last two terms related to the external field are not present in this study.

The charge of the spore, q, was calculated as a product of the surface charge density obtained from the SSPM measurement and the surface area for a rod shaped particle obtained from AFM images at different relative humidity conditions. In order for equation 4.2 to be applicable, the spore was assumed to be a spherical particle having an equivalent volume as the rod-shaped particle (Chung et al. 2010a). The radius of the model spherical particle (R) varied from 0.481 to 0.490 μm at relative humidity values ranging from 20% to 80%.

The image force is directly proportional to the dimensionless coefficient, α, but it is known that the value of α varies with the charge distribution on the particle surface. There is evidence that the charge distribution is not uniform in a real system and the partial charge distribution influences the electrostatic force (Matsuyama, Ohtsuka and Yamamoto 2008, Pollock, Burnham and Colton 1995, Techaumnat and Takuma 2009). As the uniformity of the surface charge of the particle decreases, i.e., the charges are concentrated close to the contact point on the surface, and the value of the constant increases by up to an order of magnitude. For example, α is 1.59 for a uniformly charged particle with a dielectric constant of 3 compared to 52.7 for a nonuniformly charged particle having a concentrated charge at two opposite poles of a spherical particle (Feng and Hays 2003).

In addition to the charge distribution on the sample surface, the discreteness of the nonuniform surface charge influences the electrostatic image force. According to the reference by Czarnecki and Schein (2004), a discretely charged particle can increase the electrostatic image force compared to the force for a point charged particle. The image

force for a spherical, symmetrically charged particle and a planar surface was calculated as $1+4/\pi$ (≈ 2.27) times greater than the point charged particle system, and the increase was constant with different configurations. If 1.59 is taken as the value of α for a uniformly charged, sphere-shaped spore and a discrete charge distribution is assumed on the surface of the spore, the image force is calculated as 14.6 nN at 20% of relative humidity. Because the surface charge of the spore decreases with humidity as shown in Figure 4.2, reduction of the image force is expected as relative humidity is increased (see Table 4.2).

4.4 Adhesion Force between a *Bt* Spore and Surfaces

The electrostatic force can be a significant component in the interaction between a spore and a charged surface. Forces such as van der Waals and capillary are less important for a small, spherical particle, such as a spore, than the electrostatic force due to the spore's size and the relatively small contact area between the spore and the planar surface. In addition, it was confirmed by SSPM measurements that the spore has a significant level of surface charge. The force measurement of the *Bt* spore on the mica surface by AFM supports the hypothesis that the electrostatic interaction may play a significant role in the adhesion force of the spore on electrically nonconductive materials, such as mica. The adhesion force for mica was found to be less than that for the spore and gold system in the entire range of relative humidity used in the measurements. This result implies that the magnitude of an electrostatic repulsion between similarly charged objects (the spore and the mica) is large enough to cancel out the attraction due to the van der Waals and capillary forces. A mathematical model was applied to explain the experimental observation by quantifying each component of the force (van der Waals, capillary, and electrostatic). In previous work by the authors on spore adhesion on

Table 4.2 Calculated Coulombic forces between a *Bt* spore and a mica surface and the image forces between the spore and an electrically conductive surface such as gold.

Relative Humidity [%]	$F_{Coulomb}$ [nN]	F_{image} [nN]
20	79.7	-14.6
40	68.5	-13.8
60	60.7	-12.7
80	59.0	-12.1

surfaces (Chung et al. 2010a), the adhesion force was modeled as a sum of a capillary force and a van der Waals attraction. The details to calculate each force component are discussed elsewhere (Chung et al. 2010a, Orr et al. 1975). The parameters applied in the calculation can be found in the supporting materials.

Based on the discussion presented in the preceding section, the third component of the adhesion force, the electrostatic interaction that can be neglected for electrically-conductive materials, is included. The van der Waals and capillary forces, were calculated according to methods described in the literature (Orr et al. 1975, Xiao and Qian 2000), and the electrostatic force for four different relative humidity levels is shown in Figure 4.3. According to the calculations, the repulsive electrostatic force cancels a part of the attractive capillary and van der Waals forces. Approximately 60% of the sum of the two attractive forces at 20% relative humidity, and 25% of the attractive force at 80% relative humidity are cancelled by the electrostatic force.

The calculated value of the electrostatic force (79.7 nN) is comparable to the expected value because the sum of the adhesion force components (van der Waals and capillary) is approximately -125 nN at 20% relative humidity, while the measured force is approximately -72 nN. Therefore, the expected electrostatic repulsive force is 53 nN. The electrostatic force between the spore and the mica surface decreases as the relative humidity level is increased.

This result agrees with the experimental observation of increasing adhesion force with increasing relative humidity. While the attractive component of the total adhesion force increases with relative humidity, the repulsive electrostatic force decreases with relative humidity. Thus, the total adhesion force, i.e., the sum of attractive and repulsive forces, is expected to be greater at higher humidity values. As expected, the measured adhesion force increases with increasing relative humidity. Even though the trend of the measured adhesion force with the relative humidity is similar to that predicted by the theory, the increase of the experimental adhesion force does not completely correlate

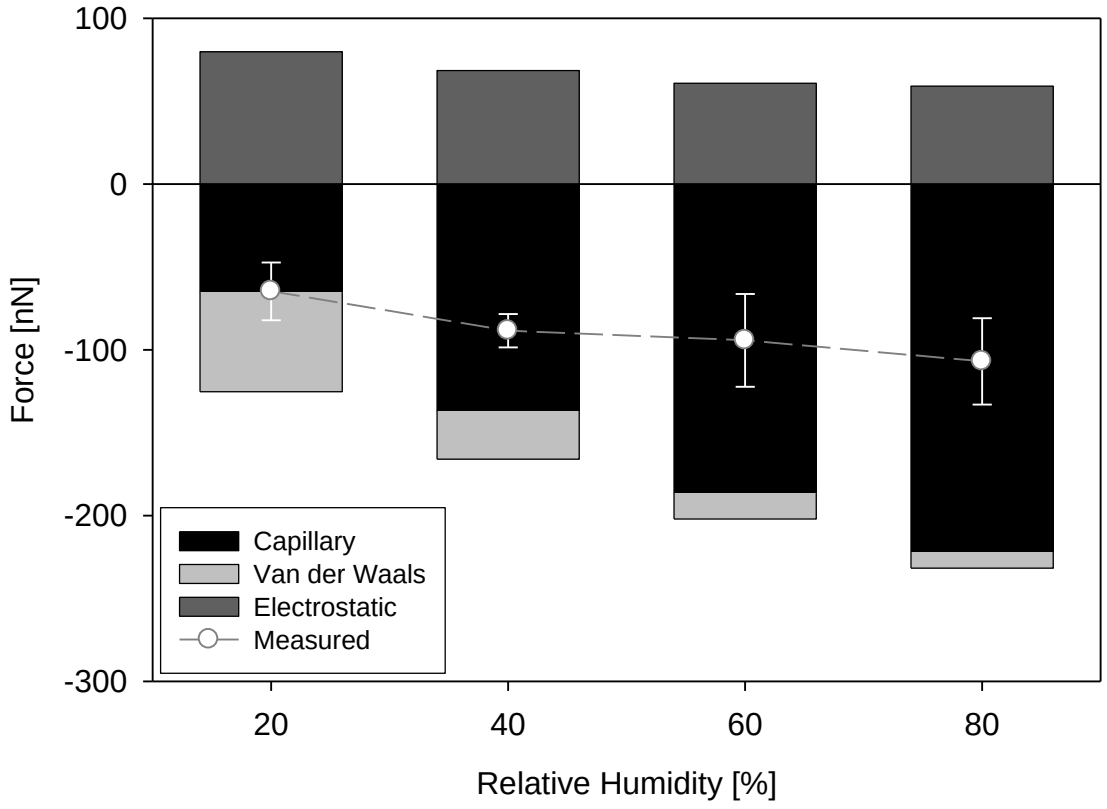

Figure 4.3 Measured adhesion force by AFM between a *Bt* spore and a mica surface and model calculation of its components: capillary, van der Waals, and electrostatic forces.

with calculations at higher humidity levels. The greater discrepancy between the measurement and the theoretical estimation at higher relative humidity levels is considered to be due to the values of the parameters used in the model. For example, the values of the contact angle and the Hamaker constant of the *Bt* spore were assumed similar to those for bacteria, which have been reported in the literature. This assumption, as well as the assumption that the permittivity of air (ε) is not affected by humidity, may have introduced some error in the calculations.

If the electrostatic force is ignored, then the capillary and van der Waals forces are the only components of the total adhesion force of the spore on an electrically conductive surface. This is because it is assumed that the surface charge of an electrically conductive surface, such as gold, dissipates fast and is neutralized by interaction with water vapor in the atmosphere at most relative humidity levels except at extremely low ones (less than 5%). In this paper, the authors note that another force can exist due to the charge on the spore surface and the corresponding polarization in the planar surface even with the spore and conductive surface system. Addition of this "image force" is expected to improve the accuracy in the estimation of the adhesion force between a charged particle and a conductive surface. Figure 4.4 depicts the measured adhesion force between the *Bt* spore and gold surface by AFM and the calculated adhesion force consisting of three components: capillary, van der Waals, and electrostatic image forces. The parameters in the capillary and van der Waals force calculation were applied as described in our previous study (Chung et al. 2010a). The calculated image force is approximately 10% of the total adhesion force for the relative humidity range 20% to 80%.

The comparison can be done at relative humidity values up to 60% because, due to experimental limitations, the adhesion force could not be measured at a higher relative humidity. The negative values of the forces represent an attractive force. The capillary and van der Waals forces are more sensitive to humidity than the image force. The total

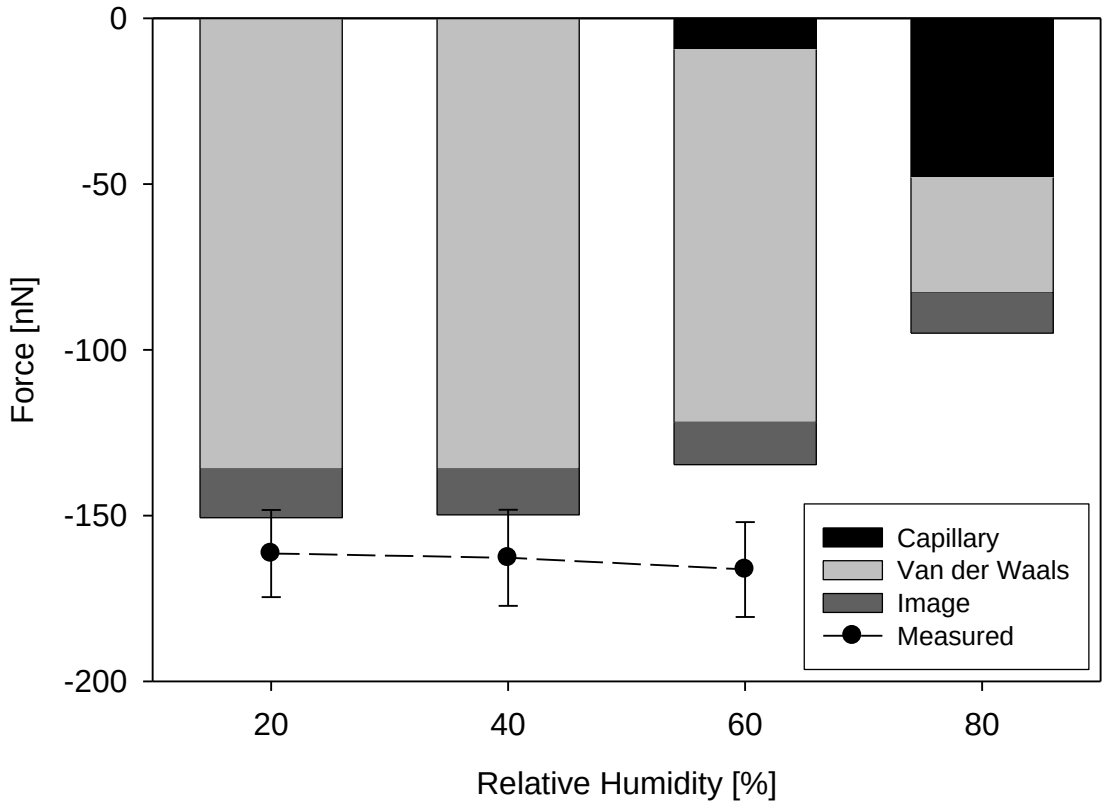

Figure 4.4 Measured adhesion force by AFM between a *Bt* spore and a gold surface and model calculation of its components: capillary, van der Waals, and electrostatic image forces.

adhesion force consists primarily of the van der Waals force at low and intermediate relative humidity levels. High contact angles of the two materials (*Bt* spore and gold) inhibit the meniscus formation between the two objects, which reduces the capillary force (Chung et al. 2010a). The van der Waals force decreases with increasing humidity and the total force shows the same trend. The image force decreases as the humidity is increased but the change is not significant. Therefore, the contribution of the image force to the total force increases. At a relative humidity between 20% and 60%, the model estimated forces are closer to the experimental values when the image force is added, which means that the addition of the image force improves the estimation of the adhesion force even though the image force is not the major component of the total adhesion force.

Although the added component of the image force improved the theoretical predictions, the discrepancy between the experimental values and model calculations for the gold surface system is greater compared to that for the mica surface system. This difference may be due to the surface roughness of the gold surface. Comparing to the atomically flat mica surface, the gold surface has some level of inherent roughness. The effect of surface roughness on the adhesion force or potential has been discussed in the literature (Schein and Czarnecki 2004, Farshchi-Tabrizi et al. 2006). Schein and Czarnecki noted that the image force is $\frac{4}{\pi}N$ times the force for one-point contact between a particle and a planar surface, where N is the number of contact points between the two objects (Schein and Czarnecki 2004). Quantifying the effect of roughness would require knowledge of N.

4.5 Summary

In the present study, the electrostatic force is investigated as one of the components of the adhesion force between *Bacillus thuringiensis* (*Bt*) spores and planar

surfaces. Two types of the electrostatic forces were introduced for two types of surfaces used; one is the electrostatic image force for an electrically conductive surface and the other is the Coulombic force for a non-conductive surface. Gold and mica were chosen as the surface material, respectively.

The surface potentials of a *Bt* spore and a non-conductive surface, such as mica, are experimentally obtained using a combined atomic force microscopy (AFM)-scanning surface potential microscopy (SSPM) technique. On the basis of experimental information, the surface charge density of the spores is estimated as 0.03 $\mu C/cm^2$ at 20% relative humidity. The surface charge of the mica and the *Bt* spore decreases with increasing humidity.

The Coulombic force is introduced for the spore-mica system and an electrostatic image force is introduced to the spore-gold system. The Coulombic force for spore-mica (both charged, non-conductive surfaces) is repulsive because the components are similarly charged, while the image force for the spore-gold system is attractive. The magnitude of both forces decreases with increasing humidity as a result of the decreasing surface charge density as humidity increases.

The electrostatic forces are added to other force components, e.g., van der Waals and capillary forces, to obtain the adhesion force for each system. The repulsive Coulombic force for the spore-mica system decreases the magnitude of the adhesion force, while the attractive image force for the spore-gold system increases the previously obtained adhesion force. The adhesion forces measured by AFM are greater than the values estimated by the model, including the electrostatic forces. It is shown that the electrostatic (Coulombic and image) forces play a significant role in the adhesion force between spores and planar surfaces.

CHAPTER 5

INTERACTIONS OF SPORES WITH PLANAR SURFACES IN AQUEOUS SOLUTIONS

So far, the adhesion force between spherical particles, especially microbial colloids such as a bacterial spores, and planar surfaces in atmospheric environments was estimated as the sum of the capillary force, van der Waals force, and electrostatic force. Experimental observations and theoretical estimations showed a good agreement. However, it is expected that the theoretical calculations can be improved if parameters that were neglected in the model, such as roughness of the interacting surfaces, were considered.

In this chapter, the interaction forces between a particle and a planar surface in aquatic environments are investigated. Two types of forces, i.e., the adhesion force and the force-distance profile, are observed between a bacterial spore and various planar surfaces. Parallel theoretical and experimental studies were conducted for both types of forces. Since ions are taken into account for the calculation of the electrostatic force in aquatic solutions, the theoretical model for the electrostatic force differs from the model used for atmospheric environments. While a qualitative agreement between modeling results and experimental data is expected, consideration of the surface roughness is needed to provide quantitative agreement at various experimental conditions.

5.1 Introduction

Microbial interactions are important in understanding how the microorganisms adhere to such common surfaces as soil particles, metal, or glass in natural or engineering environments and how they are redispersed in aquatic environments. The microbial

colloids facilitate the transport of other contaminants, such as heavy metals or they can be considered as contaminants in groundwater or subsurface systems. Previous studies on the behavior of the biocolloids using laboratory-scale or field-scale experiments have applications in contaminated groundwater treatment such as filtration, coagulation, or sedimentation, subsurface bioremediation, subsurface ecology, water-treatment system design, and risk assessment of pathogen contamination.

Bacterial spores, a dormant form of microorganisms during their life cycle, have their most outer layer (called 'spore coat') as a structural support and a barrier against external conditions (Gerhardt, Pankratz and Scherrer 1976). Inside the coat, the core contains DNA, ribosome, and enzymes, as well as protein, calcium, and dipicolinic acid which provide resistance to external stimuli such as heat, oxidizing agents, or UV radiation. The properties of the spores allow them to travel through either atmospheric or aquatic environments for a relatively long time and distance compared to the transport of its active form. This behavior can explain a global transport or dispersion of microbial colloids with regards to microbial ecology. Microbial colloids can also be used as a tracer. Biocolloids, including bacterial spores, for example, can be used as a tracer for sewage dispersion (Pang, Close and Noonan 1998).

There are many mechanisms contributing to the interaction force between two surfaces. The main interaction force components between two objects, such as a particle and a planar surface, are van der Waals force, electrostatic interaction, acid-base interaction, and steric forces (Israelachvili 1998, Elimelech et al. 1995). Electrostatic interaction occurs when the interacting bodies are electrically charged. Traditionally, the electrostatic force in an aqueous solution is calculated by using the electrical double layer theory. The electrostatic force may be a significant component for objects with a large surface area to volume ratio. The double layer is formed by the depletion of coions and concentration of counterions as a consequence of the surface charge. Near the surface exposed to the liquid, two layers are formed. Hydrated counterions adsorb onto the

surface, building an inner layer called Stern layer, while the outer layer is called the diffuse layer. The Lifshitz-van der Waals force arises from the interactive forces between the permanent or instantaneous dipoles in molecules and, for macroscopic bodies; it is calculated using the Derjaguin approximation. While the van der Waals force appears between molecules in both polar and nonpolar systems, the acid-base interaction plays a role only in polar systems.

Combination of these forces determines the total interaction force between a particle and a planar surface. The contribution of each component varies with the properties of the medium and the particle/planar-surface system such as type of materials, shape, and charged density.

Adhesion of a spore or a bacterial cell onto surfaces has been studied previously (Faille et al. 2002, Li and Logan 2004). The magnitude of the adhesion force and the effects of the material properties on the adhesion have been investigated, however, the components of the total force have not been fully examined. In this study, the forces between a *Bacillus thuringiensis* (*Bt*) spore and planar surfaces of mica and gold are investigated via experimental and theoretical methods. Within the *Bacillus* genus, *Bacillus thuringiensis* is a member of the *Bacillus cereus* group, which includes the pathogens *Bacillus cereus* and *Bacillus anthracis* that are potentially dangerous to human health. *Bacillus thuringiensis* is a reasonable representative of the *Bacillus cereus* group and an excellent substitute of the dangerous *Bacillus anthracis*. Mica and gold surfaces are also good model surfaces in terms of surface charge. Mica is known to have a high surface charge in natural environments, while gold is chosen as an electrically conductive material. The aim of the research is to provide a better understanding of the interaction of spores with model surfaces in aquatic environments.

5.2 Materials and Methods

5.2.1 Spore Characterization: Size and Zeta Potential Measurements

The size of *Bt* spores was measured using electron microscopy. Images of the spores were taken by scanning electron microscopy and scanning/transmission microscopy, and the images showed that the size of the spores varies. More than 50 spore sizes were acquired from at least five different images and averaged. The zeta potential of *Bt* spores and mica particles was measured by a zetameter (ZetaPlus, Brookhaven Instruments Corporation, Holtsville, NY) in solutions of varying pH and ionic strength. For such solutions, the measurements were repeated 15 to 25 times and averaged values were obtained. Three pH values (4.5, 7.0, and 9.5) adjusted by addition of HCl or NaOH solution and three ionic strengths (0.0001 M, 0.001M, and 0.01 M) of sodium chloride were considered resulting in nine different conditions from the 3 by 3 combination of the variables considered.

5.2.2 AFM Force Measurements

Bt spores were purchased from Raven Labs (Omaha, Nebraska). Details of the preparation of the spore AFM probes can be found elsewhere (Chung et al. 2010a). In brief, drops of spore suspension were air-dried on a filter paper, and the spores were transferred onto a micro-cantilever. Epoxy glue was used to fix a single spore on a tipless AFM cantilever. The spring constant of the spore probe was measured after mounting of the spore. The typical values were about 0.3 N/m. The *Bt* spore probes prepared, as well as various substrates such as mica and gold, were used for measurements with a multi-mode atomic force microscope (Veeco, Plainview, NY) to yield the interaction force between a spore and a substrate. Two types of forces can be measured by the AFM force mode between two objects; adhesion force (sometimes called ‘pulling-off’ force) and

force-distance curve. The force-distance curve is obtained as the AFM probe approaches the substrate, and the adhesion force is measured from the maximum deflection of the cantilever when the probe retracts from the substrate. A number of 1024 data points were recorded for each force-distance curve, as the probe approached toward and retracted from the substrate.

5.3 Theoretical Approach

5.3.1 Adhesion Forces of a Particle onto Surfaces

The adhesion force can be modeled with the assumption that the particle is attached onto the planar surface at a distance of an intermolecular spacing from the surface. In previous studies by the authors, the adhesion force between a spherical particle and a planar surface in atmospheric environments was modeled as the addition of van der Waals, capillary, and electrostatic forces (Chung et al. 2010a, Chung et al. 2010b). In an aquatic system, however, the capillary force that is due to water condensation between the surfaces does not apply. Therefore, in our theoretical approach, the adhesion force between a particle and a flat surface has been assumed to be composed of van der Waals and electrostatic interactions.

The van der Waals force has been mathematically expressed by Hamaker and Lifschitz by the integration of all interactions between atoms or molecules of the objects (Israelachvili 1998). For aqueous systems, the Hamaker constant needs to be adjusted to take into account the presence of water molecules in between the interacting surfaces. The electrostatic interaction force can be calculated using Coulomb's law. In aqueous solutions, the electrostatic force can be calculated by the electrical double-layer theory as discussed in the following paragraph.

5.3.2 Force-Distance Curves between a Particle and a Planar Surface through DLVO Theory

The second type of force measurements obtained via AFM is force-distance curves. Traditionally, the Derjaguin, Landau, Verwey and Overbeek (DLVO) theory has been used to explain the interaction between two charged colloidal particles in electrolyte solutions (Israelachvili 1998, Elimelech et al. 1995, Hiemenz and Rajagopalan 1997). The DLVO theory has also two components, the electrostatic and van der Waals interactions, whose potentials or forces can be expressed as functions of the separation distance between the two interacting surfaces. Mathematical expressions of potentials and forces between two planar surfaces, between two spherical particles, or between a particle and a planar surface have been reported in the literature (Elimelech et al. 1995, Hiemenz and Rajagopalan 1997, Dorobantu et al. 2009). The electrostatic interaction between charged particles in aqueous solutions is determined by overlapping of the electrical double layers formed by ions accumulating near the charged surfaces. The electrical double-layer potential between two planar surfaces is expressed per unit area by: $\Phi_{edl} = 64 k_B T n_\infty \kappa^{-1} \Gamma_0^2 \exp(-\kappa h)$, where k_B is the Boltzmann constant, T is the temperature, n_∞ is the number concentration of ions in the bulk solution, h is the separation distance between the surfaces, $\kappa = \left[\frac{e^2}{\varepsilon k_B T} \sum_i z_i^2 n_{i\infty} \right]^{1/2}$, and $\Gamma_0 = \frac{\exp(ze\psi_0 / 2k_B T) - 1}{\exp(ze\psi_0 / 2k_B T) + 1}$ (Hiemenz and Rajagopalan 1997). The parameters e, ε, z_i, $n_{i,\infty}$, and ψ_0 represent the charge of an electron, dielectric permittivity, charge valence, number concentration in the bulk solution of ion type i, and the surface potential, respectively. The interaction potential between two charged spheres can be given by:

$$\Phi_{edl} = \frac{2\pi r_1 r_2 n_\infty k_B T}{(r_1 + r_2)\kappa^2} \left(\phi_1^2 + \phi_2^2\right) \left[\frac{2\phi_1 \phi_2}{\phi_1^2 + \phi_2^2} \ln\left(\frac{1 + \exp(-\kappa h)}{1 - \exp(-\kappa h)} \right) - \ln\left(1 - \exp(1 - \exp(-2\kappa h))\right) \right] \qquad (5.1)$$

where r_i is the radius of the spherical particle *i* and ϕ_i is the reduced potential, which is related to the surface potential (ψ_i) by: $\phi_i = \frac{e\psi_i}{k_B T}$ (Hiemenz and Rajagopalan 1997). The interaction potential of the system of a spherical particle and a planar surface can be estimated by equation 5.1, by allowing one particle to have infinite size. The van der Waals interaction potential between two flat surfaces is given by: $\Phi_{vdw} = -(A_H / 12\pi) / h^2$ and is expressed per unit area, while the van der Waals potential between a spherical particle and a flat surface is given by:

$$\Phi_{vdw} = -A_H R / 6h \tag{5.2}$$

where A_H is the van der Waals constant and *R* is the radius of the particle (Elimelech et al. 1995). After the addition of the two potential components (i.e., for van der Waals and electrostatic interactions) between a spherical particle and a planar surface, the corresponding force can be obtained from the derivative of the total potential with respect to the separation distance.

5.4 Experimental Results

5.4.1 Spore Characterization

The length and width distributions of *Bt* spore samples obtained from electron microscopy images are shown in Figure 5.1. The graphs show normal distributions with average sizes of 1.57 μm in length and 0.86 μm in width. A spore probe used in AFM force measurements was also imaged by scanning electron microscopy (results not shown). The spore attached onto the cantilever does not have the exact average size of the

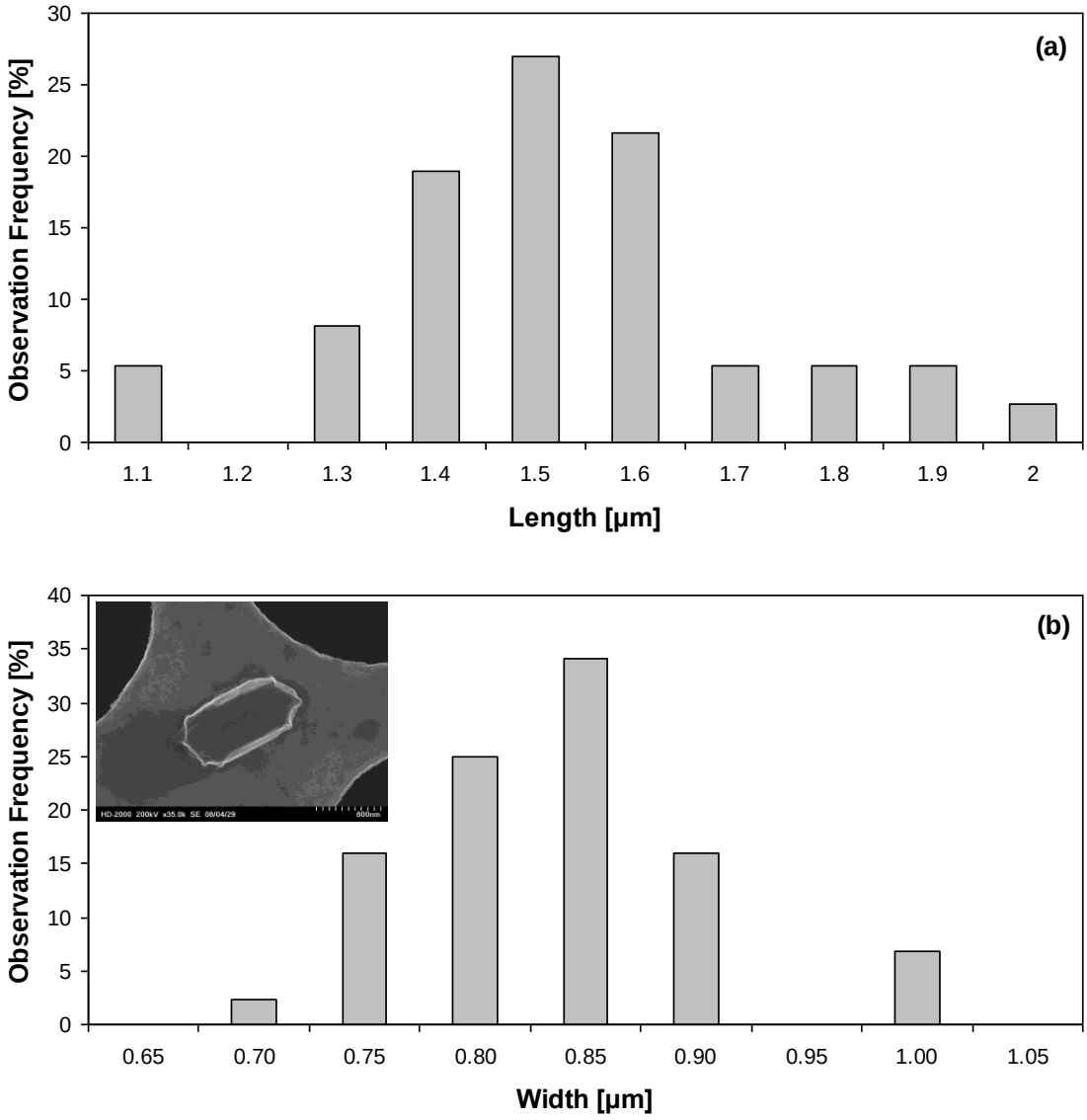

Figure 5.1 Size distribution of *Bt* spore samples. The average size of the spores is 1.57 µm long (a) and 0.86 µm wide (b).

observed *Bt* spores but it could be confirmed that its size (1.3 μm long and 0.8 μm wide) is within the expected range.

Three different pH levels and three different ionic strengths were chosen, with nine different configurations resulting from their combination, for adhesion force and force-distance measurements using AFM. Zeta potential measurements at the same conditions were conducted, as shown in Table 5.1. The observed zeta potential values of the *Bt* spores were negative for all conditions. An increase of the pH level leads to increase of the absolute value of the potential. The effects of the ionic strength were not significant in low-pH conditions but, in mid- or high-pH conditions, the zeta potential decreased with increasing ionic strength in the range of conditions used in the study.

5.4.2 Adhesion Force between a *Bt* Spore and a Surface

The adhesion force measurements are summarized in Table 5.2 and 5.3. The maximum adhesion force for the *Bt* spore-gold surface system is measured at the mid-pH level, except when the ionic strength is 0.01 M. In either lower or higher pH levels, the adhesion force is smaller than that at mid-pH conditions. Also, the adhesion force at acidic conditions (pH 4.5) is greater than at basic conditions (pH 9.5). This trend can be explained by a similar trend of the electrostatic force because the van der Waals force is expected to be constant at all conditions. The adhesion force of the spore onto the gold surface in Table 5.2 is greater than that onto the mica surface in Table 5.3; however, the trend of the adhesion force onto mica is similar to the trend of adhesion onto the gold surface. The reason that adhesion is stronger on gold is that not only is the Hamaker constant of the mica-water-spore system smaller than that of the gold-water-spore system, but also the mica surface is similarly charged with the spore surface charge, while the gold has opposite surface charge.

Table 5.1 Zeta potential measurements (in V) of *Bt* spores in different conditions of pH and ionic strength (NaCl). The reported numbers are averaged values, while the standard deviations are shown in the parentheses.

I \ pH	4.5	7.0	9.5
0.0001 M	-0.013 (0.007)	-0.038 (0.008)	-0.051 (0.006)
0.001 M	-0.014 (0.005)	-0.026 (0.006)	-0.040 (0.003)
0.01 M	-0.015 (0.006)	-0.018 (0.003)	-0.033 (0.007)

Table 5.2 AFM-measured adhesion force between a *Bt* spore and a gold planar surface in various conditions. The values in the parentheses are theoretically calculated adhesion forces, all in (nN).

I \ pH	4.5	7.0	9.5
0.0001 M	-1.94 (-15.2)	-5.34 (-15.2)	-0.16 (-15.0)
0.001 M	-1.95 (-15.3)	-2.88 (-15.3)	-1.18 (-14.7)
0.01 M	-1.91 (-15.3)	-1.73 (-15.3)	-1.28 (-14.4)

Table 5.3 AFM-measured adhesion force between a *Bt* spore and a mica planar surface in various conditions. The values in the parentheses are theoretically calculated adhesion forces, all in (nN).

I \ pH	4.5	7.0	9.5
0.0001 M	-0.20 (-8.19)	-2.30 (-8.06)	-0.04 (-8.01)
0.001 M	-0.06 (-8.02)	-0.58 (-7.83)	-0.02 (-7.59)
0.01 M	-0.92 (-7.56)	-0.25 (-7.42)	-0.01 (-6.81)

For the calculation of the adhesion force, the van der Waals and electrostatic force components were considered, while the adhesion force was modeled with the assumption of an "intermolecular spacing" between the particle and the planar surface. At this close distance, the van der Waals force is expected to be a major component of the adhesion force unless the charge of the particle or the planar surface is significant. As shown in Table 5.2 and 5.3, the overall calculated values are greater than the adhesion forces measured by AFM. This result may be attributed to the assumption of intermolecular spacing between the spore and planar surface. If, for example, the spore/planar-surface interface was not smooth at the molecular level, then the spacing allowed between the spore and the planar surface would be larger. The adhesion force of the *Bt* spore-mica surface system is measured close to zero in most of the experimental conditions (Table 5.3). The real separation distance between the *Bt* spore and the mica surface at which the van der Waals attraction and the electrostatic repulsion are equal, so that the adhesion force is zero, can be used to estimate the surface roughness of the spore by subtracting the intermolecular spacing from the 'zero-force' separation distance. From the model, the total adhesion force at most conditions is calculated close to zero at about 1.0 nm distance between the spore and mica surface. The assumed intermolecular spacing in the model was 0.275 nm (Chung et al. 2010a, Xiao and Qian 2000); therefore, the roughness of the spore can be estimated at approximately 0.725 nm. Table 5.4 summarizes the recalculated adhesion forces with a distance between the spore and the gold surface of 1.0 nm, and shows that the calculated values are closer to the AFM force measurements. Therefore, it can be concluded that the surface roughness of the spore should be considered for the estimation of the separation distance between the spore and the surface in model calculations.

Table 5.4 Calculated adhesion forces between a *Bt* spore and a gold planar surface with the assumption that the distance between the spore and the surface is 1 nm. The values are in units of (nN). Calculated adhesion forces for the spore-mica system are close to zero at all conditions.

I \ pH	4.5	7.0	9.5
0.0001 M	-1.18	-1.25	-0.98
0.001 M	-1.28	-1.25	-0.75
0.01 M	-1.30	-1.26	-0.58

5.4.3 Force-Distance Curves between a *Bt* Spore and a Planar Surface by AFM

Force-distance curves obtained using AFM for the *Bt* spore-gold surface system were compared to the calculated force-distance curves obtained from the DLVO theory using the zeta potential values of gold surface obtained from literature (Taboada-Serrano et al. 2008) (result not shown). At mid- or low-pH levels, the spore and the gold have opposite charge which caused an attractive force calculated for all separation distances. Even though the measured force-distance curves did not show an attractive force for any separation distance, there are local minima in the curves at pH values of 4.5 and 7.0. The separation distance for these local minima becomes smaller as the ionic strength increases. This result seems reasonable because the thickness of the electrical double layer becomes smaller as the ionic strength increases. The calculated force curves at higher pH values, where the *Bt* spore and gold surface are similarly charged, showed local maxima due to the repulsive electrostatic force. Even though the modeling results agree with the experimental data qualitatively, a discrepancy between the two results implies that possible sources of error need to be considered in the model. One possible explanation is that there are other components of the total interaction force besides van der Waals and electrostatic forces, which are discussed in the following section. Another possible source of error in the model is that the zeta-potential values for the gold surface used in the calculations did not represent the gold surface used in this study. The same three pH levels (4.5, 7.0, and 9.5) were considered in the reference paper (Taboada-Serrano et al. 2008), however, different ionic strengths (0.0005, 0.005, and 0.05 M) were used instead of the ionic strengths used in this study (i.e., 0.0001, 0.001, and 0.01 M). This difference may have contributed to the discrepancy between the force measurements and calculations. It should also be noted that the zeta potential was not directly measured in reference (Taboada-Serrano et al. 2008).

While the experimental results show a slight discrepancy compared to the theoretical calculations for the *Bt* spore-gold surface system, the force-distance curve calculations are more comparable to the AFM measured force-distance curves for the spore-mica surface system. As shown in Figure 5.2, when the AFM measured force-distance curve is compared to the theoretically calculated curves, the experimental results show better agreement with the particle-surface system profiles than with the surface-surface system profiles. The calculated force profile between two planar surfaces shows much greater repulsive force for the wider distance range compared to the experimentally obtained force-distance profile or the theoretical profile for particle-surface system.

Because the surface charge of the spore and mica are both negative for all conditions of pH and ionic strength used in this study, the calculated curves showed local maximum points and exponential force decay after each maximum point. As the ionic strength increases, the maximum value of the repulsive force increases and the force profile shows steeper decay. In addition, the point of the maximum force approaches the surface as the ionic strength is increased. This is because the electrical double layer becomes thinner as the ionic strength increases. Also, the charge densities of the mica surface and *Bt* spore were found to be greater at a higher ionic strength of the solution. A change in the pH did not move the maximum force point, but an increase of the pH level led to a larger peak point value in the force curves. This behavior may be explained by the fact that the measured surface charge densities of the spores increased with increasing pH values even though the surface charge density of the mica did not change with pH.

5.5 Discussion

For a living bacterial cell and a planar surface, the extended DLVO theory is often employed to explain the interaction force between a particle and a surface (Dorobantu et al. 2009, Hoek and Agarwal 2006). For the *Bt* spore-mica surface system in this study,

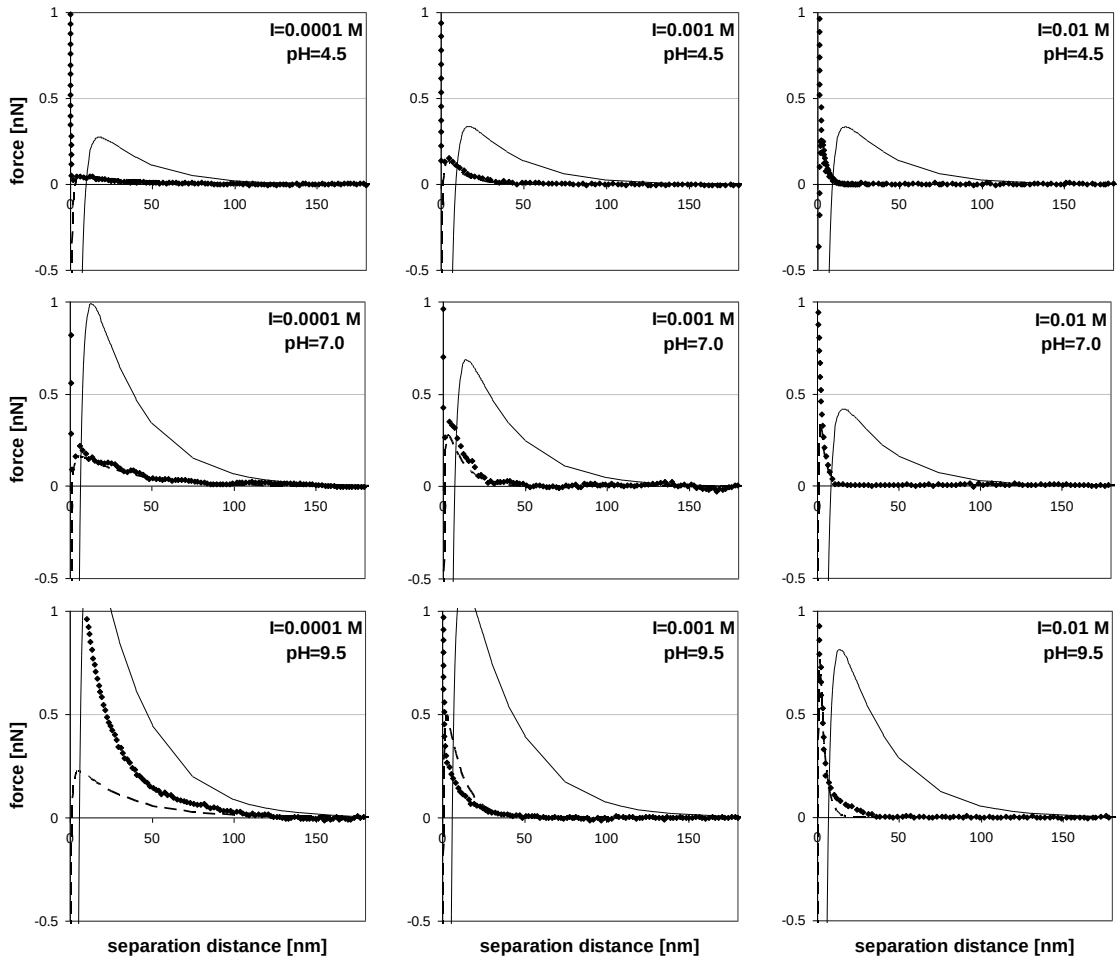

Figure 5.2 Force-distance profiles for the *Bt* spore-mica planar surface system in three different pH levels and three different ionic strength conditions. The broken line is the theoretically calculated profile for a spherical particle and planar surface system; the solid line represents the theoretically calculated profile between two planar surfaces; and the dotted line is the measured force-distance curve between the *Bt* spore probe and the mica surface using AFM.

force calculations using the DLVO theory have shown a relatively good agreement with the experimental values. The extended DLVO theory includes such terms as acid-base and steric interactions in the total potential or force calculations, in addition to the van der Waals and electrostatic interaction terms. Therefore, it can be concluded that the van der Waals and electrostatic interaction forces play important roles in the interaction between a *Bt* spore and a planar surface in an aqueous solution.

The discrepancy between the theoretical force-distance curves and experimental results for the *Bt* spore-gold surface system can be attributed to the approximate zeta potential values of the gold surface, as discussed in the previous section. Explaining the experimental force curve using the DLVO theory by modifying the zeta potential of the gold surface provided zeta potential values that described better the force measurements. From the calculated force curve that describes best the experimental results (in Figure 5.3), the zeta potential value of the gold surface was estimated as shown in Table 5.5. The estimated zeta potential values found in this way are lower than the approximate values obtained from previous work. These values are more reliable because they are directly related to the system used in this study. The zeta potential values obtained here follow the general trends of the zeta-potential with respect to pH and ionic strength. As the ionic strength increases or the pH level decreases, the absolute zeta potential values decrease.

Effects of the deformation of the particle are sometimes considered in force measurements by AFM especially for soft particles, such as living microorganisms or polymers (Petrov and Gallyamov 2007). Force measurements via AFM are conducted using a micro-cantilever that is deflected due to the interaction force between the surface and the particle attached at the end of the cantilever. Therefore, deformation of the particle, which affects the deflection, may play a role in force measurements (Capella et al. 1997). The most outer membrane of the *Bt* spore, or other spores of similar species, consists of several types of proteins and lipids and sometimes has appendages on the surface. The outer membrane or the exosporium has a certain level of flexibility and the

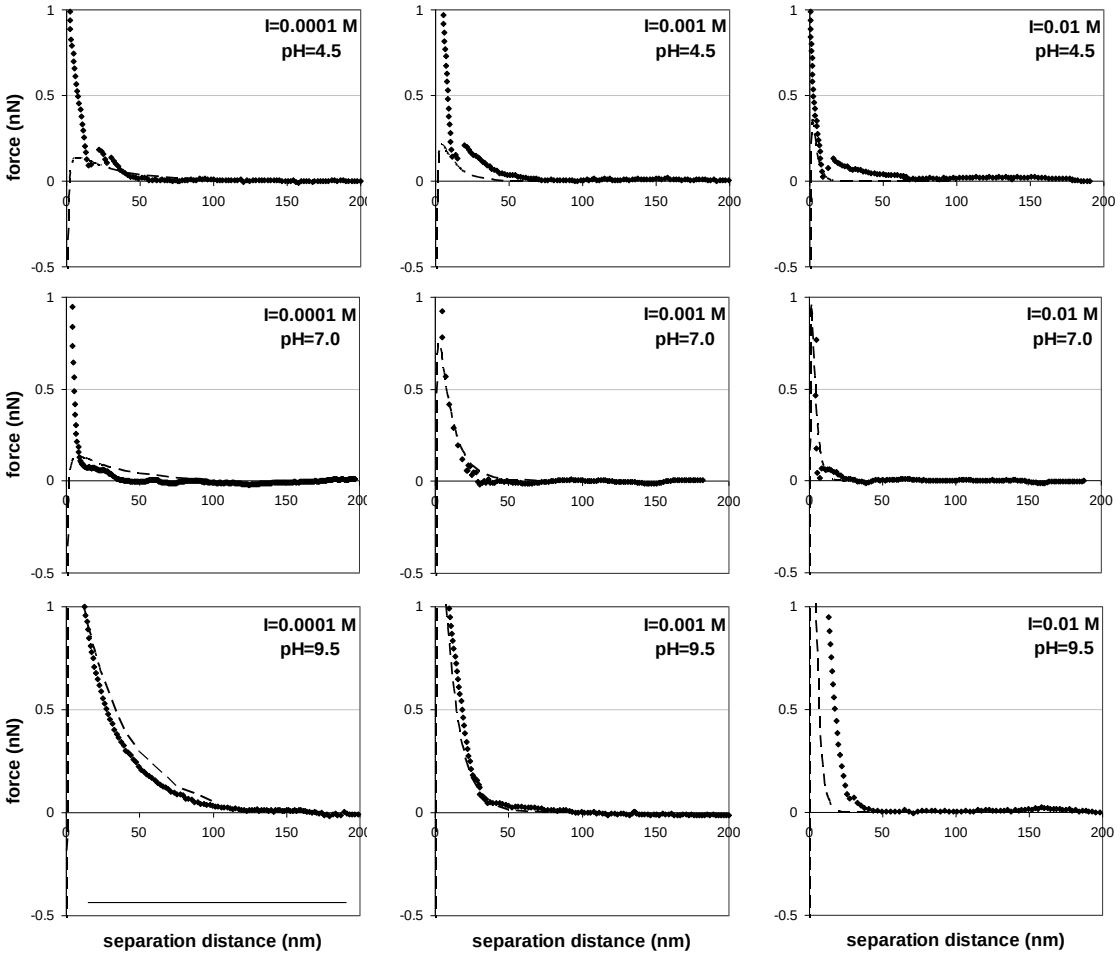

Figure 5.3 Force-distance profiles for the *Bt* spore-gold planar surface system in three different pH levels and three different ionic strength conditions. The dotted line is the measured force-distance curve between the *Bt* spore probe and the gold surface using AFM, and the broken line represents the theoretically calculated profile for a spherical particle and planar surface system.

Table 5.5 Zeta potential values of gold estimated from the experimentally obtained force-distance curves. The values are in units of (mV).

I \ pH	4.5	7.0	9.5
0.0001 M	-45	-50	-85
0.001 M	-30	-45	-55
0.01 M	-25	-40	-50

appendages have motility in aqueous solutions but, when the spore is dried in the atmosphere, the exosporium seems to cling to the inner layer and the appendages on the exosporium harden. This assumption is supported by the fact that the surface of an air-dried spore is firm and inflexible enough to be used in the AFM imaging, using a sharp silicon nitride tip, without any deformation or damage of the surfaces. Therefore, since the AFM spore probes were dried in air prior to the measurements in this study, the deformation effect of spores on the interaction forces was not considered.

5.6 Summary

In summary, this study investigated the bacterial spore interactions with planar surfaces in aquatic environments, including adhesion forces and force-distance profiles, which are influenced by the geometry and physicochemical properties of the system.

The characteristics of spores of *Bt* were determined using electron microscopy and electrokinetic measurements. The average size of the spores is 1.57 μm long and 0.86 μm wide, and the zeta potential values are negative for the solutions used in this work.

The DLVO theory was employed to predict the interaction force between the spore and planar surfaces as a function of the separation distance, and a force balance was used to explain the adhesion force or "pulling-off force." Theoretical estimations were compared to experimental measurements obtained from AFM. The results on the adhesion force suggest that the surface roughness of the *Bt* spore used in this study is about 0.7 nm. Through the force-distance profile results for the spore-gold surface system, zeta potential values of the gold planar surface were estimated.

The DLVO theory and the mathematical model describing the adhesion force were found adequate in explaining the behavior of spores in aqueous environments. Consequently, the model can be employed to describe transport and dispersion of spores in aquatic and subsurface systems. It can also be used to devise methods, such as

filtration or adsorption processes, for the removal or deactivation of spores in aqueous systems.

CHAPTER 6

INTERACTION OF SILICA NANO-PARTICLES WITH A FLAT SILICA SURFACE STUDIED BY NEUTRON REFLECTOMETRY

Studies in previous chapters of this thesis have been based on atomic force microscopy (AFM) as the experimental instrument of choice. Experimental data obtained through AFM were compared with theoretical calculations, and it was confirmed that the interaction of a *Bacillus thuringiensis* spore with planar surfaces, such as gold and mica, can be explained by the classical DLVO theory. The AFM provides information about the interaction between a single particle immobilized at the cantilever tip and a planar surface. Although the use of several AFM probes can produce a representative behavior of the interaction force, an experimental system in which a large population of particles interacts with the surface is expected to provide more realistic information. Neutron reflectometry, as described in this chapter, allows measurements involving a large particle population of particles.

In the experimental set-up of neutron reflectometry, many particles are floating in a cell and interact with a surface. The experimental data and the corresponding model analysis are expected to be explained by the classical theory. Similarly with the previous study, the original idea was to use the microbial colloidal particles in the measurements. However, silica particles were used as a sample material, instead of bacterial spores, for simplicity. It was expected that this study could demonstrate the possibility of the use of neutron reflectometry to provide a better understanding of the fundamental mechanisms behind particle-surface interactions.

6.1 Introduction

Aggregation and surface deposition of particles in aqueous solutions are widely observed phenomena in natural or engineered systems. Deposition of particles, especially nano-sized particles, on surfaces is of great interest in various environmental processes, such as transport of groundwater contaminants onto subsurfaces and remediation of contaminated water. Aggregation of suspended particles is also important because it forms aggregates, which can be easily removed from aqueous solutions. Motivated by better water quality, researchers have investigated particle aggregation and deposition through experimental and theoretical approaches.

Quartz crystal microbalance (QCM) is often used for the investigation of the behavior of colloidal particles, polymers, and lipid films, and biomolecules on surfaces (Lvov et al. 1997, Cliffel et al. 1998, Marx 2003, Keller and Kasemo 1998, Caruso et al. 1997). The device measures the change in resonance frequency of a quartz crystal resonator, which is disturbed by the accumulation or removal of particles at the surface of the resonator. It can be used to monitor the deposition rate of colloidal particles on surfaces.

Atomic force microscopy (AFM) can also be used to study the interaction of colloidal particles with a surface (Chin et al. 2002). The force-distance profile can be obtained from the deflection of the AFM cantilever as the AFM probe approaches toward or retracts from the surface. Cantilever deflection results from the interaction between the cantilever probe and the surface. While AFM provides the interaction force between a particle and a surface as a function of separation distance, QCM can detect the mass change of particles deposited on a surface.

Neutron reflectometry (NR) provides structural information of surfaces (Zhou and Chen 1995). The technique involves an incoming neutron beam at a flat surface, and its reflection from the surface is measured in terms of scattering length density as a function of depth (Russell 1990). The obtained reflectivity profile can be used to determine the

thickness, material composition, periodicity, and roughness of any thin film layered on the substrate. NR data provide the distribution of particles along the direction perpendicular to the surface, a result that cannot be provided by QCM experiments. QCM measurements provide information on particles deposited onto a surface or removed from a surface, while AFM provides force measurements between a particle and a substrate surface as a function of distance from the surface. AFM experiments involving a single particle attached to the cantilever tip provide valuable information on particle-substrate interaction, but the question is whether the measurements represent the average response of the particle population. NR measurements, on the other hand, involve a large population of particles, thus the data reflect the average behavior of the whole particle population at the surface. Moreover, the movement of the particle, which is attached on the AFM cantilever tip, is dictated by the AFM controls in terms of height and speed, while in the NR experiment, particles freely move toward and away from the surface. Thus, the behavior of a large number of colloidal particles freely floating in the medium and interacting with a surface in the NR experiments is comparable to the behavior of a real system.

Theoretical modeling, including Monte Carlo simulation (Taboada-Serrano et al. 2006) or molecular dynamics (Gargallo et al. 2003, Peters 1999), has been applied to explain particle-surface interactions and particle aggregation. Theoretical calculations are often compared to experimental data provided by AFM or QCM. However, the modeled system is hardly matched by the experimental setup because of computational limitations (Taboada-Serrano et al. 2006) or the complexity in the calculations (Taboada-Serrano et al. 2005).

NR has often been used to study surface interactions of polymer, surfactant, or biomolecules (Penfold and Thomas 1990, Fragneto-Cusani 2001, Li et al. 1998). However, this technique has not been utilized to study surface interactions of environmental particles in terms of stabilization, aggregation, and desorption. NR can be

a good alternative tool to QCM and AFM providing complementary information on the behavior of environmental nanoparticles.

6.2 Theoretical Background

6.2.1 Neutron Reflectometry Theory

NR provides structural information near an interface, in the direction normal to the surface. The instrument provides the refractive index profile normal to the interface, which is related to the scattering length density, and this information is used in the calculation of the reflectivity. The reflectivity $R(\theta)$ is calculated using the following formula (Russell 1990, Fragneto-Cusani 2001, Grundy et al. 1988):

$$R(\theta) = r_{0,1} r_{0,1}^{*} \tag{6.1}$$

where $r_{0,1}$ is the reflection coefficient and $r_{0,1}^{*}$ is the complex conjugate of the reflection coefficient. The reflectivity for a multi-layer system is:

$$r_{n-1,n} = \frac{r'_{n-1,n} + r'_{n,n+1} \exp(2id_n k_n)}{1 + r'_{n-1,n} r'_{n,n+1} \exp(2id_n k_n)} \tag{6.2}$$

where you have n^{th} and $(n-1)^{th}$ layers. Here, k is the scattering vector within the species (normal to a surface), and d is the thickness of the species.

The momentum transfer perpendicular to the surface is given by (Ankner and Felcher 1999):

$$Q_z = k_{zf} - k_{zi} = \frac{4\pi}{\lambda}\sin\theta \tag{6.3}$$

where λ is the wavelength of the incident beam and θ is the angle of the beam with the surface. The momentum transfer is used in the calculation of the reflection of neutrons in which the incident and reflected beam wave vectors (k_i, k_f) enter and exit the surface at the same angle θ. The critical value of Q is obtained from: $Q_c^2 = 16\pi(b_i/V_i) + 16\pi(b/V)$, where b_s/V_s is the scattering length density (SLD) of the incident medium and b/V is the SLD of the subphase. SLD = b_j/V_j where V and b are the volume and neutron scattering length of atom j, respectively.

The experimentally obtained neutron reflectivity curve is analyzed by finding the model best describing the experimental data. The model contains a series of layers of different scattering densities and thicknesses along the normal distance from the surface.

6.2.2 Potential Calculation

For the purpose of comparison with the NR result, potential calculations are performed using the Derjaguin-Landau-Verwey-Overbeek (DLVO) theory. In the DLVO theory, the potential energy is mathematically expressed as a function of the separation distance between a spherical particle and a planar surface; in an aqueous solution, as the sum of two components, the electrostatic and van der Waals interactions (Hiemenz and Rajagopalan 1997):

$$\Phi = \frac{4\pi\zeta_{particle}\zeta_{surface} r \exp(-\kappa d)}{\varepsilon\kappa^2} - \frac{A_H r}{6d} \tag{6.4}$$

where ζ is the zeta-potential of a particle or a surface, r is the radius of the particle, κ is the inverse of the Debye length, ε is the permittivity, A_H is the Hamaker constant, and d is the distance between the particle and the surface. The first term in the formula represents the electrostatic interaction between a particle and a flat surface, while the second term represents the van der Waals interaction. The electrostatic interaction or electrical double-layer potential between charged surfaces in aqueous solutions is originated by accumulated ions near the charged surfaces to form the electrical double layers, while the van der Waals interaction arises from quantum-induced instantaneous polarization multipoles in molecules. The zeta-potentials needed in the calculations were measured using a zeta-meter for SiO_2 particles. For the flat surface, it was assumed that the zeta potential value is the same as that of a spherical particle of the same material.

6.3 Materials and Methods

6.3.1 Materials

Tetraethyl orthosilicate (TEOS, ≥99%) used in the preparation of the particles was purchased from Aldrich. Absolute ethanol (200 proof) was obtained from Decon Labs, and $NH_3 \cdot H_2O$ (28-30%, ACS) was purchased from BDH. All chemicals were used as received. Deionized water with 18.2 MΩ·cm resistivity was processed from a Millipore ultra-pure water system.

6.3.2 Nanoparticle Synthesis and Characterization

Colloidal SiO_2 nanoparticles were prepared by hydrolysis of TEOS in an alcohol medium in the presence of water and ammonia, according to a procedure originally described by Stöber *et al*. (1968). Hydrolysis and condensation of the TEOS monomers

catalyzed by ammonia provide stable spherical SiO_2 nanoparticles. In the modified synthesis procedure (Wang et al. 2003b, Wang et al. 2003a), two solutions of equal volume were rapidly mixed under vigorous stirring at controlled temperature of 23℃ or 50℃. One of the solutions contained ethanol and TEOS; and the other included ethanol, water, and ammonia. The total volume of the solutions was 250 ml with final concentrations of 0.3 M TEOS, 0.12 M NH_3, and 9.0 M H_2O. The reaction was allowed to continue with moderate stirring for two hours at the controlled temperatures and then at room temperature for 12 hours. After the synthetic reaction was completed, the SiO_2 particles were collected by centrifugation and washed with deionized water three times, then further purified by dialysis using dialysis tubes (Pierce Snake Skin^{TM}, 10,000 molecular weight cutoff) in deionized water.

Direct imaging of SiO_2 nanoparticles was obtained by a Hitachi S4700 scanning electron microscope (SEM) under an acceleration voltage of 10 kV. The average particle diameter, size distribution, and zeta potential of SiO_2 nanoparticles were determined by dynamic light scattering (DSL) with a Brookhaven 90Plus/ZetaPlus instrument. With initial reaction temperatures of 23℃ and 50℃, the resulting SiO_2 nanoparticles were 95.3 nm and 24.7 nm in average diameters with polydispersity 5.7% and 10.2% respectively, as determined by DSL measurements. The SiO_2 nanoparticles are negatively charged in water with ζ potentials of -47.9 mV and -51.7 mV for the 100-nm and 25-nm particles, respectively. Typical SEM images are shown in Figure 6.1.

6.3.3 Neutron Reflectometry

The neutron reflectivity study was conducted at the Spallation Neutron Source (SNS, Oak Ridge, TN) on the variable wavelength Liquid Reflectometer (Ankner et al. 2008). The wavelength band used were $2.5 < \lambda < 6$ Å, with the seven incident angle (θ =

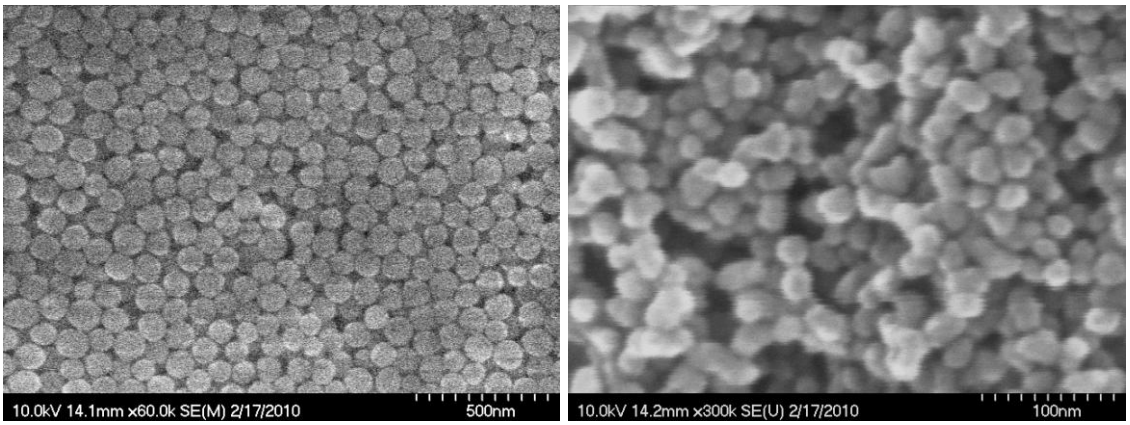

Figure 6.1 Electron microscopy images of synthesized SiO_2 nanoparticles. Nominal size: 100 nm (left), 25 nm (right).

0.15°, 0.25°, 0.45°, 0.65°, 0.85°, 1.6°, and 2.8°). The resolution ($\delta Q/Q$) of the instrument under the conditions used to collimate the neutron beam was determined by fitting the reflectivity data from D_2O and it was found to be 0.078. The experimental setup used for these measurements can be found in Figure 6.2.

The coherent scattering length densities (SLDs) of H_2O, SiO_2, $SiOx$, and Si (substrate) were calculated as -5.60×10^{-7}, 4.18×10^{-6}, 3.20×10^{-6}, and 2.07×10^{-6}, respectively, in units of $Å^{-2}$. A pure D_2O measurement was made to scale the H_2O data appropriately. Since H_2O has a negative SLD, the square root of Q_c^2 will yield an imaginary number, hence H_2O cannot achieve total reflection. Correction due to incoherent scattering and absorption was insignificant. Neutron reflectivity curves were calculated from the assumed SLD profiles and compared with measurements. This procedure was carried out carefully by utilizing statistical error minimization techniques until the agreement between the calculated reflectivity and the experimental reflectivity data was acceptable.

The ionic strength of the solution was adjusted with NaCl solution. Starting with a low ionic strength (0.0001 M) solution, we added concentrated NaCl solution to reach higher ionic-strength conditions. Between each experiment, the surface was cleaned by using an ultrasonic device, and the NR cell was cleaned by flushing the cell several times with deionized water in order to remove the particles deposited on the surface or remaining inside the cell.

To check the influence of time on particle deposition onto the surface, we repeated several times the experiment of one sample solution, without changing the sample solution. One cycle, with six different angles for each experiment, lasted for 40 minutes, and several randomly selected samples were repeated for measurements up to 10 cycles.

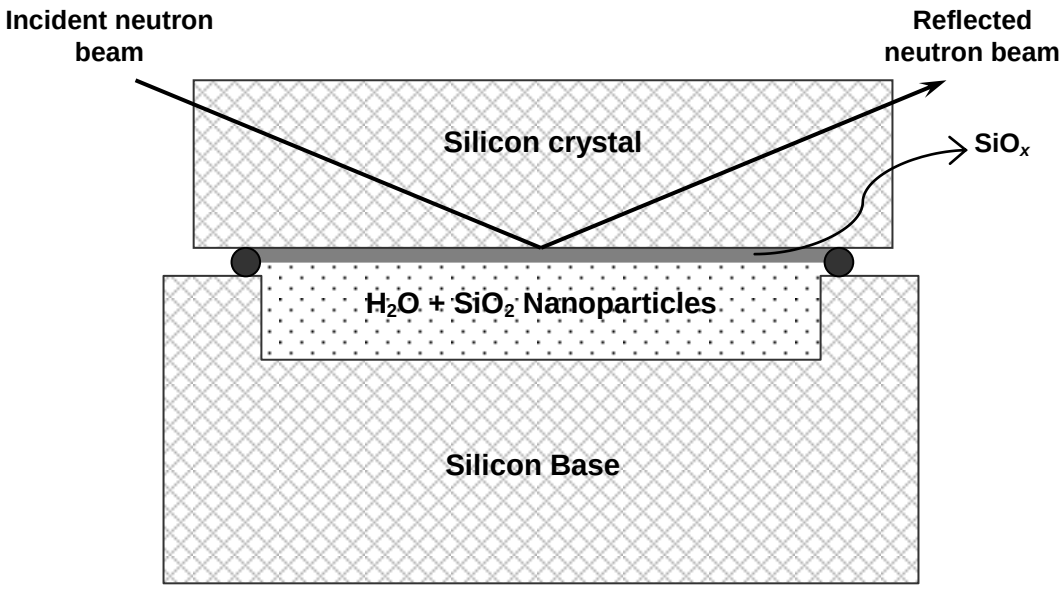

Figure 6.2 Schematic of the neutron reflectometry cell.

6.4 Results and Discussion

Experimental data obtained from NR and their analyzed results in terms of concentration profiles are presented in Figure 6.3 for 25-nm silica-particle suspensions in three different ionic-strength conditions (0.0001 M, 0.01 M, and 1 M). The description of the layers in the analyzed data is summarized in Tables 6.1. The model describing the experimental data is evaluated by a factor called χ^2. The χ^2 value indicates how closely the modeling results match the NR data. Lower χ^2 value means better description of the experimental data by the model. The χ^2 values of the analyzed results are acceptable for all conditions. The χ^2 value for the 1-M NaCl solution is higher than at other conditions, but still the lowest achievable. Experimental data and analysis for 100-nm silica particle suspensions in different ionic strengths similarly obtained by NR are summarized in the Figure 6.4 and Table 6.2.

Reproducibility measurements did not show significant differences for experiments run at the same conditions. The sample of 100-nm silica particles in 2-M NaCl solution was tested for 10 cycles and the results are shown in Figure 6.5. As shown in Figure 6.5, the resulting curves from the first and the last runs, which had more than 6 hours time in between, do not show a difference when they are plotted on the same graph. This result implies that particle deposition reached equilibrium within an hour.

DLVO calculations for the interaction of a 25-nm silica particle and a flat silica surface in three different solutions of ionic strengths, i.e., 0.0001 M, 0.01 M, and 1 M NaCl are shown in Figure 6.6 in order to qualitatively explain the particle distribution near the surface. An energy barrier was observed near the surface in the potential-distance profiles for low ionic-strength solutions (0.0001 M and 0.01 M NaCl), while no energy barrier was observed in the 1-M solution. When there is an energy barrier close to the flat surface, the particles are expected not to approach the surface. Therefore, a

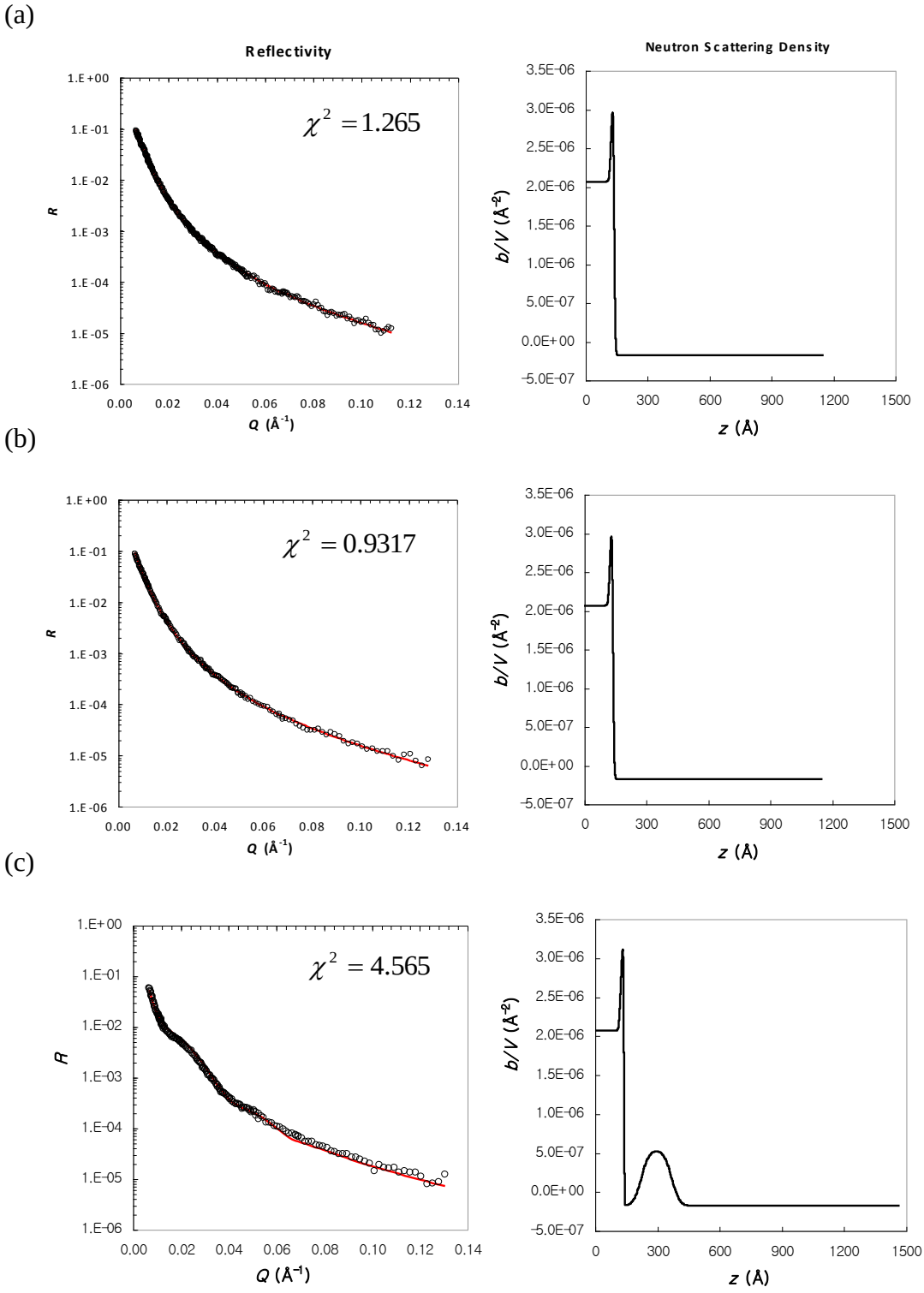

Figure 6.3 Neutron reflectivity data, model, and scattering density (b/V) versus layer depth (z), used to fit the data. Fitting results for 25-nm silica particles in three different solutions of ionic strength: 0.0001 M (a), 0.01 M (b), 1 M (c) NaCl.

Table 6.1 Model Parameters for 25-nm SiO_2 particles in 0.0001 M, 0.01 M, 1 M NaCl solution.

0.0001 M				0.01 M				1 M			
Slab	*b/V* (10^{-6} Å $^{-2}$)	*d* (Å)	σ (Å)	Slab	*b/V* (10^{-6} Å $^{-2}$)	*d* (Å)	σ (Å)	Slab	*b/V* (10^{-6} Å $^{-2}$)	*d* (Å)	σ (Å)
Si SiO_x	2.07 3.02	100.0 15.5	15.5 15.5	Si SiO_x	2.07 3.02	100.0 15.5	15.5 15.5	Si SiO_x	2.07 3.02	100.0 15.5	15.5 15.5
8.0 wt% SiO_2	-0.172	1000.0	10.0	8.0 wt% SiO_2	-0.172	1000.0	10.0	8.0 wt% SiO_2 25 nm SiO_2 8.0 wt% SiO_2	-0.172 0.531 -0.172	84.0 146.0 1000.0	5.0 70.0 70.0

(a)

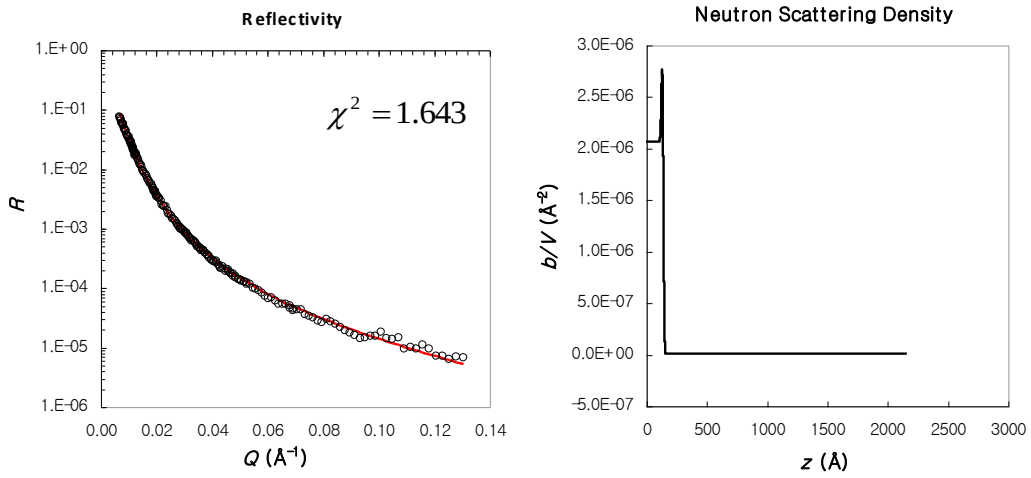

(b)

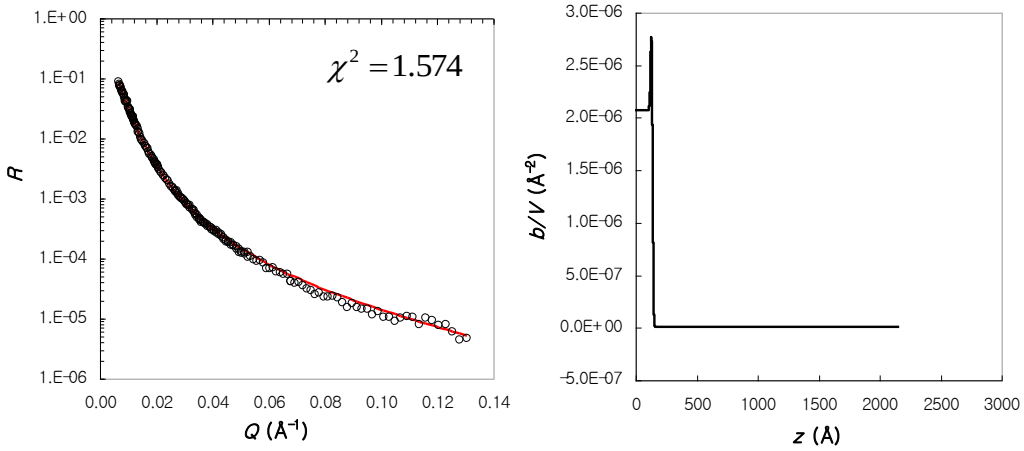

(c)

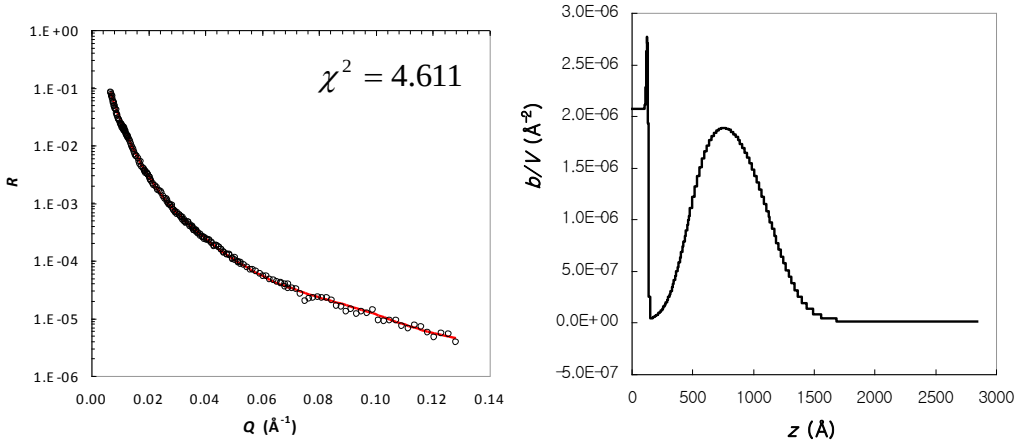

Figure 6.4 Neutron reflectivity data, model, and scattering density (b/V) versus layer depth (z), used to fit the data. Fitting results for 100-nm silica particles in solutions of various ionic strengths: 0.0001 M (a), 0.01 M (b), 0.1 M (c), 1 M (d), and 2 M (e) NaCl.

(d)

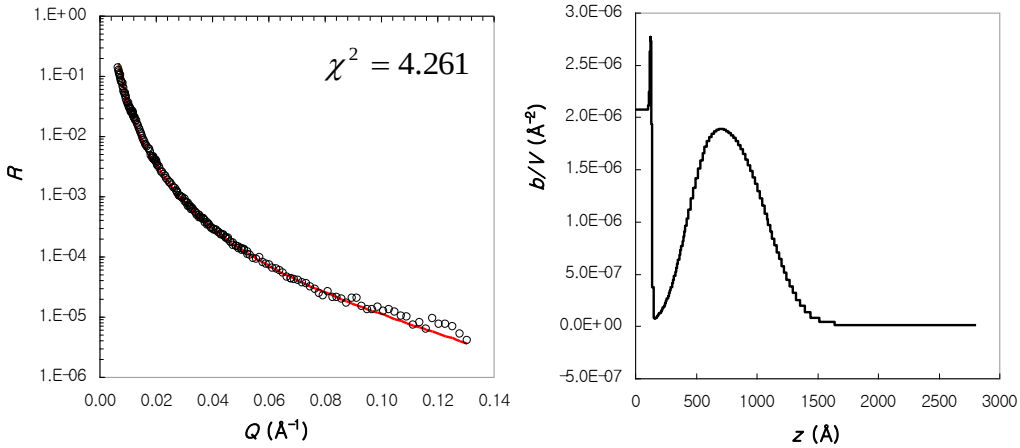

(e)

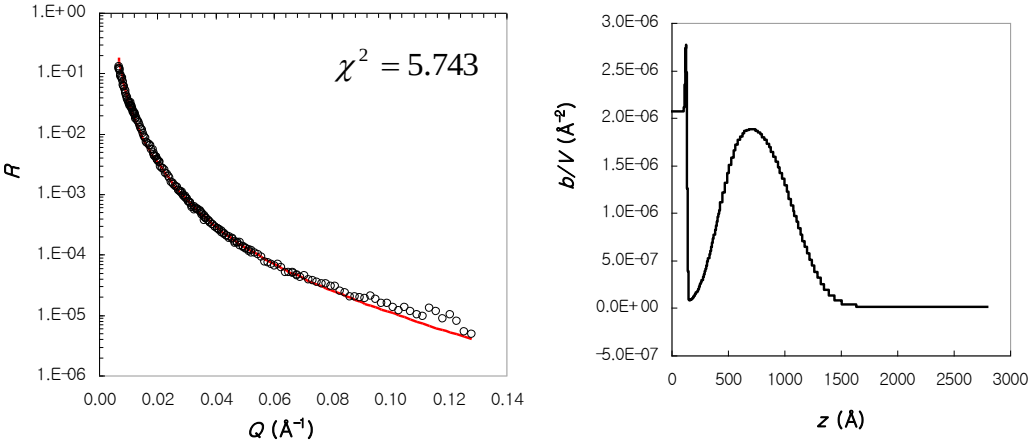

Figure 6.4 Neutron reflectivity data, model, and scattering density (b/V) versus layer depth (z), used to fit the data. Fitting results for 100-nm silica particles in solutions of various ionic strengths: 0.0001 M (a), 0.01 M (b), 0.1 M (c), 1 M (d), and 2 M (e) NaCl (Continued).

Table 6.2 Model Parameters for 100-nm SiO_2 particles in 0.0001 M, 0.01 M, 0.1 M, 1 M, and 2 M NaCl solution.

0.0001 M				0.01 M				0.1 M			
Slab	*b/V* (10^{-6} Å $^{-2}$)	*d* (Å)	*σ* (Å)	Slab	*b/V* (10^{-6} Å $^{-2}$)	*d* (Å)	*σ* (Å)	Slab	*b/V* (10^{-6} Å $^{-2}$)	*d* (Å)	*σ* (Å)
Si SiO_x	2.07 3.02	100.0 15.5	15.5 15.5	Si SiO_x	2.07 3.02	100.0 15.5	15.5 15.5	Si SiO_x	2.07 3.02	100.0 15.5	15.5 15.5
12.0 wt% SiO_2	0.00948	1000.0	15.0	12.0 wt% SiO_2	0.00948	1000.0	15.0	12.0 wt% SiO_2 100 nm SiO_2 12.0 wt% SiO_2	0.00948 2.0 0.00948	330.0 720.0 1000.0	15.5 330.0 500.0

Table 6.2 Model Parameters for 100-nm SiO_2 particles in 0.0001 M, 0.01 M, 0.1 M, 1 M, and 2 M NaCl solution (Continued).

1 M				2 M			
Slab	*b/V* (10^{-6} Å $^{-2}$)	*d* (Å)	σ (Å)	Slab	*b/V* (10^{-6} Å $^{-2}$)	*d* (Å)	σ (Å)
Si SiO_x	2.07 3.02	100.0 15.5	15.5 15.5	Si SiO_x	2.07 3.02	100.0 15.5	15.5 15.5
12.0 wt% SiO_2 100 nm SiO_2 12.0 wt% SiO_2	0.00948 2.0 0.00948	310.0 720.0 1000.0	15.5 310.0 500.0	12.0 wt% SiO_2 100 nm SiO_2 12.0 wt% SiO_2	0.00948 2.0 0.00948	300.0 720.0 1000.0	15.5 300.0 500.0

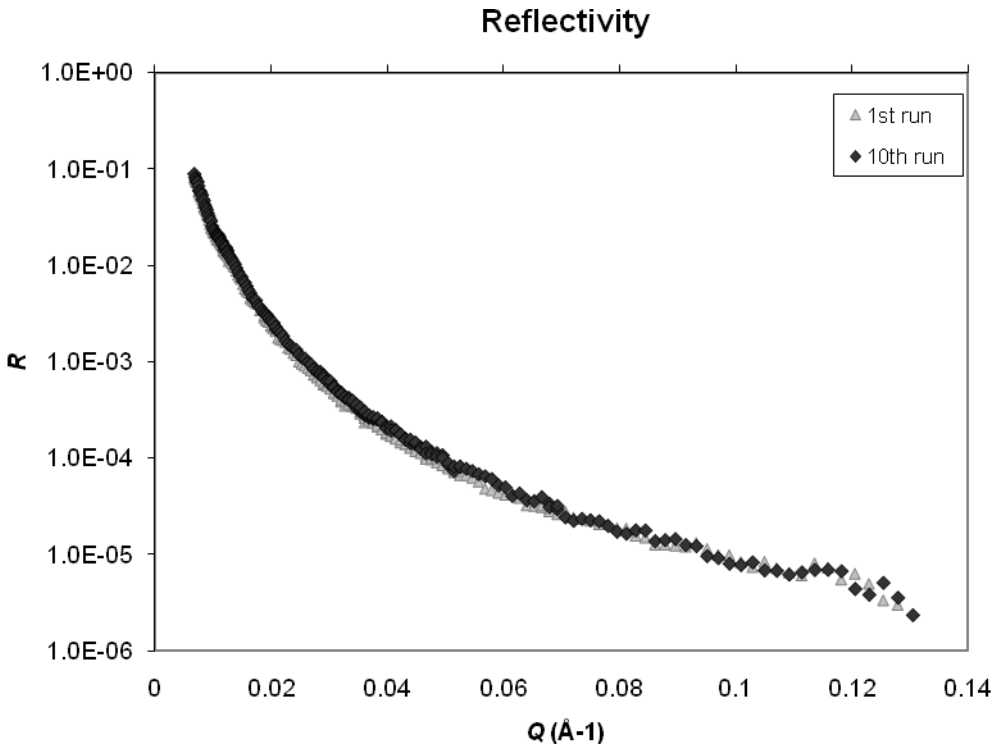

Figure 6.5 Repeated neutron reflectometry results for 100-nm silica particles in 2-M NaCl solution.

(a)

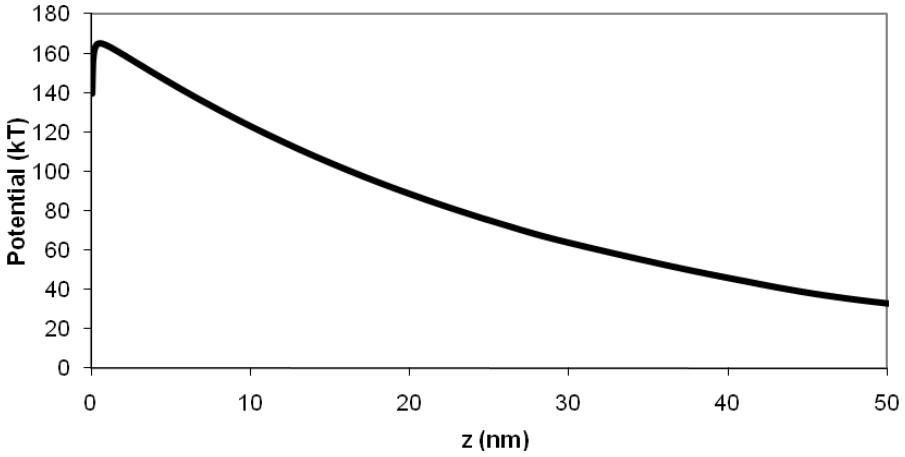

(b)

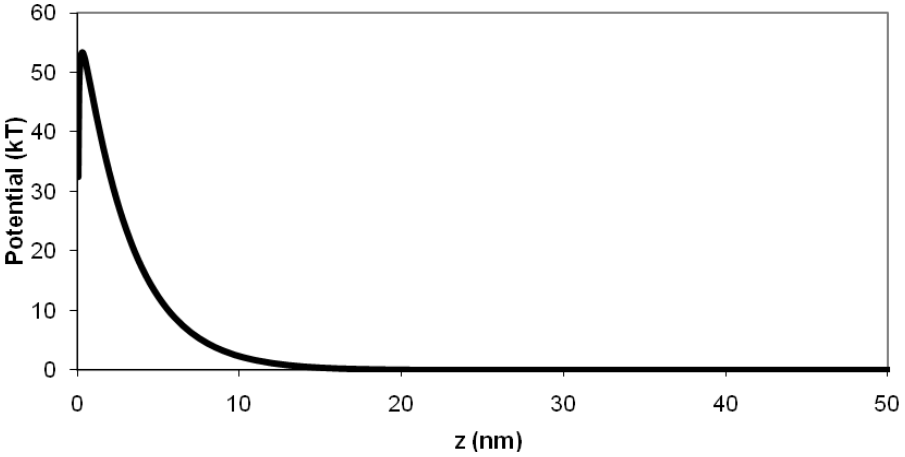

(c)

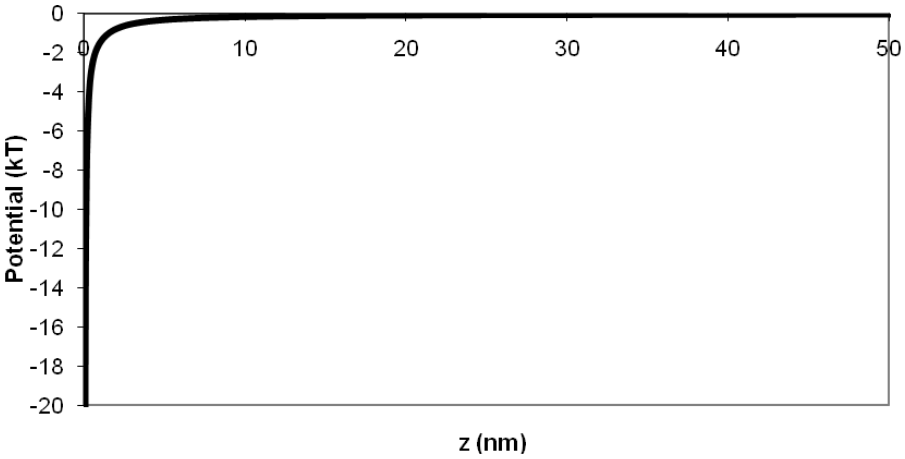

Figure 6.6 DLVO calculations for 25-nm silica particle solutions in three different solutions of ionic strength: 0.0001 M (a), 0.01 M (b), 1 M (c) NaCl.

particle concentration close to zero was expected at the surface, increasing up to the bulk concentration away from the surface. The concentration of particles in the analyzed modeling results, however, is the same as the bulk solution (8.18 wt% for 25-nm SiO_2 particle) for the entire *z* range as shown in Figure 6.3 and Table 6.1. This behavior indicates that the resolution or sensitivity of the NR measurements is not high enough to determine the thickness of a possible H_2O layer between the flat surface and the particles. Better contrast can be obtained by using D_2O.

The experiment with 25-nm particles in 1-M NaCl solution showed different results from the other concentrations with this particle size. In higher ionic-strength solutions, where DLVO calculations showed no energy barrier, the particles are attracted to the silica surface. The formation of a SiO_2 monolayer was observed in the neutron data. Since these particles are spherical in shape, a 3-layer slab model was used to fit the data as shown in Figure 6.7. The 84 Å layer closest to the silicon oxide (SiO_x) layer consists of a 42 Å $\left(=84-\left(\frac{1}{6}\right)250\right)$ layer of H_2O on which the SiO_2 particles float. The SiO_2 disk layer was found to be 146 Å thick (Table 6.1). From this information, the particle diameter was determined as 21.9 nm, which is very close to the particle size obtained from electron microscopy. The areal density of the spheres was extracted from the data by calculating the packing fraction. The closest packing possible for spheres in a plane is a triangular lattice or honeycomb. The maximum packing fraction was determined to be 0.907 in a monolayer using the honeycomb construction as the real fraction of circular cylindrical disks to hexagonal prism in two dimensions. The packing fraction (*F*) can be calculated using the scattering length densities of the SiO_2, H_2O, and the system of measurement: $(b/V)_{Measurement} = F(b/V)_{SiO_2} + (1-F)(b/V)_{H_2O}$. The actual packing fraction found in this system is 0.23.

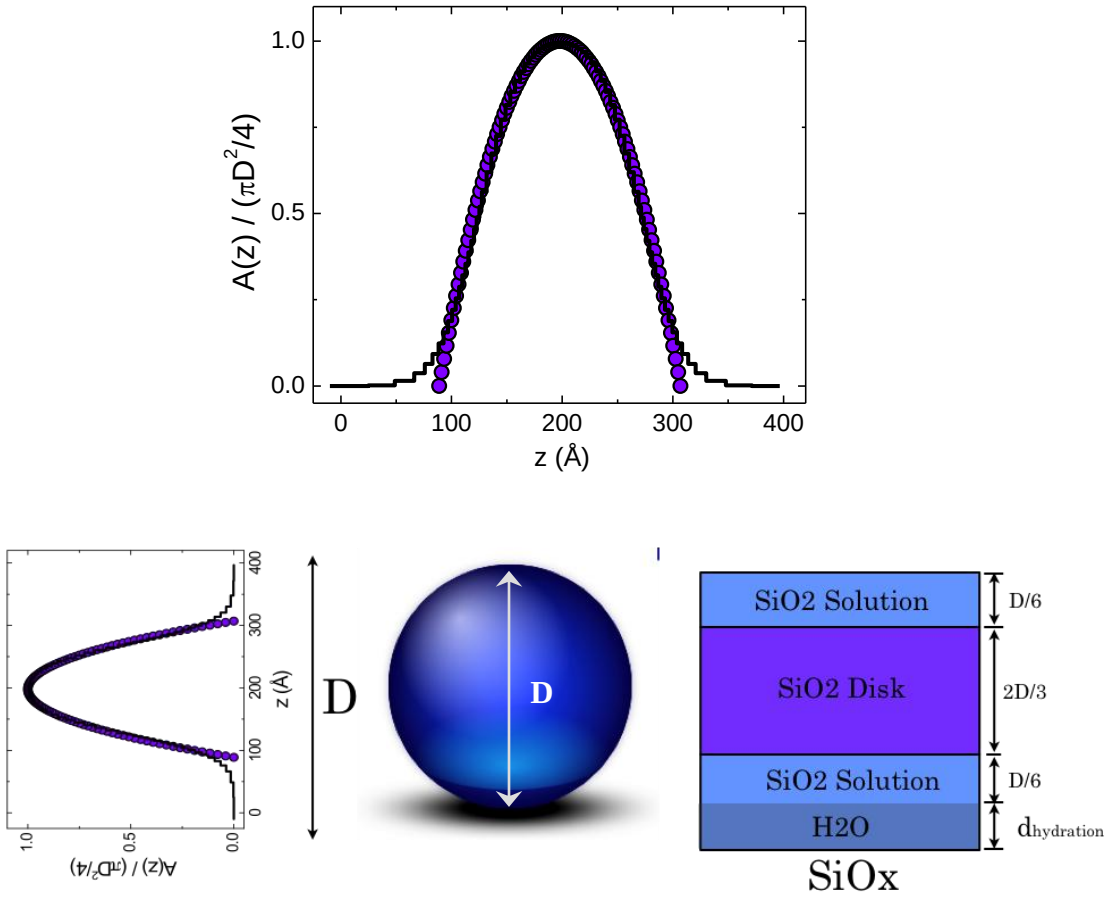

Figure 6.7 Model representation of the layers next to the surface with deposited SiO_2 particles.

At the end of the experiment, when the NR cell was disassembled, it was observed that the particle suspension had undergone gelation. This observation was made only for the 25-nm particles in high ionic-strength solution. During gelation, the particles aggregate with each other, forming large aggregates in which the particles are frozen in space. This phenomenon occurs in suspensions of high concentration of particles, undergoing rapid aggregation (Zackrisson et al. 2008). Not only the size, but also the variation of size and shape of the aggregates might have caused the unexpected results observed in this experiment (Smith and Zukoski 2006).

The 100-nm silica particle suspensions behave in the same manner as for 25-nm particles as shown in Figure 6.4 and Table 6.2. In low ionic-strength systems (0.0001 M and 0.01 M NaCl), the scattering length density plots showed the flat concentration profile with the concentration of bulk solution (i.e., 12 wt% SiO_2). Although potential calculations by the DLVO theory showed an energy barrier close to the surface (Figure 6.8), which means that a depletion of the particles was expected near the surface, the concentration of the particles is uniform in the entire system. High ionic-strength solutions (0.1 M, 1 M, and 2 M) for the 100-nm silica particle suspensions also showed similar behavior to that of the 25-nm particle suspensions in high ionic strength conditions. The model shows that particle deposition has been occurred. In 1-M NaCl solution, the depth of SiO_2 disk layer was 720 Å. Based on the model, the diameter of the particles was calculated at 108 nm, and the H_2O layer was determined to be 130 Å deep. The actual packing fraction in this system was calculated as 0.54. The reason that the packing fraction of the 25-nm particles was lower than this value is the strong attractive force between the particles that let to gelation of the 25-nm particles. Although all the suspensions with ionic strength from 0.1 M to 2 M NaCl have shown the same monolayer formations, the depths of the water layer on which the silica particles float varied slightly with the solution ionic strength. The thickness of the H_2O layer decreased from 150 Å to 120 Å as the ionic strength increases. From this information, it can be concluded that the

(a)

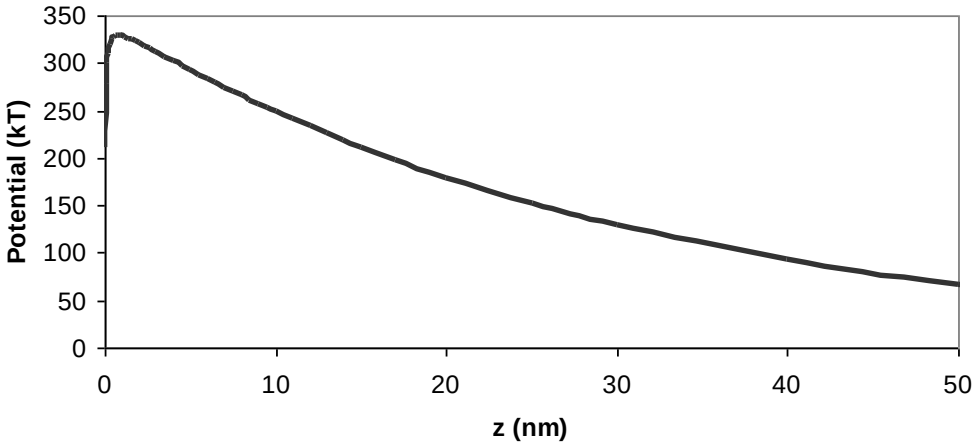

(b)

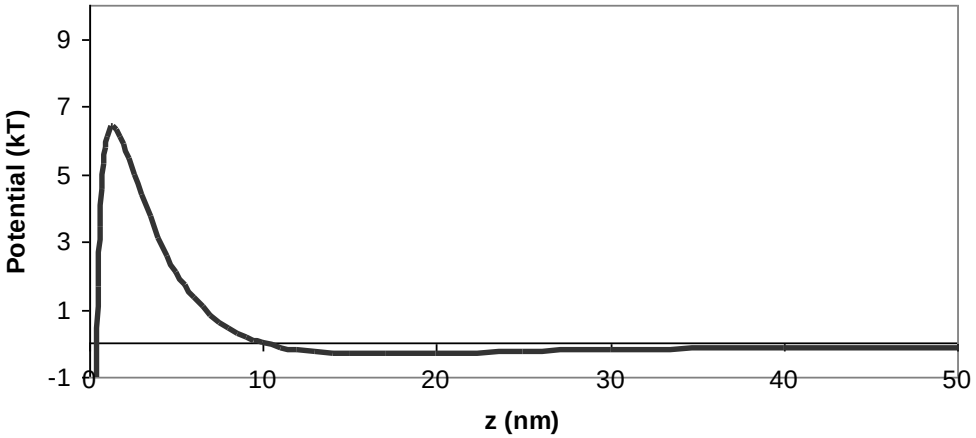

(c)

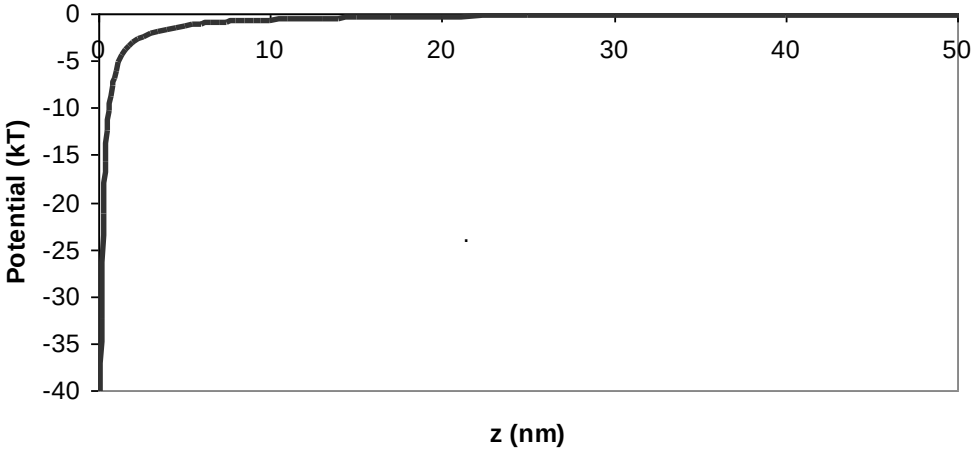

Figure 6.8 DLVO calculations for 100-nm silica particles in solutions of various ionic strengths: 0.0001 M (a), 0.01 M (b), 0.1 M (c), 1 M (d), and 2 M (e) NaCl.

(d)

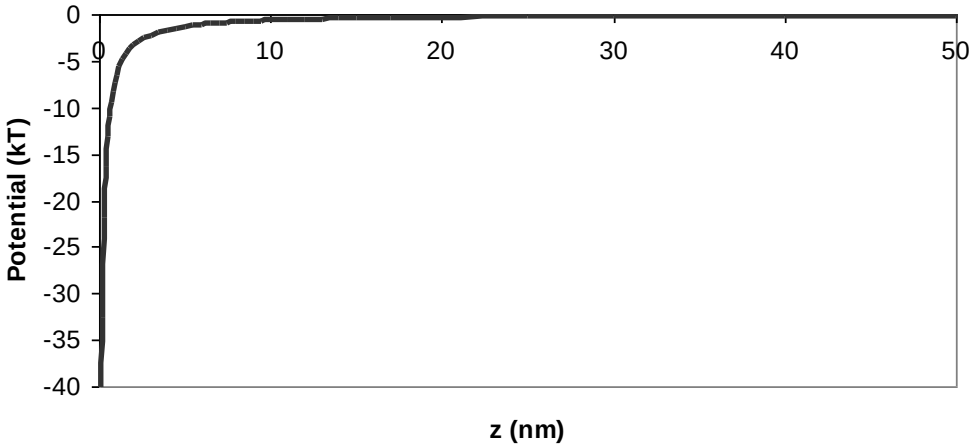

(e)

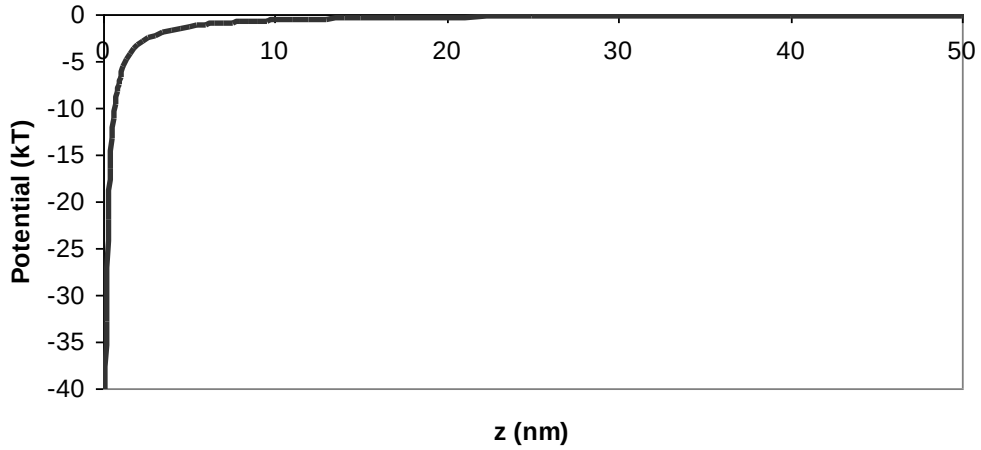

Figure 6.8 DLVO calculations for 100-nm silica particles in solutions of various ionic strengths: 0.0001 M (a), 0.01 M (b), 0.1 M (c), 1 M (d), and 2 M (e) NaCl (Continued).

silica particle monolayer is formed closer to the planar surface as the ionic strength increases.

6.5 Summary

Through this study, the possibility that NR could be used as a tool to investigate particle deposition at a flat surface in aqueous solutions was tested. This experimental method has some advantages compared to other experimental tools, such as observation of particles within several nanometers from the surface and observation over a large population of particles that represent very well the behavior of the whole system. The results agree reasonably well with DLVO calculations between a particle and a surface, but there are also some disagreements that need to be further studied. Results of such studies can be used to predict aggregation between particles, as well as deposition on filter materials and membranes.

CHAPTER 7

CONCLUSIONS AND RECOMMENDATIONS

This research combines experimental and theoretical investigations of the interactions between colloidal particles and planar surfaces in atmospheric and aqueous environments. The adhesion or detachment of the particles onto or from the surfaces, the force-distance profiles between a particle and a surface, and the concentration profile of particles near a surface as a result of the surface charge were examined.

Measurements of the adhesion force of microbial colloids on surfaces obtained using atomic force microscopy (AFM) and theoretical calculations have significance in the characterization of the adhesion force and its components. Quantitative information of the total adhesion force and knowledge of the possible contributing forces help delineate the effect of relative humidity, hydrophobicity of surfaces, surface charge, and other properties of the materials involved on the adhesion force.

The force-distance profile data obtained by AFM and calculated by the classical DLVO theory indicate that the interaction force or potential energy between a microbial particle and a surface in aquatic solutions is influenced by the chemistry of the solution, e.g., pH or ionic strength. The values of the zeta potential of the surfaces, which are directly affected by the pH and ionic strength of the solution, determine the magnitude of the electrostatic interaction.

Knowledge gained from neutron reflectometry has significance in visualizing the distribution of particles near a charged surface in an aqueous solution. The study provides information on the concentration profile of particles at the surface and in the solution near the surface.

Through experimental data obtained from various techniques and model calculations of the adhesion force and the force-distance profile, the following conclusions can be stated:

- It was shown through AFM measurements that the adhesion force of microbial colloids on planar surfaces in atmospheric environments is a strong function of the relative humidity. A theoretical treatment assumed that the adhesion force consists of the van der Waals, capillary, and electrostatic forces. The capillary meniscus between interacting surfaces is not formed below a certain level of the relative humidity, which depends upon the hydrophobicity of the material expressed by the contact angle, thus the adhesion force is composed only of van der Waals and electrostatic forces in low relative humidity conditions. At higher humidity values, the condensed water between the particle and the surface forms a meniscus that causes a decrease of the van der Waals force and an increase of the capillary force. The electrostatic force decreases with increasing relative humidity as a result of decreasing surface charge. This study can be used to build criteria for decontamination of surfaces that have attached particulate contaminants such as bioaerosols on them in atmospheric environments. Because the adhesion force depends on humidity, the relative humidity level on which the adhesion force is minimized could be determined based on the geometry and material properties of the surfaces.

- A possible explanation of the discrepancy observed between theoretical model calculations and AFM measurements of the adhesion force is the surface roughness of the spore and planar surface, which is neglected in the model. The roughness of the *Bt* spore was observed in AFM, SEM, and STEM images. An estimation of the surface roughness was indirectly obtained through the adhesion

force measurements in aqueous solutions between the spore and planar surfaces. By comparison of the AFM measurements and theoretical calculations, the surface roughness of *Bt* spores that describes best the measurements was determined.

- Force-distance profiles between the *Bt* spore and planar surfaces in aqueous solutions were obtained using AFM. Based on the measured zeta potentials of the spore and surfaces, the force-distance curves were calculated through the DLVO theory. The results indicated that the interactions between spores and planar surfaces are influenced by the properties of the solution, such as pH and ionic strength. The DLVO theory was adequate in explaining the interactions between the spores and planar surfaces used in this study, therefore, it can be concluded that the van der Waals and electrostatic interaction forces are dominant components of the interaction between a *Bt* spore and a planar surface in an aqueous solution. It should be noted here that the capillary force does not exist in aqueous solutions. The implications of this study include treatment of contaminated water by filtration, coagulation, and sedimentation. We can control the conditions of the system in order to induce attractive or repulsive forces between particulate contaminants and surfaces. In addition, control of the pH or salt concentration in the solution can help the recovery of used filter media. Similarly, applications of this study can be found in water treatment systems.

- Further experimental investigation of the interactions between colloidal particles and planar surfaces was carried out using neutron reflectometry. This experimental technique provides structural information of the distribution of a large population of particles near surfaces. The theory predicts that the potential energy is highly dependent on the ionic strength. For 0.0001 and 0.01 M NaCl

solutions, the particles concentration near the surface obtained from NR is the same as the bulk concentration, while depletion of particles near the surface was expected because of the repulsion that the DLVO theory predicts. This result may be due to inadequate resolution of the measurements and calls for further investigation. In contrast, in solutions of higher ionic strength, where the theoretical calculations show an attractive force between the particle and the surface and particles, a high concentration of adsorbed particles is observed near the flat silica surface. The study confirmed that neutron reflectometry is a promising tool for the investigation of particle-surface interactions in order to provide insight into the deposition of particles onto planar surfaces.

In this study, theoretical model calculations were compared to experimental measurements. Through this comparison, the mechanisms of interaction phenomena between a particle and a surface can be identified. The implications of this research are two-fold: (i) the mechanisms and parameters involved in particle interactions with environmental surfaces are identified, contributing to the understanding of the phenomenon, and (ii) the results may help us devise better means for the removal of spores and other biological particles from environmental surfaces.

Although this research identified the mechanisms of particle-surface interactions, further work is needed both experimentally and theoretically to improve the agreement quantitatively. It is known that the point of contact between a particle and a planar surface affects the adhesion force of the particle onto the surface in atmospheric conditions. Therefore, the roughness of both the particle and planar surface should have an influence on the adhesion due to the changes it can cause in the number of contact points and the separation distance between the particle and the surface. Consideration of the point of contact and the separation distance will enable us to predict more accurately the adhesion force components.

Although the DLVO theory explains the interaction between a *Bt* spore and a planar surface adequately, several studies on the adhesion of living bacterial cells onto surfaces pointed out that hydrophobicity plays a role in the adhesion force. Although the effect of hydrophobicity is incorporated in terms of the contact angle in the capillary force model, it is recommended to consider additional force components in the DLVO model, such as acid-base or hydrophobic interactions, especially for the adhesion of microbial colloids.

Further work using neutron reflectometry is also recommended and is currently pursued as an extension of this research. Although the neutron reflectometry experiments confirmed its potential for the investigation of particle-surface interactions, various factors need to be examined in order to obtain better resolution in the measurements. More experiments are recommended to include a variety of materials for the particles, such as microbial colloids and nanoparticle contaminants, and different solution conditions, such as ionic strength and pH. Experimental results that do not show a good agreement with the classical DLVO theory may need to be compared with other theoretical calculations such as the extended DLVO theory and molecular simulations. Furthermore, it is recommended to use neutron reflectometry to obtain a better understanding of the electrical double layer at the solid-liquid interface by studying ion, rather than particle, distribution near the surface.

REFERENCES

Abu-Lail, N. I.; Camesano, T. A., Specific and nonspecific interaction forces between *Escherichia coli* and silicon nitride, determined by Poisson statistical analysis. *Langmuir* **2006**, 22 (17), 7296-7301.

Ankner, J. F.; Felcher, G. P., Polarized-neutron reflectometry. *Journal of Magnetism and Magnetic Materials* **1999**, 200 (1-3), 741-754.

Ankner, J. F.; Tao, X.; Halbert, C. E.; Browning, J. F.; Kilbey, S. M.; Swader, O. A.; Dadmun, M. S.; Kharlampieva, E.; Sukhishvili, S. A., The SNS liquid reflectometer. *Neutron News* **2008**, 19 (3), 14-16.

Asay, D. B.; Barnette, A. L.; Kim, S. H., Effects of water adsorption on silicon oxide nano-asperity adhesion in ambient conditions. *Contact Angle Wettability Adhesion* **2009**, 6, 65-79.

Biggs, S.; Cain, R. G.; Dagastine, R. R.; Page, N. W., Direct measurements of the adhesion between a glass particle and a glass surface in a humid atmosphere. *Journal of Adhesion Science and Technology* **2002**, 16 (7), 869-885.

Bovallius, A.; Bucht, B.; Roffey, R.; Anas, P., Long-range air transmission of bacteria. *Applied and Environmental Microbiology* **1978**, 35 (6), 1231-1232.

Bowen, W. R.; Lovitt, R. W.; Wright, C. J., Direct quantification of *Aspergillus niger* spore adhesion to mica in air using an atomic force microscope. *Colloids and Surfaces a-Physicochemical and Engineering Aspects* **2000**, 173 (1-3), 205-210.

Brown, D. G.; Jaffe, P. R., Effects of nonionic surfactants on the cell surface hydrophobicity and apparent Hamaker constant of a *Sphingomonas* sp. *Environmental Science & Technology* **2006**, 40 (1), 195-201.

Butt, H. J.; Farshchi-Tabrizi, M.; Kappl, M., Using capillary forces to determine the geometry of nanocontacts. *Journal of Applied Physics* **2006**, 100 (2) 024312.

Camesano, T. A.; Unice, K. M.; Logan, B. E., Blocking and ripening of colloids in porous media and their implications for bacterial transport. *Colloids and Surfaces a-Physicochemical and Engineering Aspects* **1999**, 160 (3), 291-308.

Capella, B.; Baschieri, P.; Frediani, C.; Miccoli, P.; Ascoli, C., Force-distance curves by AFM - A powerful technique for studying surface interactions. *Ieee Engineering in Medicine and Biology Magazine* **1997**, 16 (2), 58-65.

Caruso, F.; Rodda, E.; Furlong, D. F.; Niikura, K.; Okahata, Y., Quartz crystal microbalance study of DNA immobilization and hybridization for nucleic acid sensor development. *Analytical Chemistry* **1997**, 69 (11), 2043-2049.

Chada, V. G. R.; Sanstad, E. A.; Wang, R.; Driks, A., Morphogenesis of *Bacillus* spore surfaces. *Journal of Bacteriology* **2003**, 185 (21), 6255-6261.

Chin, C. J.; Yiacoumi, S.; Tsouris, C., Influence of metal ion sorption on colloidal surface forces measured by atomic force microscopy. *Environmental Science & Technology* **2002**, 36 (3), 343-348.

Chung, E.; Kweon, H.; Yiacoumi, S.; Lee, I.; Joy, D. C.; Palumbo, A. V.; Tsouris, C., Adhesion of spores of *Bacillus thuringiensis* on a planar surface. *Environmental Science & Technology* **2010a**, 44 (1), 290-296.

Chung, E.; Yiacoumi, S.; Lee, I.; Tsouris, C., The role of the electrostatic force in spore adhesion. *Environmental Science & Technology* **2010b**, 44 (16), 6209-6214.

Cliffel, D. E.; Bard, A. J.; Shinkai, S., Electrochemistry of tert-butylcalix 8 arene - C-60 films using a scanning electrochemical microscope - Quartz crystal microbalance. *Analytical Chemistry* **1998**, 70 (19), 4146-4151.

Costerton, J. W.; Stewart, P. S.; Greenberg, E. P., Bacterial biofilms: A common cause of persistent infections. *Science* **1999**, 284 (5418), 1318-1322.

Cross, N. L.; Picknett, R. G., *Particle adhesion in the presence of a liquid film*. Butterworths: London, 1963.

Custodio, E. *Groundwater Protection and Contamination*, Special edition based on selected papers of The Global Importance of Groundwater in the 21st Century: Proceedings of the International Symposium on Groundwater Sustainability in Alicante, Spain. NGWA Press: Westerville, OH, 2006.

Czarnecki, W. S.; Schein, L. B., Electrostatic force acting on a spherically symmetric charge distribution in contact with a conductive plane. *Journal of Electrostatics* **2004**, 61 (2), 107-115.

de Kerchove, A. J.; Weronski, P.; Elimelech, M., Adhesion of nonmotile *Pseudomonas aeruginosa* on "soft" polyelectrolyte layer in a radial stagnation point flow system: Measurements and model predictions. *Langmuir* **2007**, 23 (24), 12301-12308.

Dorobantu, L. S.; Bhattacharjee, S.; Foght, J. M.; Gray, M. R., Analysis of force interactions between AFM tips and hydrophobic bacteria using DLVO theory. *Langmuir* **2009**, 25 (12), 6968-6976.

Driks, A., The dynamic spore. *Proceedings of the National Academy of Sciences of the United States of America* **2003**, 100 (6), 3007-3009.

Elimelech, M.; Gregory, J.; Jia, X.; Williams, R. A., *Particle Deposition and Aggregation: Measurement, Modeling and Simulation*. Butterworth-Heinemann: Oxford, 1995.

Emerson, R. J.; Camesano, T. A., Nanoscale investigation of pathogenic microbial adhesion to a biomaterial. *Applied and Environmental Microbiology* **2004**, 70 (10), 6012-6022.

Faille, C.; Jullien, C.; Fontaine, F.; Bellon-Fontaine, M. N.; Slomianny, C.; Benezech, T., Adhesion of *Bacillus* spores and *Escherichia coli* cells to inert surfaces: role of surface hydrophobicity. *Canadian Journal of Microbiology* **2002**, 48 (8), 728-738.

Farshchi-Tabrizi, M.; Kappl, M.; Cheng, Y. J.; Gutmann, J.; Butt, H. J., On the adhesion between fine particles and nanocontacts: An atomic force microscope study. *Langmuir* **2006**, 22 (5), 2171-2184.

Feng, J. Q.; Hays, D. A., Relative importance of electrostatic forces on powder particles. *Powder Technology* **2003**, 135, 65-75.

Feng, J. Q.; Hays, D. A., Theory of electric field detachment of charged toner particles in electrophotography. *Journal of Imaging Science and Technology* **2000**, 44 (1), 19-25.

Fowlkes, W. Y.; Robinson, K. S., The electrostatic force on a dielectric sphere resting on a conducting substrate. In *Particle on Surfaces: 1. Detection, Adhesion, and Removal*, Mittal, K. L., Ed. Plenum: New York, **1988**; 143-155.

Fragneto-Cusani, G., Neutron reflectivity at the solid/liquid interface: examples of applications in biophysics. *Journal of Physics-Condensed Matter* **2001**, 13 (21), 4973-4989.

Fuzzi, S.; Mandrioli, P.; Perfetto, A., Fog droplets - An atmospheric source of secondary biological aerosol particles. *Atmospheric Environment* **1997**, 31 (2), 287-290.

Gargallo, R.; Hunenberger, P. H.; Aviles, F. X.; Oliva, B., Molecular dynamics simulation of highly charged proteins: Comparison of the particle-particle particle-mesh and reaction field methods for the calculation of electrostatic interactions. *Protein Science* **2003**, 12 (10), 2161-2172.

Gerhardt, P.; Pankratz, H. S.; Scherrer, R., Fine-structure of *Bacillus thuringiensis* spore. *Applied and Environmental Microbiology* **1976**, 32 (3), 438-440.

Giorno, R.; Bozue, J.; Cote, C.; Wenzel, T.; Moody, K. S.; Mallozzi, M.; Ryan, M.; Wang, R.; Zielke, R.; Maddock, J. R.; Friedlander, A.; Welkos, S.; Driks, A., Morphogenesis of the *Bacillus anthracis* spore. *Journal of Bacteriology* **2007**, 189 (3), 691-705.

Griffin, D. W., Terrestrial microorganisms at an altitude of 20,000 m in Earth's atmosphere. *Aerobiologia* **2004**, 20 (2), 135-140.

Grundy, M. J.; Richardson, R. M.; Roser, S. J.; Penfold, J.; Ward, R. C., X-ray and neutron reflectivity from spread monolayers. *Thin Solid Films* **1988**, 159, 43-52.

Hahn, M. W.; O'Melia, C. R., Deposition and reentrainment of Brownian particles in porous media under unfavorable chemical conditions: Some concepts and applications. *Environmental Science & Technology* **2004**, 38 (1), 210-220.

Hartley, P. G.; Larson, I.; Scales, P. J., Electrokinetic and direct force measurements between silica and mica surfaces in dilute electrolyte, solutions. *Langmuir* **1997**, 13 (8), 2207-2214.

Hartmann, G. C.; Marks, L. M.; Yang, C. C., Physical models for photoactive pigment electrophotography. *Journal of Applied Physics* **1976**, 47 (12), 5409-5420.

Harvey, R. W.; Metge, D. W.; Shapiro, A. M.; Renken, R. A.; Osborn, C. L.; Ryan, J. N.; Cunningham, K. J.; Landkamer, L., Pathogen and chemical transport in the karst limestone of the Biscayne aquifer: 3. Use of microspheres to estimate the transport potential of *Cryptosporidium parvum oocysts*. *Water Resources Research* **2008**, 44 (8), W08429.

Hays, D. A. Adhesion of charged-particles. *Journal of Adhesion Science and Technology* **1995**, 9 (8), 1063-1073.

Hays, D. A.; Sheflin, J. C. Electrostatic adhesion of ion and triboelectric-charged particles. *Journal of Electrostatics* **2005**, 63 (6-10), 687-692.

Hiemenz, P. C.; Rajagopalan, R., *Principles of Colloid and Surface Chemistry*. 3rd ed.; Marcel Dekker: New York, 1997.

Ho, J.; Duncan, S., Estimating aerosol hazards from an anthrax letter. *Journal of Aerosol Science* **2005**, 36 (5-6), 701-719.

Hoek, E. M. V.; Agarwal, G. K., Extended DLVO interactions between spherical particles and rough surfaces. *Journal of Colloid and Interface Science* **2006**, 298 (1), 50-58.

Husmark, U.; Ronner, U., Forces involved in adhesion of *bacillus-cereus* spores to solid-surfaces under different environmental-conditions. *Journal of Applied Bacteriology* **1990**, 69 (4), 557-562.

Israelachvili, J., *Intermolecular and Surface Forces*. 2nd ed.; Academic Press: San Diego, 1998.

Jacobs, H. O.; Leuchtmann, P.; Homan, O. J.; Stemmer, A., Resolution and contrast in Kelvin probe force microscopy. *Journal of Applied Physics* **1998**, 84 (3), 1168-1173.

Jiang, G. M.; Noonan, M. J.; Ratecliffe, T. J., Effects of soil matric suction on retention and percolation of *Bacillus subtilis* in intact soil cores. *Water Air and Soil Pollution* **2006**, 177 (1-4), 211-226.

Kalinin, S.; Gruverman, A., *Scanning Probe Microscopy: Electrical and Electromechanical Phenomena at the Nanoscale*. Springer Science+Business Media, LLC: New York, NY, 2007; Vol. I & II.

Keller, A. A.; Auset, M., A review of visualization techniques of biocolloid transport processes at the pore scale under saturated and unsaturated conditions. *Advances in Water Resources* **2007**, 30, 1392-1407.

Keller, C. A.; Kasemo, B., Surface specific kinetics of lipid vesicle adsorption measured with a quartz crystal microbalance. *Biophysical Journal* **1998**, 75 (3), 1397-1402.

Kellogg, C. A.; Griffin, D. W., Aerobiology and the global transport of desert dust. *Trends in Ecology & Evolution* **2006**, 21 (11), 638-644.

Kim, M.; Boone, S. A.; Gerba, C. P., Factors that influence the transport of *Bacillus cereus* spores through sand. *Water Air and Soil Pollution* **2009**, 199 (1-4), 151-157.

Kinoshita, T.; Bales, R. C.; Yahya, M. T.; Gerba, C. P., Bacteria transport in a porous-medium - retention of *bacillus* and *pseudomonas* on silica surfaces. *Water Research* **1993**, 27 (8), 1295-1301.

Kumar, G.; Smith, S.; Jaiswal, R.; Beaudoin, S., Scaling of van der Waals and electrostatic adhesion interactions from the micro- to the nano-scale. *Journal of Adhesion Science and Technology* **2008**, 22 (5-6), 407-428.

Kuske, C. R., Current and emerging technologies for the study of bacteria in the outdoor air. *Current Opinion in Biotechnology* **2006**, 17 (3), 291-296.

Lai, A. C. K.; Wang, K.; Chen, F. Z., Experimental and numerical study on particle distribution in a two-zone chamber. *Atmospheric Environment* **2008**, 42 (8), 1717-1726.

Lee, I.; Justus, B. L.; Lee, J. W.; Greenbaum, E., Molecular photovoltaics and surface potentials at the air-water interface. *Journal of Physical Chemistry B* **2003**, 107 (51), 14225-14230.

Li, B. K.; Logan, B. E. Bacterial adhesion to glass and metal-oxide surfaces. *Colloids and Surfaces - B* **2004**, 36, (2), 81-90.

Li, Z. X.; Thirtle, P. N.; Weller, A.; Thomas, R. K.; Penfold, J.; Webster, J. R. P.; Rennie, A. R., Some improvements and extensions of the application of specular neutron reflection to the study of interfaces. *Physica B-Condensed Matter* **1998**, 248, 171-183.

Lin, Y., *Mars technology program planetary protection technology development*. In Aerospace Conference, IEEE: 2006.

Lvov, Y.; Ariga, K.; Onda, M.; Ichinose, I.; Kunitake, T., Alternate assembly of ordered multilayers of SiO_2 and other nanoparticles and polyions. *Langmuir* **1997**, 13 (23), 6195-6203.

Madigan, M. T.; Martinko, J. M.; Parker, J., *Brock biology of microorganisms*. 10th ed.; Prentice Hall: Englewood Cliffs, NJ, 2002.

Marx, K. A., Quartz crystal microbalance: A useful tool for studying thin polymer films and complex biomolecular systems at the solution-surface interface. *Biomacromolecules* **2003**, 4 (5), 1099-1120.

Matsuyama, T.; Ohtsuka, M. A.; Yamamoto, H., Measurement of force curve due to electrostatic charge on a single particle using atomic force microscope. *Kona-Powder and Particle* **2008**, 26, 238-245.

Ong, Y. L.; Razatos, A.; Georgiou, G.; Sharma, M. M., Adhesion forces between *E-coli* bacteria and biomaterial surfaces. *Langmuir* **1999**, 15 (8), 2719-2725.

Orr, F. M.; Scriven, L. E.; Rivas, A. P., Pendular rings between solids - meniscus properties and capillary force. *Journal of Fluid Mechanics* **1975**, 67 (FEB25), 723-742.

Ouyang, Q.; Ishida, K.; Okada, K. Investigation of micro-adhesion by atomic force microscopy. *Applied Surface Science* **2001**, 169, 644-648.

Pang, L. P.; Close, M.; Goltz, M.; Noonan, M.; Sinton, L., Filtration and transport of *Bacillus subtilis* spores and the F-RNA phage MS2 in a coarse alluvial gravel aquifer: Implications in the estimation of setback distances. *Journal of Contaminant Hydrology* **2005**, 77 (3), 165-194.

Pang, L. P.; Close, M.; Noonan, M., Rhodamine WT and *Bacillus subtilis* transport through an alluvial gravel aquifer. *Ground Water* **1998**, 36 (1), 112-122.

Pang, L.; Close, M.; Flintoft, M., Attenuation and transport characteristics of cadmium, zinc and lead in selected New Zealand aquifer systems. *Journal of Hydrology* (Wellington North) **2004**, 43 (2), 95-110.

Penfold, J.; Thomas, R. K., The application of the specular reflection of neutrons to the study of surfaces and interfaces. *Journal of Physics-Condensed Matter* **1990**, 2 (6), 1369-1412.

Peters, M. H., Fokker-Planck equation, molecular friction, and molecular dynamics for Brownian particle transport near external solid surfaces. *Journal of Statistical Physics* **1999**, 94 (3-4), 557-586.

Petrov, A. B.; Gallyamov, R. R., Polymer surface deformation under semicontact-mode AFM scanning. *Russian Microelectronics* **2007**, 36 (3), 164-170.

Plomp, M.; Leighton, T. J.; Wheeler, K. E.; Malkin, A. J., The high-resolution architecture and structural dynamics of *Bacillus* spores. *Biophysical Journal* **2005**, 88 (1), 603-608.

Pollock, H. M.; Burnham, N. A.; Colton, R. J. Attractive forces between micron-sized particles: A patch charge model. *Journal of Adhesion* **1995**, 51 (1-4), 71-86.

Prier, K. R. S.; Lighthart, B.; Bromenshenk, J. J., Adsorption model of aerosolized bacterial spores (*Bacillus subtilis* variety *niger*) onto free-flying honey bees (*Hymenoptera* : *Apidae*) and its validation. *Environmental Entomology* **2001**, 30 (6), 1188-1194.

Redmond, C.; Baillie, L. W. J.; Hibbs, S.; Moir, A. J. G.; Moir, A., Identification of proteins in the exosporium of *Bacillus anthracis*. *Microbiology-Sgm* **2004**, 150, 355-363.

Reshetin, V. P.; Regens, D., Evaluation of malignant *anthrax* spore dispersion in high-rise buildings. *Journal of Engineering Physics and Thermophysics* **2004**, 77 (6).

Reshetin, V. P.; Regens, J. L., Simulation modeling of *anthrax* spore dispersion in a bioterrorism incident. *Risk Analysis* **2003**, 23 (6), 1135-1145.

Russell, T. P., X-ray and neutron reflectivity for the investigation of polymers. *Materials Science Reports* **1990**, 5 (4), 171-271.

Schein, L. B.; Czarnecki, W. S. Proximity theory of toner adhesion. *Journal of Imaging Science and Technology* **2004**, 48 (5), 699-704.

Sedin, D. L.; Rowlen, K. L., Adhesion forces measured by atomic force microscopy in humid air. *Analytical Chemistry* **2000**, 72 (10), 2183-2189.

Shao, P., Measurement of dielectric surface charge density and total charge density of a condenser. *Physical Review Letters* **1959**, 2 (2), 41-43.

Sheng, X. X.; Ting, Y. P.; Pehkonen, S. O., Force measurements of bacterial adhesion on metals using a cell probe atomic force microscope. *Journal of Colloid and Interface Science* **2007**, 310 (2), 661-669.

Smith, D. J.; Griffin, D. W.; Schuerger, A. C., Stratospheric microbiology at 20 km over the Pacific Ocean. *Aerobiologia* **2010**, 26 (1), 35-46.

Smith, W. E.; Zukoski, C. F., Role of solvation forces in the gelation of fumed silica-alcohol suspensions. *Journal of Colloid and Interface Science* **2006**, 304 (2), 348-358.

Stöber, W.; Fink, A.; Bohn, E. J., Controlled growth of monodisperse silica spheres in the micron size range. *Journal of Colloid and Interface Science* **1968**, 26, 62-69.

Taboada-Serrano, P.; Chin, C. J.; Yiacoumi, S.; Tsouris, C., Modeling aggregation of colloidal particles. *Current Opinion in Colloid & Interface Science* **2005**, 10 (3-4), 123-132.

Taboada-Serrano, P.; Vithayaveroj, V.; Hou, C. H.; Yiacoumi, S.; Tsouris, C., Comparison between effective electrode/electrolyte interface potential and applied potential for gold electrodes. *Industrial & Engineering Chemistry Research* **2008**, 47 (10), 3525-3531.

Taboada-Serrano, P.; Yiacoumi, S.; Tsouris, C., Behavior of mixtures of symmetric and asymmetric electrolytes near discretely charged planar surfaces: A Monte Carlo study. *Journal of Chemical Physics* **2005**, 123 (5), 054703.

Taboada-Serrano, P.; Yiacoumi, S.; Tsouris, C., Electrostatic surface interactions in mixtures of symmetric and asymmetric electrolytes: A Monte Carlo study. *Journal of Chemical Physics* **2006**, 125 (5), 11.

Takeuchi, M. Adhesion forces of charged particles. *Chemical Engineering Science* **2006**, 61 (7), 2279-2289.

Techaumnat, B.; Kadonaga, M.; Takuma, T., Analysis of electrostatic adhesion and detachment of a nonuniformly charged particle on a conducting plane. *Ieee Transactions on Dielectrics and Electrical Insulation* **2009**, 16 (3), 704-710.

Techaumnat, B.; Takuma, T., Analysis of the electrostatic force on a dielectric particle with partial charge distribution. *Journal of Electrostatics* **2009**, 67 (4), 686-690.

Thio, B. J. R.; Lee, J. H.; Meredith, J. C., Characterization of ragweed pollen adhesion to polyamides and polystyrene using atomic force microscopy. *Environmental Science & Technology* **2009**, 43 (12), 4308-4313.

Thio, B. J. R.; Meredith, J. C., Quantification of *E-coli* adhesion to polyamides and polystyrene with atomic force microscopy. *Colloids and Surfaces B-Biointerfaces* **2008**, 65 (2), 308-312.

Ubbink, J.; Schar-Zammaretti, P., Probing bacterial interactions: integrated approaches combining atomic force microscopy, electron microscopy and biophysical techniques. *Micron* **2005**, 36 (4), 293-320.

Utrup, L. J.; Werner, K.; Frey, A. H., Minimizing pathogenic bacteria, including spores, in indoor air. *Journal of Environmental Health* **2003**, 66 (5), 19-24.

Vadillo-Rodriguez, V.; Logan, B. E., Localized attraction correlates with bacterial adhesion to glass and metal oxide substrata. *Environmental Science & Technology* **2006**, 40 (9), 2983-2988.

Vane, L. M.; Zang, G. M., Effect of aqueous phase properties on clay particle zeta potential and electro-osmotic permeability: Implications for electro-kinetic soil remediation processes. *Journal of Hazardous Materials* **1997**, 55 (1-3), 1-22.

Venkateswaran, K.; Chung, S.; Allton, J.; Kern, R., Evaluation of various cleaning methods to remove *Bacillus* spores from spacecraft hardware materials. *Astrobiology* **2004**, 4 (3), 377-390.

Waar, K.; van der Mei, H. C.; Harmsen, H. J. M.; de Vries, J.; Atema-Smit, J.; Degener, J. E.; Busscher, H. J., Atomic force microscopy study on specificity and non-specificity of interaction forces between *Enterococcus faecalis* cells with and without aggregation substance. *Microbiology-Sgm* **2005**, 151, 2459-2464.

Wang, W.; Gu, B. H.; Liang, L. Y.; Hamilton, W. A., Fabrication of near-infrared photonic crystals using highly-monodispersed submicrometer SiO_2 spheres. *Journal of Physical Chemistry B* **2003a**, 107 (44), 12113-12117.

Wang, W.; Gu, B. H.; Liang, L. Y.; Hamilton, W., Fabrication of two- and three-dimensional silica nanocolloidal particle arrays. *Journal of Physical Chemistry B* **2003b**, 107 (15), 3400-3404.

Watano, S.; Hamashita, T.; Suzuki, T., Removal of fine powders from film surface. I. Effect of electrostatic force on the removal efficiency. *Chemical & Pharmaceutical Bulletin* **2002**, 50 (9), 1258-1261.

Westbrook, J. K.; Isard, S. A., Atmospheric scales of biotic dispersal. *Agricultural and Forest Meteorology* **1999**, 97 (4), 263-274.

Westphal, A. J.; Price, P. B.; Leighton, T. J.; Wheeler, K. E., Kinetics of size changes of individual *Bacillus thuringiensis* spores in response to changes in relative humidity. *Proceedings of the National Academy of Sciences of the United States of America* **2003**, 100 (6), 3461-3466.

Xiao, X. D.; Qian, L. M., Investigation of humidity-dependent capillary force. *Langmuir* **2000**, 16 (21), 8153-8158.

Yang, K. L.; Yiacoumi, S.; Tsouris, C., Canonical Monte Carlo simulations of the fluctuating-charge molecular water between charged surfaces. *Journal of Chemical Physics* **2002**, 117 (1), 337-345.

Zackrisson, A. S.; Pedersen, J. S.; Bergenholtz, J., A small-angle X-ray scattering study of aggregation and gelation of colloidal silica. *Colloids and Surfaces a-Physicochemical and Engineering Aspects* **2008**, 315 (1-3), 23-30.

Zhou, X. L.; Chen, S. H., Theoretical foundation of x-ray and neutron reflectometry. *Physics Reports-Review Section of Physics Letters* **1995**, 257 (4-5), 223-348.

VITA

EUNHYEA CHUNG

CHUNG was born in Seoul, Republic of Korea. She received a Bachelor of Science in Civil, Urban and Geosystem Engineering from Seoul National University, Seoul, Korea in 2002, and a Master of Science in Civil, Urban and Geosystem Engineering from Seoul National University, Seoul, Korea in 2004, before coming to Georgia Tech to pursue a doctorate in Environmental Engineering. In spring 2006, she joined the applied colloid and surface research group of Dr. Sotira Yiacoumi and completed her Ph.D. degree in May 2011.